PNE-217F

FINAL REPORT

379

Plowshare / peaceful uses for nuclear explosives

UNITED STATES ATOMIC ENERGY COMMISSION / PLOWSHARE PROGRAM

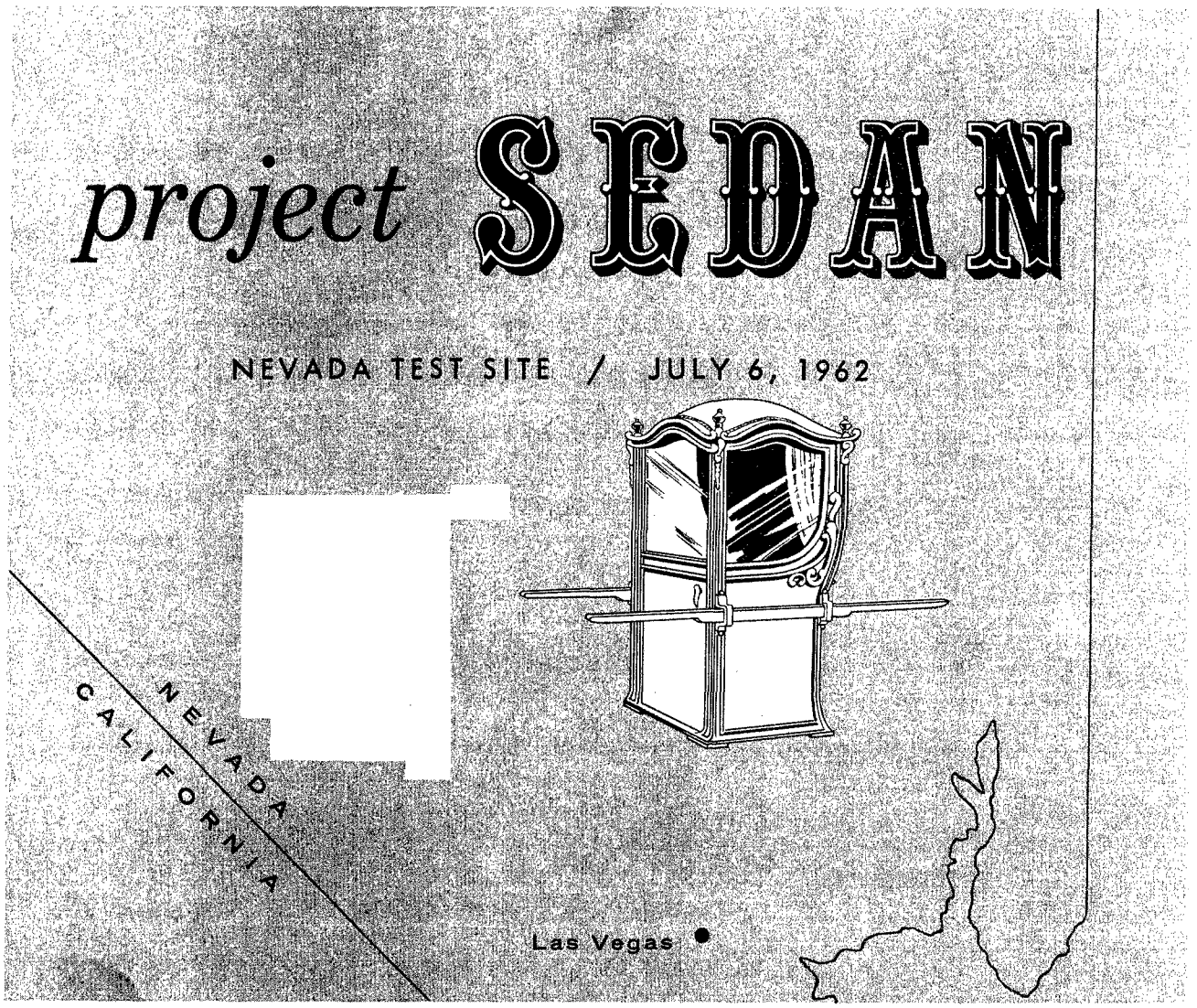

Mass Distribution and Throwout Studies

R. H. Carlson / W. A. Roberts

THE BOEING COMPANY

May 63 ISSUED: AUGUST 6, 1963

LEGAL NOTICE

USAEC Division of Technical Information Extension, Oak Ridge, Tennessee

PROJECT SEDAN

PNE-217F

MASS DISTRIBUTION AND THROWOUT STUDIES

R. H. Carlson
W. A. Roberts

The Boeing Company
Seattle, Washington

May 1963

ABSTRACT

Analysis of data collected at 117 sampling stations indicates that areal density varies inversely as distance raised to the 4.3 power. Circumferential variation in areal density was significant along all sampling rings; the ratio of highest observation to lowest was 37, 7, 10, and 32 at incremental distances in crater radii of 3.5, 4.7, 7, and 9.3 respectively. The total ejecta mass represented about 58 percent of the mass inferred from the apparent crater volume suggesting that about 37 percent of the crater volume was caused by compression of the surrounding desert alluvium. One half of the total mass of material ejected was deposited between the crater edge and two crater radii, whereas 97 percent of the total ejecta mass was deposited within ten crater radii. The ejecta profile exhibited a two-layer system, the lower layer consisting of the fine material ejected in mass or bulk. The upper layer consisted of larger particulate materials which were subjected to atmospheric influence when ejected along their ballistic trajectories. The missile-like material in the upper layer and the discrete masses of alluvium which created hundreds of impact craters probably were deposited late in the time history of ejecta deposition.

ACKNOWLEDGMENTS

It is not possible to credit all who were involved in this project; however, there are several whose contributions cannot go unrecognized. The efforts of each of the following persons have been instrumental in the success of this project: Phillip T. Anderson, Thomas P. Day, Joan K. Dickhaut, Charles V. Fulmer, Allan B. Jenkins, Glen D. Jones, Mary Lou Keefe, Nancy A. Owen, and Charles R. Wauchope.

Among those who assisted in the field aspects of this experiment, personnel from Lawrence Radiation Laboratory-Nevada and Holmes and Narver were particularly helpful.

SEDAN CRATER

CONTENTS

CONTENTS

CONTENTS

CONTENTS

FIGURES (Continued)

CHAPTER 1

INTRODUCTION

1.1 OBJECTIVES

The primary objective of this project was to obtain quantitative data on distribution of ejecta on the ground surface surrounding a nuclear crater. These data are necessary to define the fallback portion of the apparent crater lip, both radially and circumferentially. Both areal density and thickness data were to be obtained and appropriate functional relationships developed. The typical crater sketch shown in Figure 1.1 illustrates the fallback or ejecta region to be defined by this experiment.

Secondary objectives of this project were: (1) to determine the outer limit of the base surge deposit and ballistic ejecta, (2) to survey certain designated areas for significant natural geologic missiles; recording their size, weight, and location, (3) to determine particle size distribution and comminution (particle fracturing resulting from the explosive shock) existing at certain designated stations, (4) to determine particle size distribution relative to position within the ejecta profile, and (5) to map impact craters and determine their origin.

1.2 BACKGROUND

Determination of the extent and distribution of crater ejecta and associated radioactivity is a major problem that must be evaluated before peaceful projects for nuclear explosive harbor and canal excavation can be

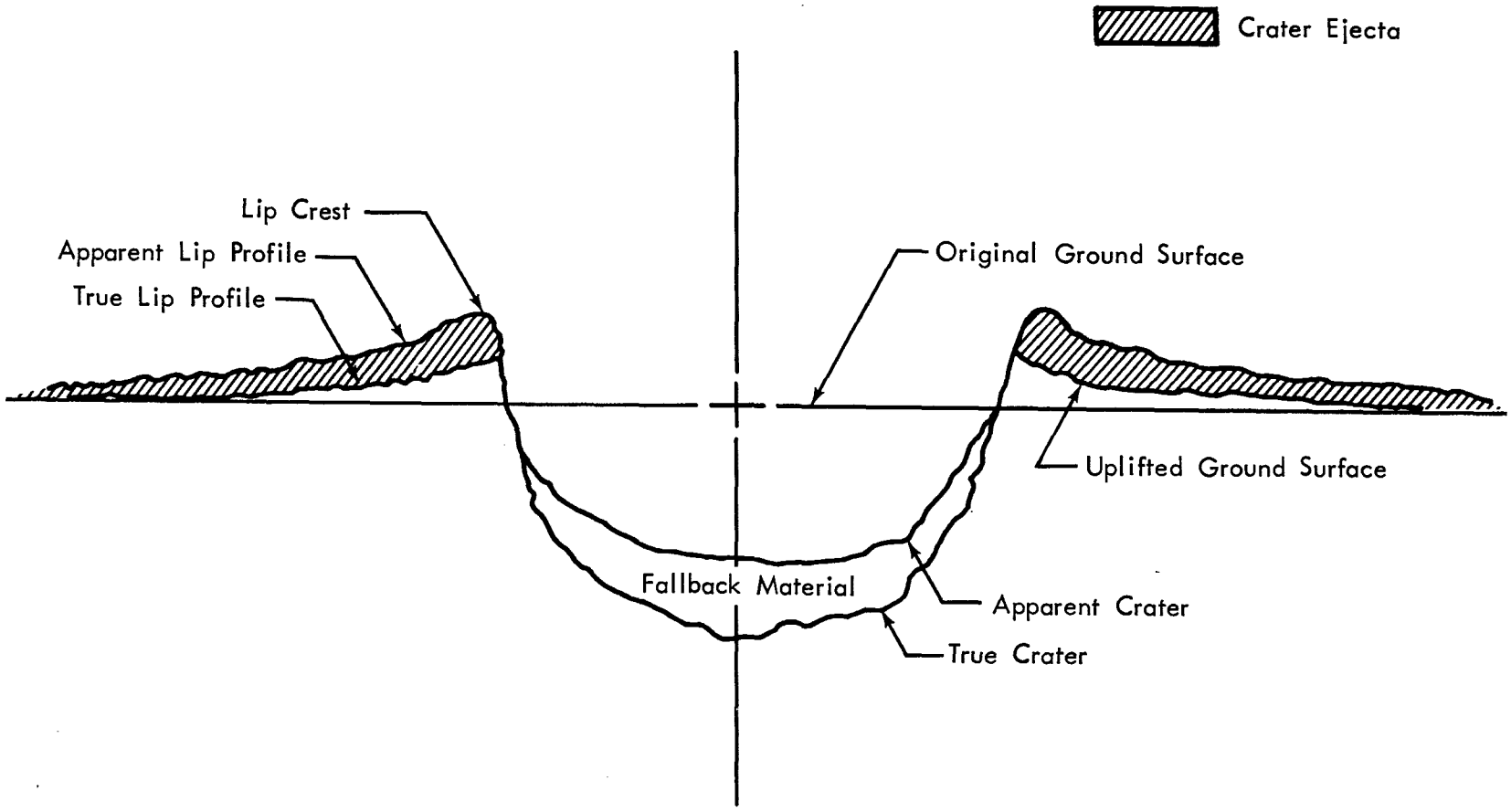

Figure 1.1 Cross-sectional profile of typical crater.

safely accomplished. From a military standpoint, crater ejecta may prove troublesome to such surface components of hardened underground structures as entrance hatchways, blast valves, and exhaust ducts and to various weapons systems communication antennas.

Nuclear cratering experiments conducted before the recent weapons test moratorium did not include projects designed specifically for measuring crater ejecta mass distribution. Available ejecta data on past tests stems from recorded crater lip profiles, data on upthrust of the ground surface adjacent to the crater, and long-range observations of fallout quantities. This information is not sufficient, however, to determine ejecta areal density variations over the entire region of interest from both Plowshare and military standpoints.

Detailed examination of aerial photographs taken of both nuclear and high explosive craters shows relatively large quantities of ejecta beyond the conventional crater lip. (The conventional crater lip is usually considered to extend a radial distance of two crater radii from ground zero.) Ejecta is generally distributed in the region adjacent to the crater in a rayed pattern characterized by a relatively large amount of debris concentrated in longitudinal mounds, radially oriented. These mounds are not necessarily continuous from their outer extremity inward to the conventional crater lip and may sometimes be tangential to the crater rather than radial.

Previous quantitative measurements of crater ejecta have been made on several high explosive cratering shots. The ejecta relationships resulting from

these experiments are summarized in Table 1.1. Experiments described in References 1 through 4 consisted of physically sampling the debris to determine its distribution. Early experimental work of a similar nature was done by Engineering Research Associates (Reference 5). Existing ejecta data are not sufficient to derive empirical relationships whereby ejecta quantities can be confidently predicted for nuclear cratering shots regardless of burst depth, medium, or charge characteristics.

Most previous work done to determine the shape and extent of the outer crater lip profile has been empirical. In a recent study the crater lip profile has been reconstructed using data obtained from known positions of origin and termination of identifiable missiles artificially introduced into the anticipated crater region for a high explosive cratering shot (Reference 6).

TABLE 1.1 SUMMARY OF HIGH EXPLOSIVE EJECTA DATA

Shot	Energy Release		Burst Depth	Apparent Crater Radius	Apparent Crater Depth	Relationship*	Range**	Medium	Reference
	kg	tons	m	m	m		m		
Stagecoach Shot 2	1.8×10^4	20	5.2	15.4	7.2	$\delta = \frac{5.03 \times 10^5}{D^{2.48}}$	73 to 485	Desert alluvium	1
Shot 3	1.8×10^4	20	10.4	17.9	8.9	$\delta = \frac{4.42 \times 10^5}{D^{2.35}}$	73 to 334	Desert alluvium	1
Scooter	4.5×10^5	500	38.1	46.8	22.9	$\delta = \frac{9.1 \times 10^6}{D^{2.6}}$	457 to 980	Desert alluvium	2
White Tribe (Average for nine shots)	5.2×10^3	5.8	0	5.3	2.5	$\delta = \frac{8.93 \times 10^4}{D^{2.73}}$	15 to 167	Caliche	3
Suffield 100 Ton	9.1×10^4	100	0	21.3	6.2	$\delta = \frac{2.56 \times 10^8}{D^{3.65}}$	37 to 427	Silt and clay	4

* These relationships were developed by mathematically fitting a single straight line to a log plot of the data.

δ = areal density in kg/m^2

D = range in meters

** Region within which data were obtained.

CHAPTER 2

EXPERIMENTAL PROCEDURE

2.1 SHOT PARTICIPATION

The Sedan shot was burst at 194 meters (635 feet) beneath the ground surface in Area 10 on the Nevada Test Site. The geologic medium is desert alluvium, a recent sedimentary deposit of poorly sorted clay, silt, sand and occasional lenses of gravel containing rock fragments ranging in size from pebbles to boulders. The shot detonated on July 6, 1962 resulted in an energy release equivalent to $9.1 \pm 1.4 \times 10^7$ kg (100 ± 15 kt) of TNT. The apparent crater is about 182 meters (600 feet) in radius and 99 meters (320 feet) in depth.

2.2 STATION LAYOUT

Ejecta station locations were based on a predicted crater radius of 213 meters (700 feet) (Reference 7). Sampling rings X, A, B, C, D, E, F, and G were located at distances from ground zero of 1 3/4, 2, 2 1/2, 3, 4, 5, 6, and 8 predicted crater radii, respectively. The range of radial distances over which stations were located was chosen to cover the possible variations of explosive yields. Radial sampling lines, spaced at fifteen-degree intervals, were numbered sequentially from 1 to 24 in a clockwise direction, line 1 being coincident with the N 15° E bearing. The prevailing wind direction for July is directly from the south. All ejecta station locations relative to ground zero and the predicted crater boundary are shown in Figure 2.1. Stations were located by Holmes and Narver survey teams to an accuracy of

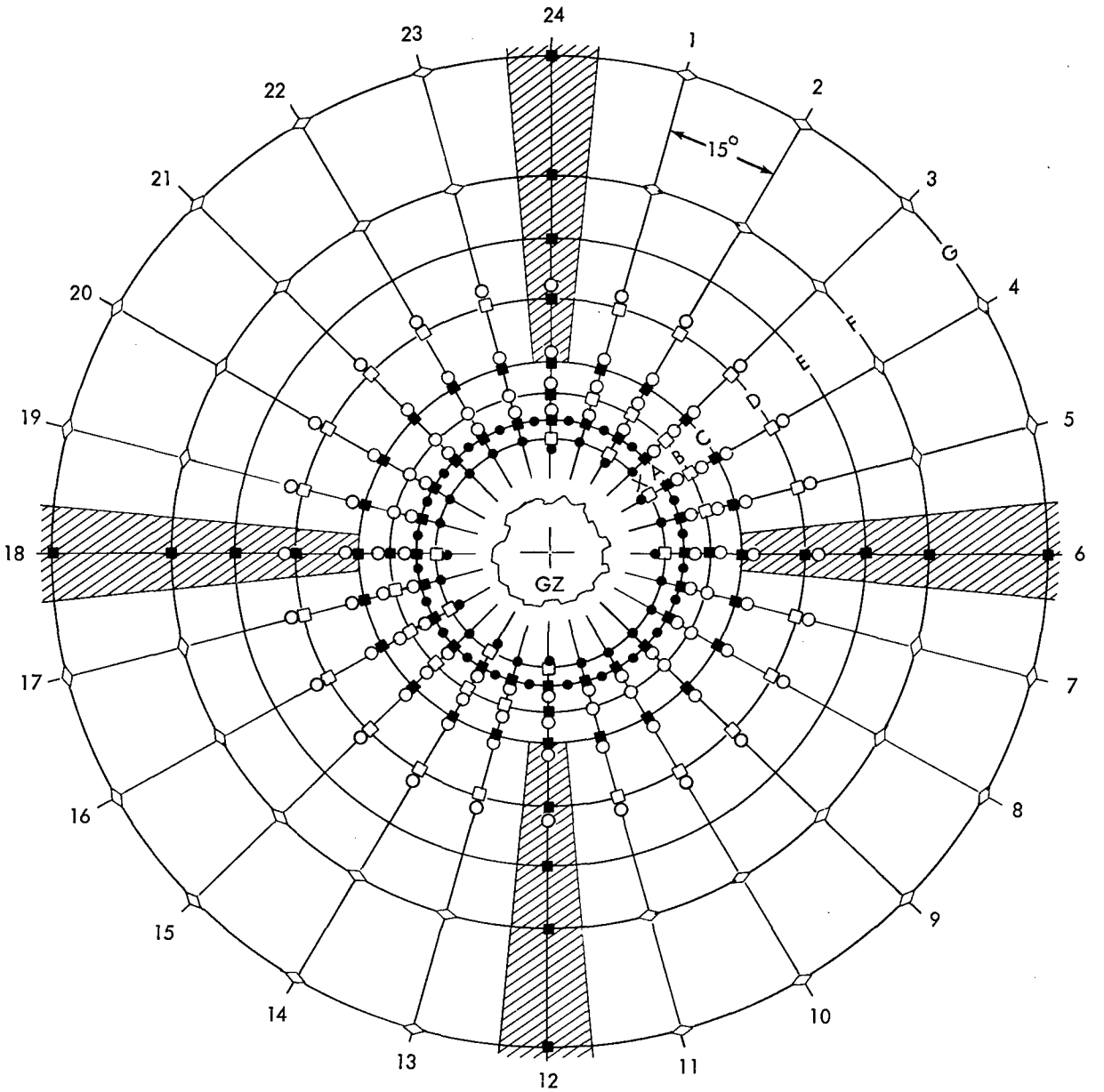

RING	RADIAL DISTANCE, Meters
G	1707
F	1280
E	1067
D	853
C	640
B	533
A	427
X	373

SYMBOLS

- □ Secondary Tarps
- ■ Primary Tarps
- ○ Pipe
- ● Flexible Rod
- ◇ Trays
- ▨ Missile Survey Area

Figure 2.1 Station layout.

$\pm$30.5 cm ($\pm$ 1 foot).

All tarp stations were cleared of random debris and plastic trays were placed along F and G rings on the afternoon of D - 1 day.

2.3 DESCRIPTION OF STATIONS

Two methods were used to obtain data on mass distribution of crater ejecta. Areal density was determined by weighing ejecta samples obtained from tarp and tray stations. (A tarp station consists of a heavy canvas tarpaulin securely fastened to the ground surface.) Vertical pipes and rods were installed to gage ejecta thickness by marking the pre-shot position of the original ground surface and post-shot position of the ejecta surface on the same pipe. Spray paint of various colors was used to record ground surface and ejecta surface positions on rods and pipes.

The 68 primary tarp stations consisted of one or more 60- by 120-cm (2- by 4-foot) heavy canvas tarps oriented so that the shorter dimension was coincident with the radial direction from ground zero. Tarp stations were located along the north, east, south, and west radial lines at the X, A, B, C, D, E, F, and G rings. Tarps were also placed at fifteen-degree intervals along the A and C rings. Radial stations were designed to sample approximately 0.2 percent and circumferential stations about 1.2 percent of the circumferences at their respective distances from ground zero. Tarps were fastened to the ground with steel spikes approximately 25 cm in length.

Thirty-eight secondary tarp stations, each consisting of a single 120-cm (4- by 4-foot) square tarp, were located so that twenty were on the D circle, ten on the B circle, and eight on the X circle.

Twenty-four vertical 1.3-cm (1/2-inch) steel pipes were located along each of the A, B, C, and D circles. The height of pipe protruding above the ground surface was approximately 150, 120, 120, and 60 cm (5, 4, 4, and 2 feet) along the A, B, C, and D circles, respectively. All vertical pipe segments were fastened by a standard coupling to a 60-cm (2-foot) section driven into the ground. Pipe sections were metal, stamped with station locations for identification after recovery.

Twenty-four flexible steel rods were located along both the X and A rings. Each rod was 240 cm (8 feet) long with 90 cm (3 feet) driven into the ground. All rods and pipes were spray painted to designate original ground surface immediately after installation.

Twenty plastic trays, approximately 25 by 36 by 8 cm (10 x 13 x 3 inches) were located along both the F and G circles at intersections of all radial lines except 6, 12, 18, and 24. Each tray was held in place with light steel cable and four 20-cm (8-inch) steel spikes. Trays were positioned late on D - 1 day to avoid accumulation of pre-shot random debris.

The sampling array consisted of a total of 196 different stations that could yield 290 ejecta areal density and thickness measurements. Table 2.1 is a summary of all ejecta stations. Figure 2.2 shows typical pre-shot

TABLE 2.1 SUMMARY OF EJECTA SAMPLING STATIONS

Ring	Distance from Ground Zero			Number of Stations				
				Primary Tarp	Secondary Tarp	Pipe	Flexible Rod	Tray
	m	ft	α^*					
G	1707	5600	8	4				20
F	1280	4200	6	4				20
E	1067	3500	5	4				
D	853	2800	4	4	20	24		
C	640	2100	3	24		24		
B	533	1750	2 1/2	4	10	24		
A	427	1400	2	24		24	24	
X	373	1225	1 3/4		8		24	
Totals				68	38	96	48	40

*Range divided by predicted apparent crater radius.

Station X24 - 4 ft by 4 ft tarp same as those used along D circle.

Station C23

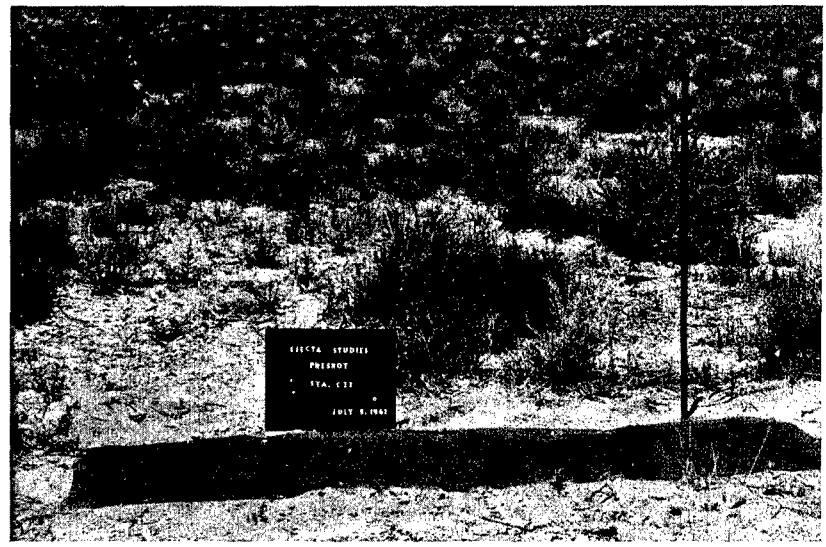

Station G24 - Note five 2 ft by 4 ft tarps required at this range. (1,700 meters)

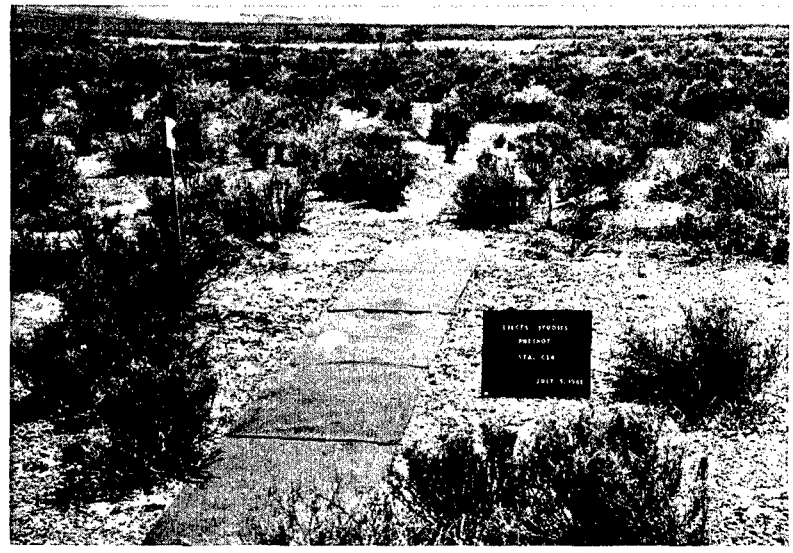

Figure 2.2 Pre-shot photographs of ejecta sampling stations.

photographs of ejecta sampling stations.

2.4 SAMPLING TECHNIQUES

Areal density samples were taken in several ways. At all primary tarp stations with the exception of the C stations, the areal density was determined by weighing tarp and sample together and subtracting the tarp weight. Areal densities at F and G tray stations were determined in the same way.

At closer stations where the ejecta thickness was greater, other techniques were used to measure the areal density. Bottomless aluminum alloy boxes of known cross-sectional area (1 ft^2 and 2 ft^2) were used in obtaining samples on the D tarps. The box was forced down into the ejecta until its lower edge rested on the tarp. The material inside the aluminum form was then removed and weighed.

At several of the D stations where the original tarp was missing or badly damaged and at most C stations, a thin-wall sampler having a cross-sectional area of 93 cm^2 (0.1 ft^2) was used. When using the thin-wall sampler, ejecta was excavated until the pre-shot ground surface was identified. A steel plate was then driven horizontally coincident with the pre-shot surface and used as the base to which the sample was taken. Recovery apparatus are shown in Figure 2.3.

The thin-walled sampler could not be completely driven to the original

One square foot sampler in place during recovery at Station D3.

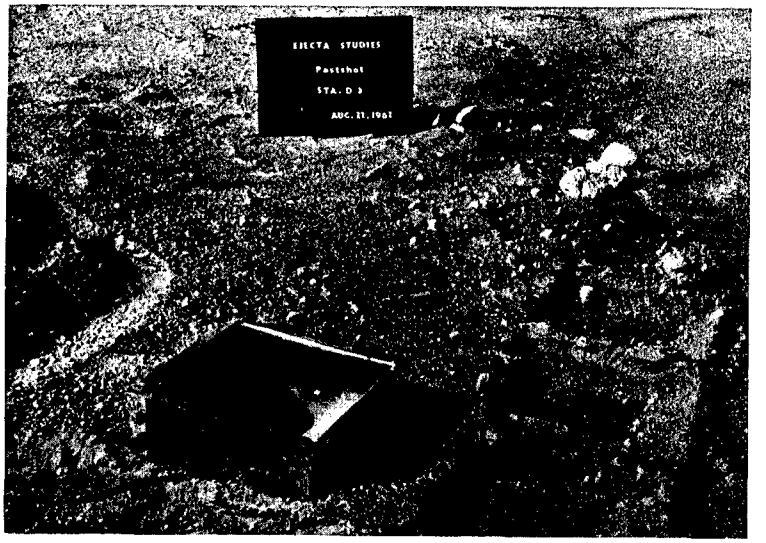

Thin wall sampler.

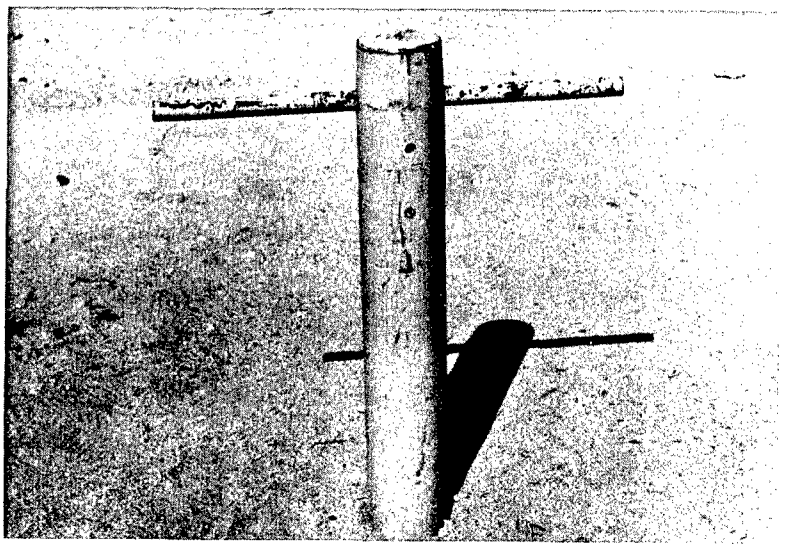

One and two square foot samplers.

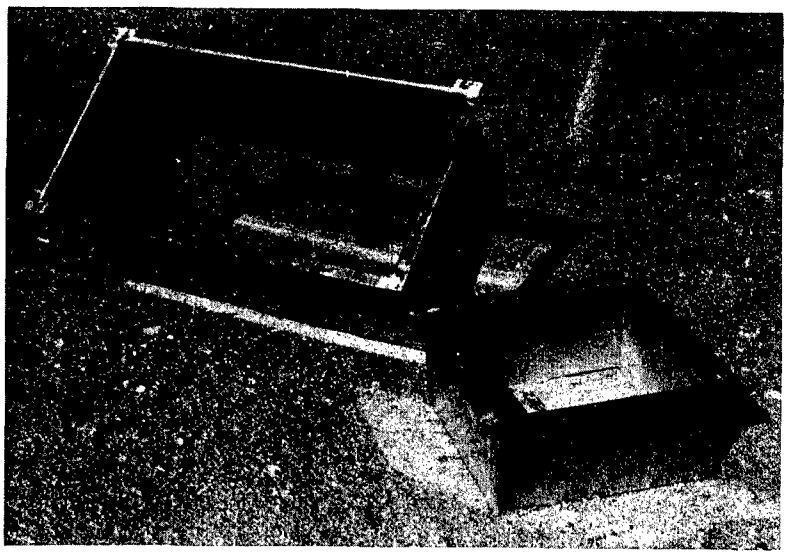

Figure 2.3 Recovery apparatus.

ground surface when the debris exceeded about 0.5 meters in depth. Ejecta depths were obtained using hand excavation techniques for thicknesses between 0.5 meters and 1.0 meters. A bulldozer was used for excavation where thicknesses were greater than one meter.

CHAPTER 3

RESULTS

3.1 EJECTA MASS DISTRIBUTION

3.1.1 Areal Density. Direct areal density measurements were made at all G and E stations, at 23 F and D stations, at 18 C stations, at 2 B stations, and at the A6 station (see Figure 2.1). At other stations, the great depth of ejecta permitted only vertical measurement of ejecta thickness (see Tables A.1, A.3, and A.4). Post-shot photographs of several sampling stations are shown in Figure 3.1. The ejecta thickness at station A24 was 3.8 meters (12.5 feet), the maximum thickness measured at any of the sampling stations. Ejecta areal densities and corresponding thicknesses for all stations at which samples were recovered are given in Table 3.1.

An ejecta density of 1.5 gm/cm^3 has been used herein whenever ejecta areal density and thickness conversions are required (see Section 3.1.6). An ejecta isopach map of ejecta thickness is shown in Figure 3.2.

Areal density as a function of range is plotted in Figure 3.3. The range of observations and the arithmetic mean are shown for each radial distance. Also shown is the exponential function which best fits the mean data using the method of least squares. The equation of this line is:

$$\delta = \frac{6.98 \times 10^{14}}{D^{4.3}}$$

Where: δ = areal density in kg/m^2

Station A24
(425 meters)

Station D8
(850 meters)

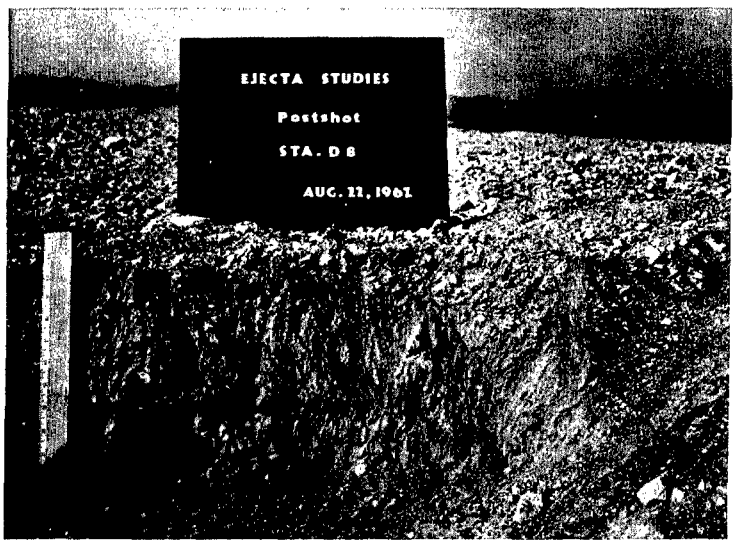

Station F9
(1270 meters)

Figure 3.1 Post-shot stations.

TABLE 3.1 EJECTA QUANTITIES AT RECOVERED STATIONS

Station	Areal Density	Thickness	Station	Areal Density	Thickness	Station	Areal Density	Thickness
	kg/m^2	cm		kg/m^2	cm		kg/m^2	cm
G1	8.10	0.54	F5	42.7	2.9	D5	147	9.8
G2	6.15	0.41	F6	10.2	0.68	D6	89.3	6.0
G3	8.93	0.60	F7	58.9	3.8	D7	191	13
G4	7.71	0.51	F8	--	--	D8	262	19
G5	16.9	1.1	F9	55.7	3.7	D9	118	7.9
G6	3.08	0.21	F10	17.6	1.2	D10	101	6.8
G7	6.54	0.44	F11	37.6	2.5	D11	53.6	3.6
G8	41.0	2.7	F12	25.1	1.7	D12	95.2	6.4
G9	30.3	2.0	F13	63.4	4.3	D13	87.6	5.8
G10	4.59	0.31	F14	58.5	3.9	D14	78.5	5.2
G11	3.76	0.25	F15	35.4	2.4	D15	177	12
G12	3.08	0.21	F16	39.5	2.6	D16	124	8.3
G13	4.59	0.31	F17	18.0	1.2	D17	134	9.0
G14	10.9	0.73	F18	7.62	0.50	D18	42.0	2.8
G15	11.3	0.75	F19	66.9	4.5	D19	108	7.2
G16	7.37	0.49	F20	17.2	1.2	D20	--	--
G17	6.15	0.41	F21	44.2	2.9	D21	114	7.6
G18	1.27	0.08	F22	52.8	3.5	D22	78.0	5.2
G19	6.93	0.46	F23	48.6	3.2	D23	57.4	3.8
G20	1.42	0.10	F24	6.69	0.45	D24	38.2	2.6
G21	3.37	0.22	E6	62.1	4.1	C1	557	37.8
G22	9.33	0.62	E12	21.9	1.5	C2	1050	70.2
G23	8.69	0.58	E18	23.1	1.5	C3	664	44.2
G24	1.86	0.12	E24	19.5	1.3	C4	626	41.7
F1	19.6	1.3	D1	129	8.7	C5	563	37.5
F2	37.0	2.5	D2	91.2	6.1	C6	323	22.0
F3	24.0	1.6	D3	104	6.9	C7	800	53.3
F4	52.5	3.5	D4	125	8.4	C8	499	33.3

TABLE 3.1 EJECTA QUANTITIES AT RECOVERED STATIONS (CONTINUED)

Station	Areal Density	Thickness	Station	Areal Density	Thickness	Station	Areal Density	Thickness
	kg/m^2	cm		kg/m^2	cm		kg/m^2	cm
C9	1010	67.1	C21	83.4	5.6	B14	1740	116
C10	529	35.2	C22	69.5	4.6	B15	2470	165
C11	2560	171	C23	193	12.9	B16	1600	107
C12	632	42.1	C24	561	37.5	B17	2420	162
C13	1190	79.2	B1	2060	137	B18	633	45.7
C14	293	19.6	B2	2380	159	B24	2190	155
C15	1390	93.0	B3	1420	94.5			
C16	869	57.9	B4	1280	85.3	A6	610	40.8
						A12	2190	146
C17	664	44.2	B5	2652	177	A18	1100	73.2
C18	229	15.3	B6	416	27.8	A24	5710	381
C19	83.4	5.6	B12	1280	85.3			
C20	88.9	5.9	B13	2790	186			

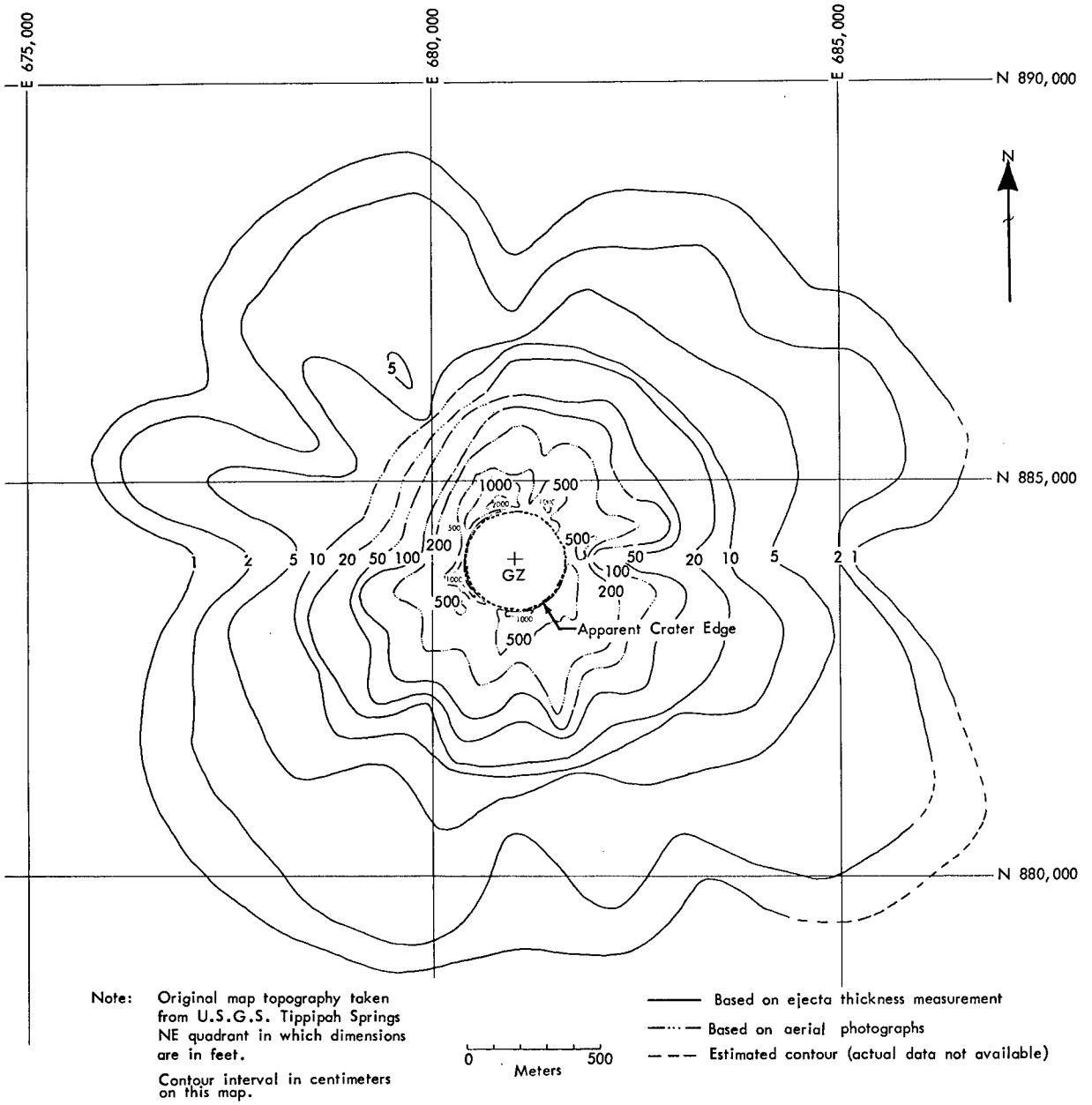

Figure 3.2 Isopach map of ejecta thickness.

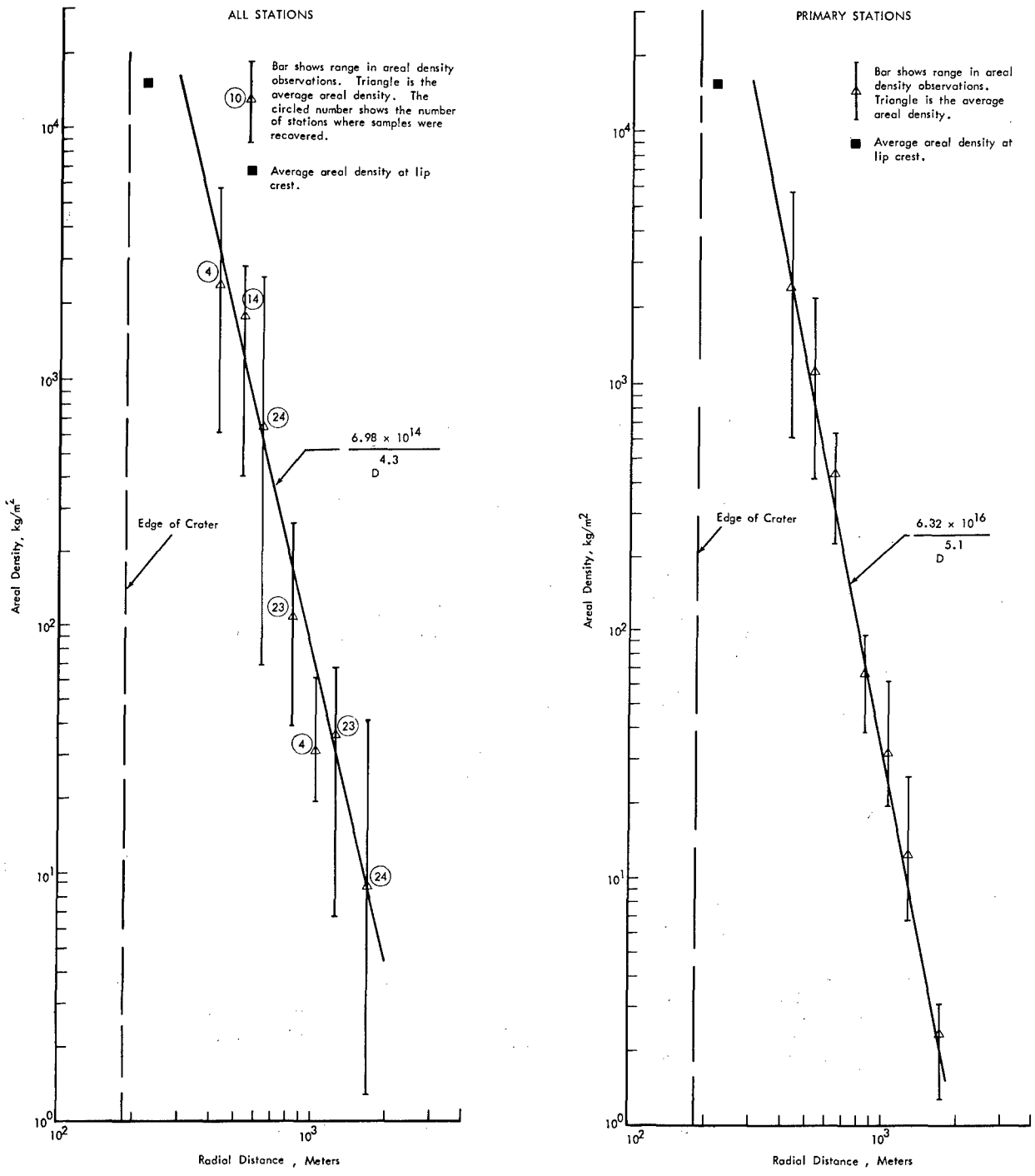

Figure 3.3 Areal density as a function of distance.

D = radial distance from ground zero in meters

Average areal densities and ranges of observations for the four primary sampling lines are also shown in Figure 3.3 along with the exponential relationship which has been mathematically fitted to these data. The equation of this line is:

$$\delta = \frac{6.32 \times 10^{16}}{D^{5.1}}$$

Average areal density data are summarized in Table 3.2.

Few data were recovered from the flexible rod stations. Only three of 24 pipes installed along the D ring were found in a vertical position. Other pipes located in the debris were either severely bent or broken. The mass of ejecta caused sufficient drag to bend or break the pipes and flexible rods.

The thickness of ejecta at the few locations where pipes remained standing is listed in Table A.5 of the appendix. The gaged thicknesses at Stations D2, D11, and D22 were 8.2, 3.7, and 2.8 cm, respectively. The thicknesses calculated from the areal density measurements at these stations were 6.1, 3.6, and 5.2 cm, respectively. The average gaged thickness at these three stations was 4.9 cm, which is fortuitously close to the average calculated thickness of 5.0 cm for these same stations. Ejecta thickness at a pipe is, of course, for a single very small area while areal density measurements result in an average thickness for a much larger relative area.

3.1.2 Vertical Layering. There is distinct stratification in the ejecta beyond the crater edge. At the lip crest, the layering is multiple and marked

TABLE 3.2 AVERAGE AREAL DENSITIES

Ring	Radial Distance from Ground Zero	Areal Density					
		Radius 6	Radius 12	Radius 18	Radius 24	Average Primary Radii	Average All Radii
	m	kg/m2					
G	1707	3.08	3.08	1.27	1.86	2.32	8.89
F	1280	10.2	25.1	7.62	6.69	12.4	36.6
E	1067	62.1	21.9	23.1	19.5	31.6	31.6
D	853	89.3	95.2	42.0	38.2	66.2	111
C	640	328	632	229	561	438	647
B	533	416	1280	633	2180	1130	1810
A	427	610	2190	1100	5710	2400	2400

by both particle sorting and color. This is illustrated in Figure 3.4. Beyond the lip crest multiple layering does not appear to be present. In general, two distinct layers can be observed and correlated at the A, B, and C rings. A third layer, uppermost in the sequence, was deposited from the base surge cloud and was almost completely removed by winds prior to recovery. The extent of this deposit is discussed in Section 3.1.3.

The lower of the two observable layers consists of poorly sorted material, light brown to light yellow-brown in color. The material of which this layer consists was probably ejected from the crater in bulk or in mass, being relatively unaffected by the atmosphere during its flight. Fused silicates or other fused alluvial material were not evident macroscopically when this layer was sampled. The thickness of this lower layer was between 1 cm and 3.8 meters. This layer is usually referred to herein as the bulk ejecta layer.

The upper layer is generally light grey in color and is between 1 and 15 cm in thickness. It is poorly sorted and contains considerable fused material in addition to pebbles, cobbles, sand, and silty material. The present upper debris layer and the remaining portion of the base surge deposit when combined are equivalent, in distribution of grain size, to the bulk ejecta of the lower layer. This layer is usually referred to herein as the missile ejecta layer.

The thicknesses of the upper and lower ejecta layers were measured at locations where samples were taken for grain size determinations. These measurements are given in Table 3.3.

West rim of Sedan Crater looking South. (Note layering in debris above the original ground surface.)

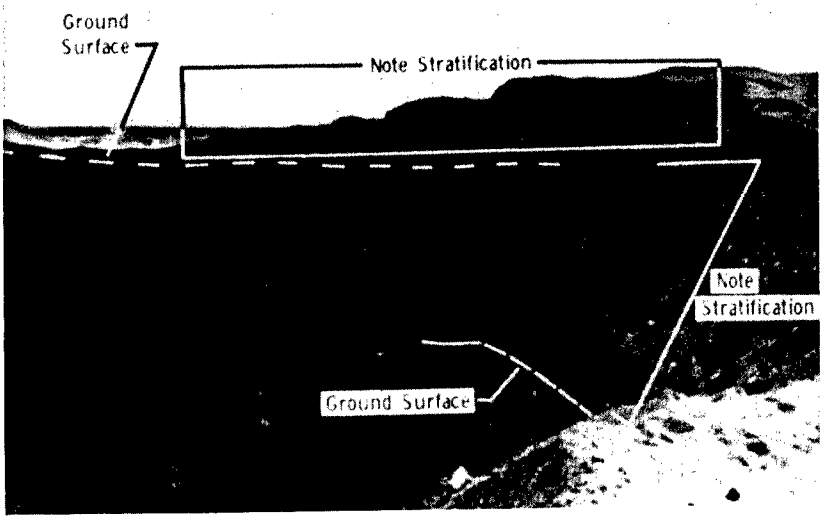

West rim of Sedan Crater looking North. (Note layering in debris near worker.) Original ground surface is not exposed here, but lies between the two outcrops of the massive unit originally just below the surface.

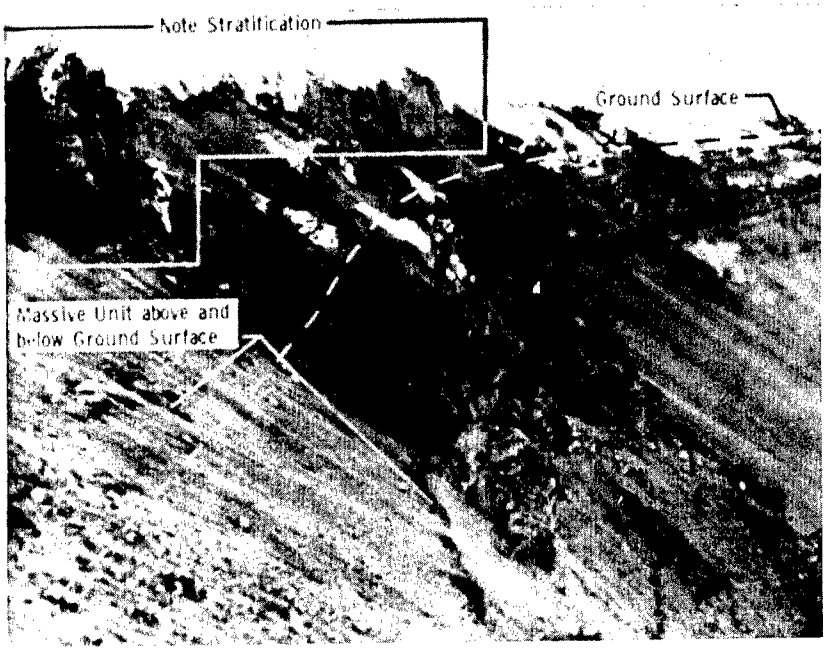

Figure 3.4 Stratification of ejecta at lip crest.

TABLE 3.3 THICKNESS OF EJECTA LAYERS

Station	Thickness		Station	Thickness	
	Upper Layer	Lower Layer		Upper Layer	Lower Layer
	cm	cm		cm	cm
C24	3.0	34.5	C8	5.1	28.2
C23	3.0	9.9	C7	5.1	48.2
C22	2.3	2.3	C6	6.0	16.0
C21	5.6		C5	6.0	31.5
C20	3.0	2.9	C4	6.0	35.7
C19	4.5	1.1	C3	6.0	38.2
C18	5.1	10.2	C2	6.0	64.2
C17	5.7	38.5			
C16	5.1	52.8	B24	4.5	151
C15	5.7	88.3	B18	9.0	36.7
C14	3.8	15.8	B12	6.4	78.9
C13	5.7	73.5	B6	8.0	19.8
C12	5.7	36.4	A24	3.0	378
C11	6.4	164	A18	6.9	66.3
C10	5.7	29.5	A12	15.0	131
C9	6.4	60.7	A6	9.0	31.8

Figure 3.5 shows the extent of the bulk and missile ejecta layers.

3.1.3 Base Surge Deposit. When material thrown upward as a dirt column from an underground cratering shot falls back to earth, it produces a secondary expanding cloud of fine soil particles known as the base surge. This secondary cloud moves outward from the center of the explosion; its transported load of contaminated soil particles eventually settling out over a large area. The extent of the base surge area depends on burst depth, geologic medium, energy release, etc. Because of the significance of the base surge in connection with Plowshare cratering projects, its extent on Sedan was documented. Similar documentation is available for the Teapot ESS crater.

The edge of the base surge deposit was taken from aerial photographs made by the Naval Office of Radiological Defense Laboratories (NRDL) on D + 1 day. The upwind deposit is easily discernible. Crosswind and particularly downwind, the base surge deposit edge is gradational and diffuse and locally indeterminate. Figure 3.6 is a map showing this base surge deposit edge as determined from the NRDL aerial photographs.

3.1.4 Grain Size Distribution. A total of 53 ejecta samples were sorted into size groups to (1) determine average sorting of ejecta particulate within the region sampled, (2) determine possible particulate size differences between samples recovered from trays and others recovered from tarps, and (3) define the difference in grain size distribution of the two distinct ejecta layers. The grain size distribution is listed in Tables A.9 and A.10 of the appendix.

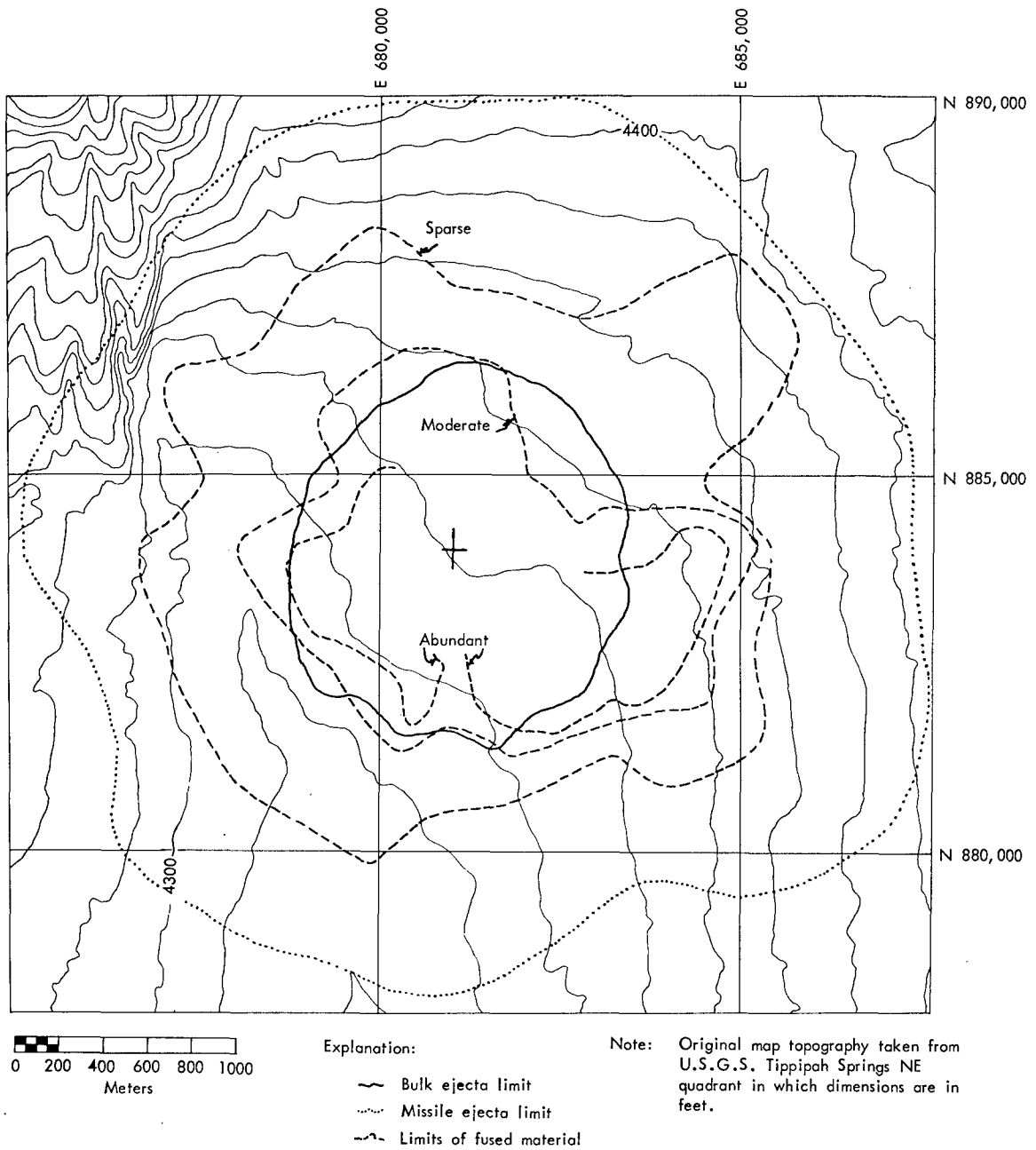

Figure 3.5 Outer limits for bulk ejecta, missile ejecta, and fused material.

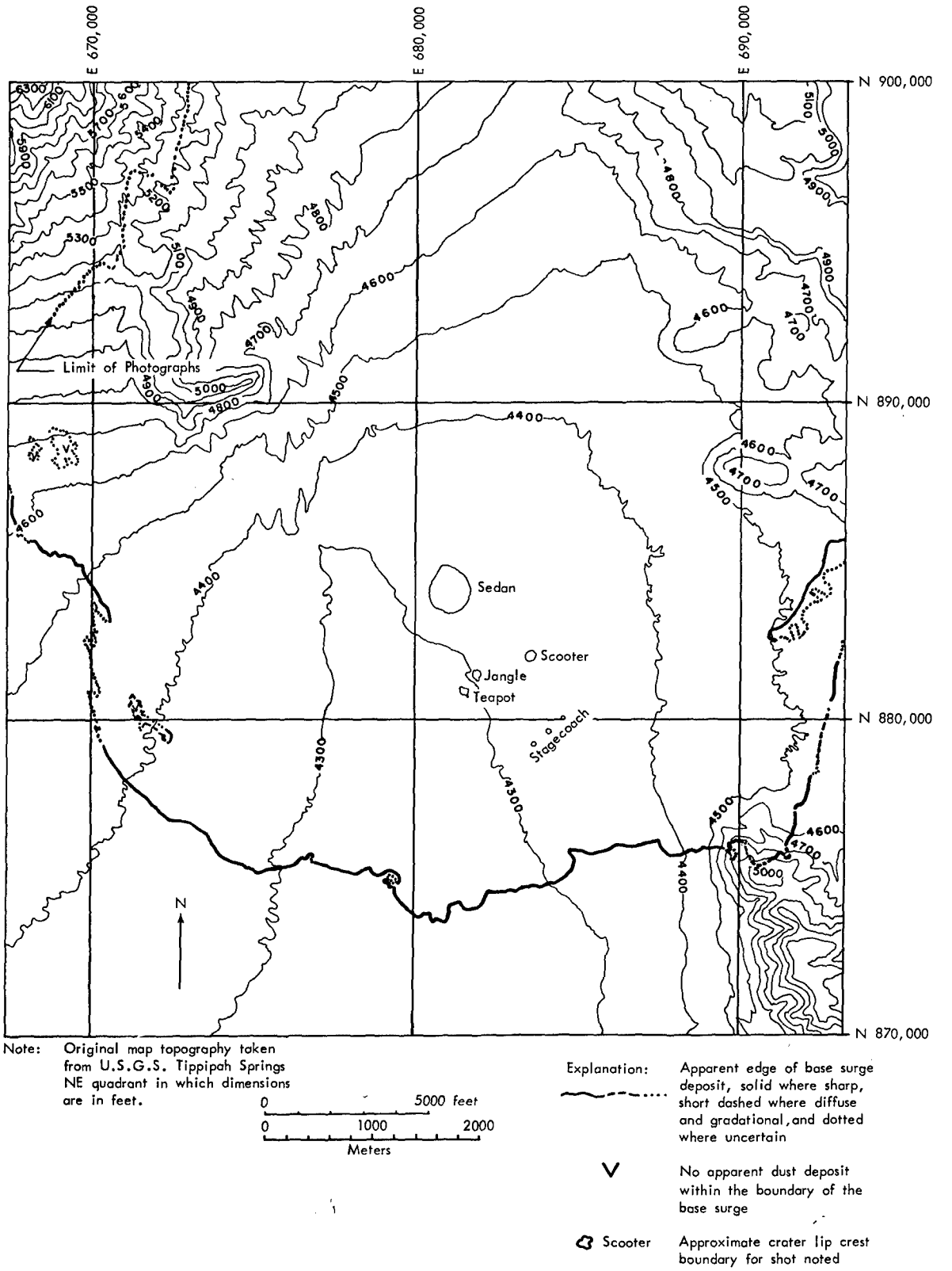

Figure 3.6 Outer limit of base surge deposit.

Figure 3.7 shows the grain size distribution for samples collected along the G, F, D, C, B, and A rings. Also shown in Figure 3.7 is the grain size distribution for the in situ pre-shot desert alluvium.

3.1.5 Circumferential Variation. The variation of the quantity of ejecta at a constant radial distance is illustrated in Figure 3.8 for sampling rings G, F, D, C, and B. Areal densities vary by a factor of about 30 along the G ring, 10 along the F ring, 7 along the D ring, 37 along the C ring, and 7 in the two quadrants sampled along the B ring. The tray at F8 was not recovered, but was in a region of relatively high areal density. The tarp at D20 was buried beneath the throwout from a large impact crater.

3.1.6 Volumetric Ejecta Density. Twelve post-shot determinations were made of in situ volumetric ejecta density. These data are summarized in Table A.7 of the appendix. The average density was 1.5 gm/cm^3 (94 lb/ft^3). All conversions of ejecta areal density and ejecta thickness made herein are based on this average volumetric density.

Typical pre-shot field densities in Area 10 on the Nevada Test Site are as follows: at a depth of 60 cm, 1.4 gm/cm^3; at 90 cm, 1.6 gm/cm^3; at 120 cm, 1.5 gm/cm^3; at 3 meters, 1.5 gm/cm^3; and at 4.5 meters, 1.4 gm/cm^3 (Reference 8). The average density is about 1.5 gm/cm^3.

3.2 MISSILES AND IMPACT CRATERS

3.2.1 Missile Survey. A missile survey was made along the four primary

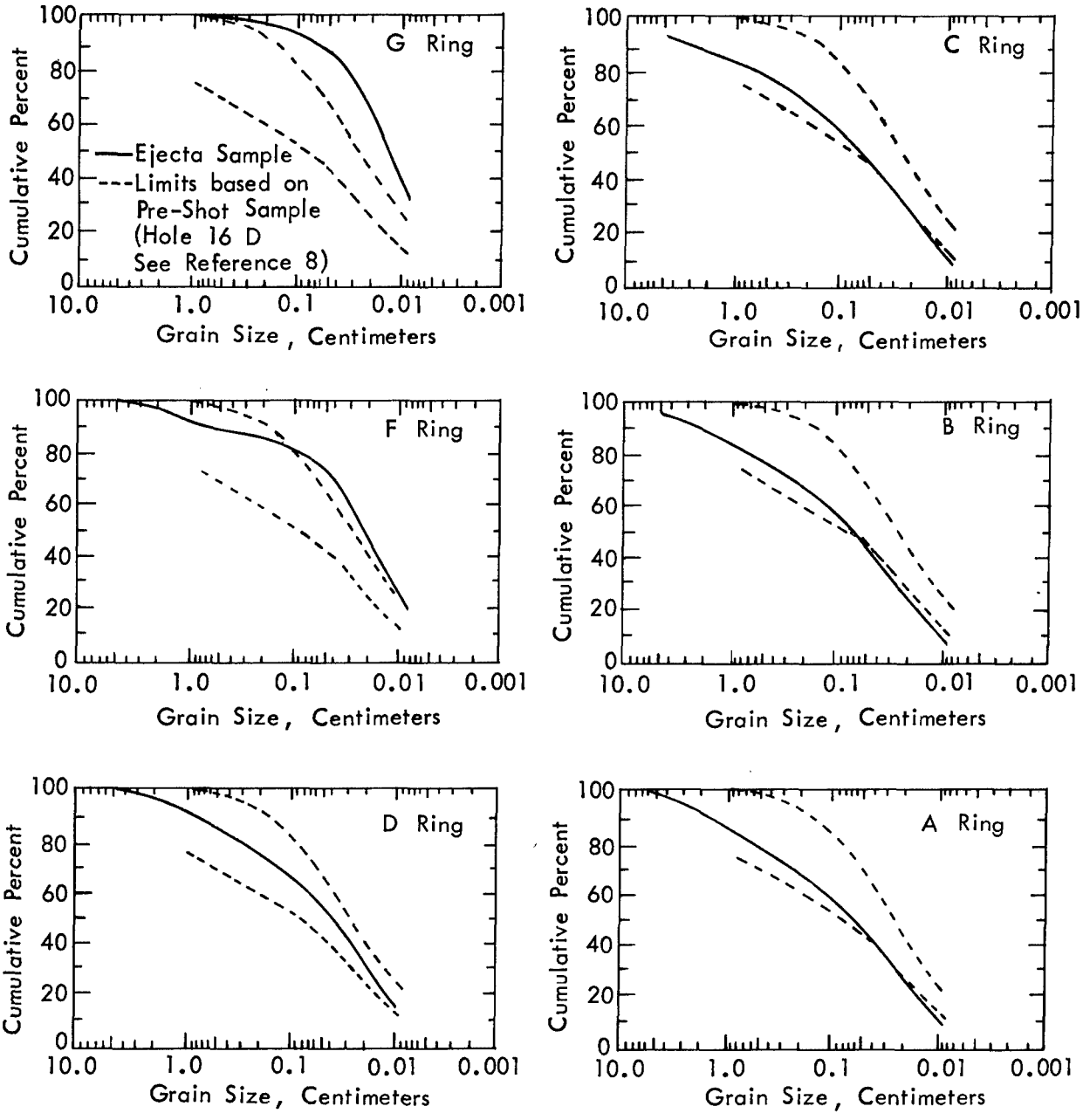

Figure 3.7 Grain size distribution curves for ejecta samples.

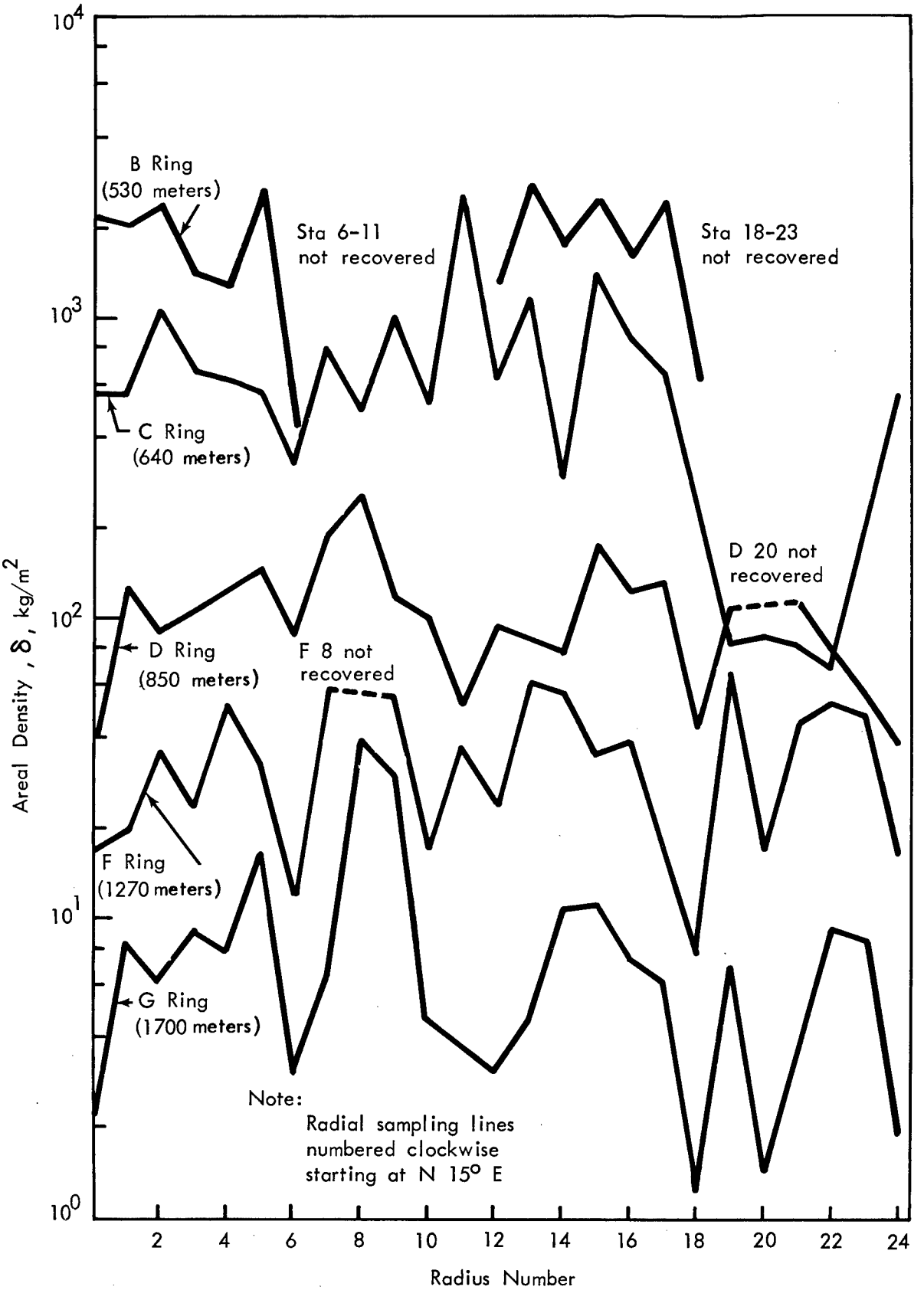

Figure 3.8 Circumferential variations of areal density.

sampling radii (missiles as used here refer to natural geologic material, either boulders or discrete ejecta masses, which are ballistically ejected from the crater). Resulting data are given in Table A.8. Missile locations are shown in Figure A.1.

3.2.2 Impact Craters. Numerous impact craters are located on the ground surface around the Sedan crater. Small craters having diameters on the order of a few feet were associated with missiles which were investigated in connection with the missile study described in Section 3.2.1. These small craters are located at ranges as great as 2,140 meters from ground zero. Numerous impact craters with lip-to-lip diameters of several tens of feet are located out to radial distances of almost 1,300 meters. Many of these impact craters are visible in the aerial photograph shown in Figure 3.9. A large impact crater with a lip-to-lip diameter of about 7.3 meters was observed along the F ring (1,280 meters) at a bearing of about N 70° W from ground zero. The largest impact crater visible on aerial photographs is located at a radial distance of about 300 meters at a bearing of S 80° W from ground zero. The distribution of the impact craters with a diameter greater than about 3 meters is shown in Figure 3.10.

Nine impact craters were excavated by bulldozer in an attempt to determine the nature of the missiles that formed the craters. A diagrammatic composite section of the impact craters that were excavated is shown in Figure 3.11. Most impact craters were caused by discrete masses of alluvium; however, there were a few documented cases where craters were caused by single boulders or other kinds

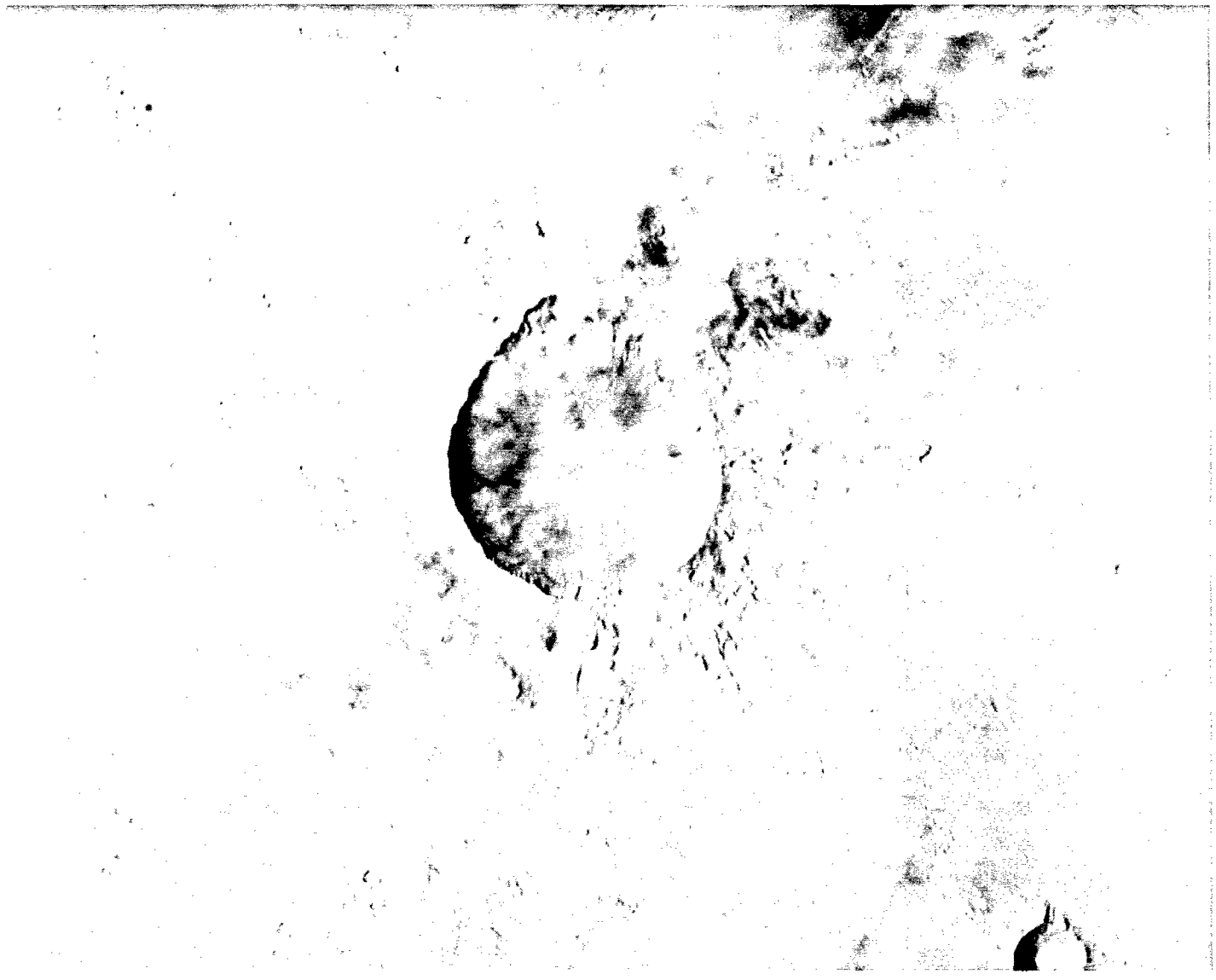

Figure 3.9 Aerial photograph showing impact craters.

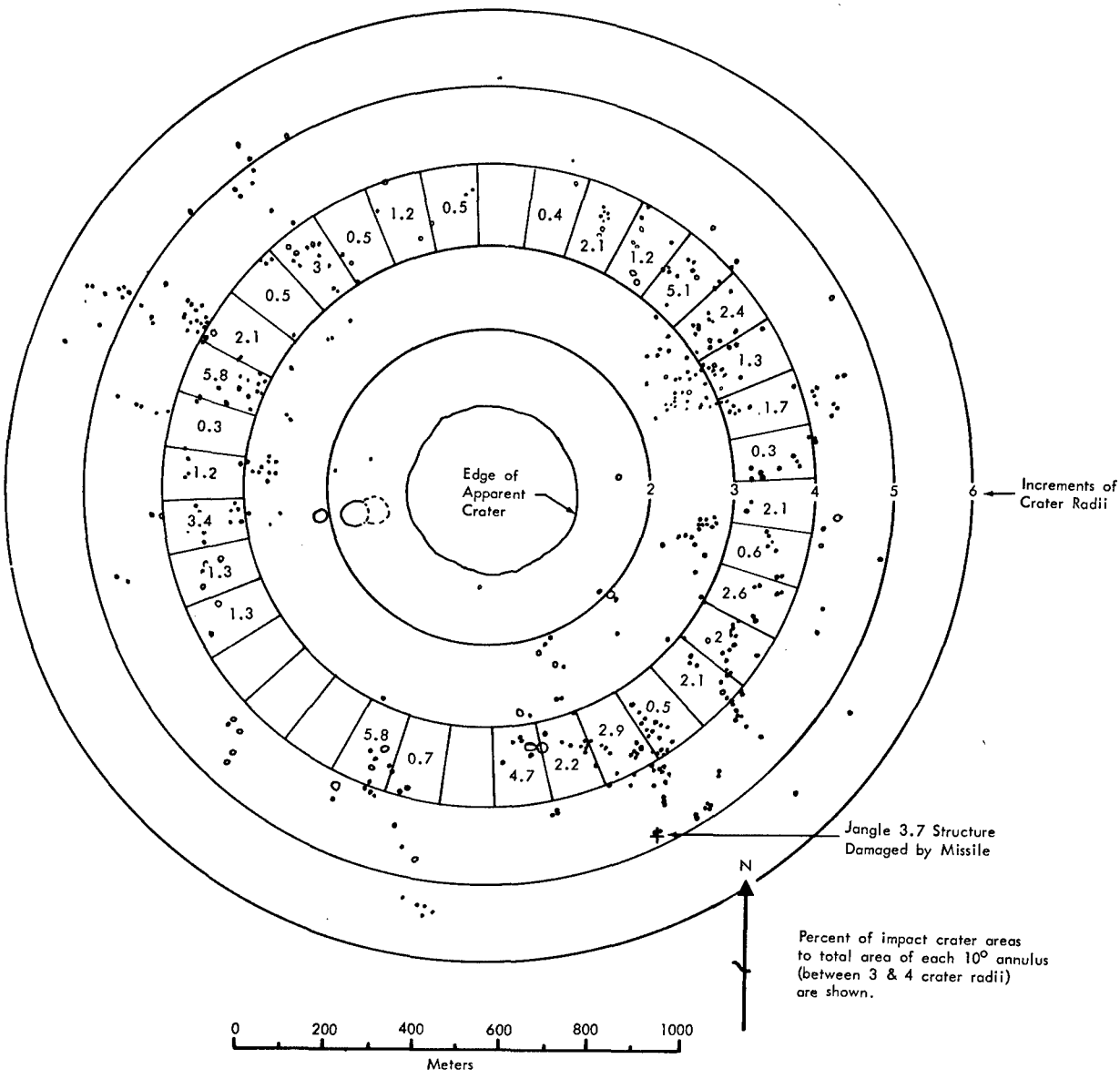

Figure 3.10 Distribution of large impact craters.

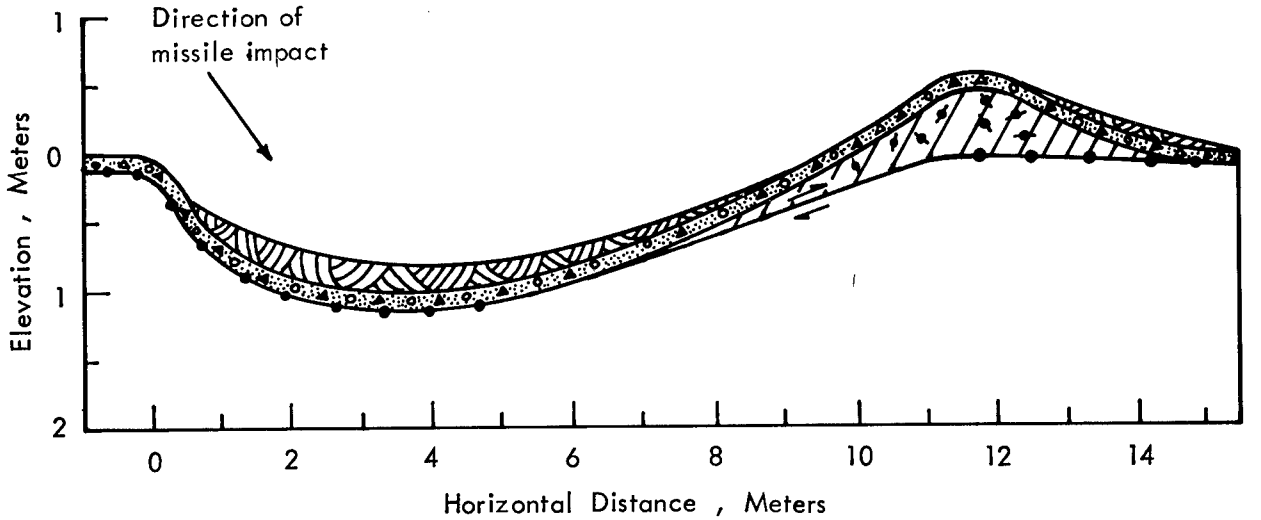

EXPLANATION

Original Ground Surface with traces of original vegetation and organic debris.

Shear plane where ricocheting missile has removed earth from impact area.

Post Ejecta
Aeolian deposit of fine to coarse sand and fused material.

Missile and Earth displaced from impact crater area. Contains some vegetation fragments.

Ejecta
Missile-type ejecta.

Original ground in place.

Figure 3.11 Diagrammatic section of impact crater.

of debris. A small crater (about two meters in diameter) located approximately at 26 meters S 35° W of Station C11 was formed by a melted and ablated portion of steel casing material with fused alluvial material adhering to it. Typical impact craters are illustrated in Figure 3.12.

Several impact craters contain central conical mounds of ejecta. The elevations of these central peaks is higher than the encircling lip crest. Hand excavation of one of these unusual craters revealed the central mound to be poorly sorted alluvial material, not stratified, but covered by a shallow layer of missile-type debris.

Excavation of impact craters revealed that the crater surface appeared to be covered by the missile ejecta layer noted at the ejecta collection stations, indicating that impact craters were formed prior to the deposition of the missile-type debris. Where both types of debris were present, the layer was relatively uniform along the crater floor where recognizable, indicating that bulk ejecta was deposited prior to the impacting missile.

Figure 3.11 shows an interpretive diagrammatic cross section of an impact crater and represents a composite of features detected in one or more of the impact craters. The missile forming the impact crater was apparently a large discrete mass of alluvium ejected as a ballistic unit. During impact, the earth compacted and bulged radially outward.

The outward bulge of soil was sheared off as it rose by the ricocheting mass of impacting alluvium. The outward high lip remaining after the crater

Impact crater 853 meters from ground zero. (Lip to lip diameter about 11 meters.)

Large impact crater on D ring (Note boulder in background which probably caused crater.)

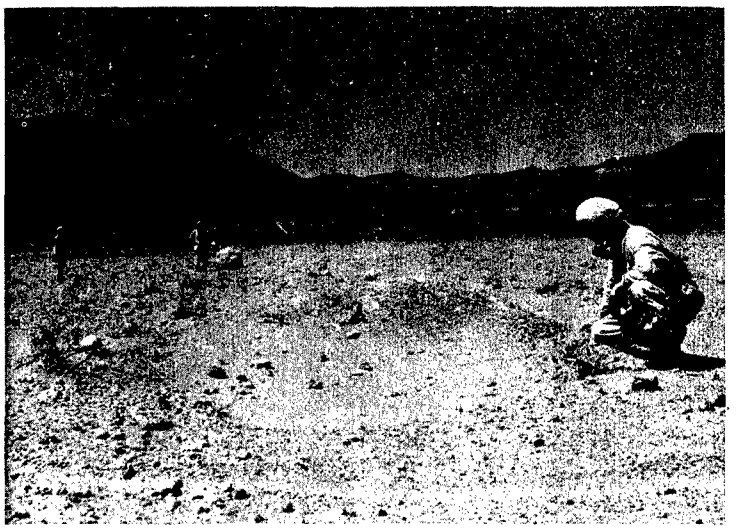

Large impact crater on F ring (Missile which caused crater is not evident.)

Figure 3.12 Impact craters.

formation appears to be a mixture of soil displaced from the impact crater and missile debris. Much of the displaced soil and missile debris was deposited radially outward from ground zero and beyond the impact crater.

3.2.3 Range of Ballistic Throwout. The edge of ballistically ejected debris occurs at or beyond 2,140 meters from ground zero, this being the radial distance observed for the outermost missile and its splash crater. This particular missile, an 11.3-kg (25-pound) boulder, was found along the bearing (S 60° E) coincident with a major ejecta concentration or ray extending outward from the crater.

3.3 LIP CREST AND GROUND SURFACE UPTHRUST

The original ground surface was identified at several locations along the inner edge of the Sedan crater. The elevation of this surface was determined by leveling (using a pocket transit) to known elevations on the crater rim. The location of the original ground surface before the shot was established by the pre-shot topographic map. The pre-shot and post-shot levels of the ground surface are shown in Figure 3.13, establishing an approximate value for the permanent uplift at the crater edge. The permanent uplift at the crater edge is about 3 meters (10 ± 1 feet).

Also shown in Figure 3.13 is the variation of the lip crest. These data were obtained using the topographic map of the Sedan crater made from aerial stereophotographs and locating points around the lip crest at major slope changes.

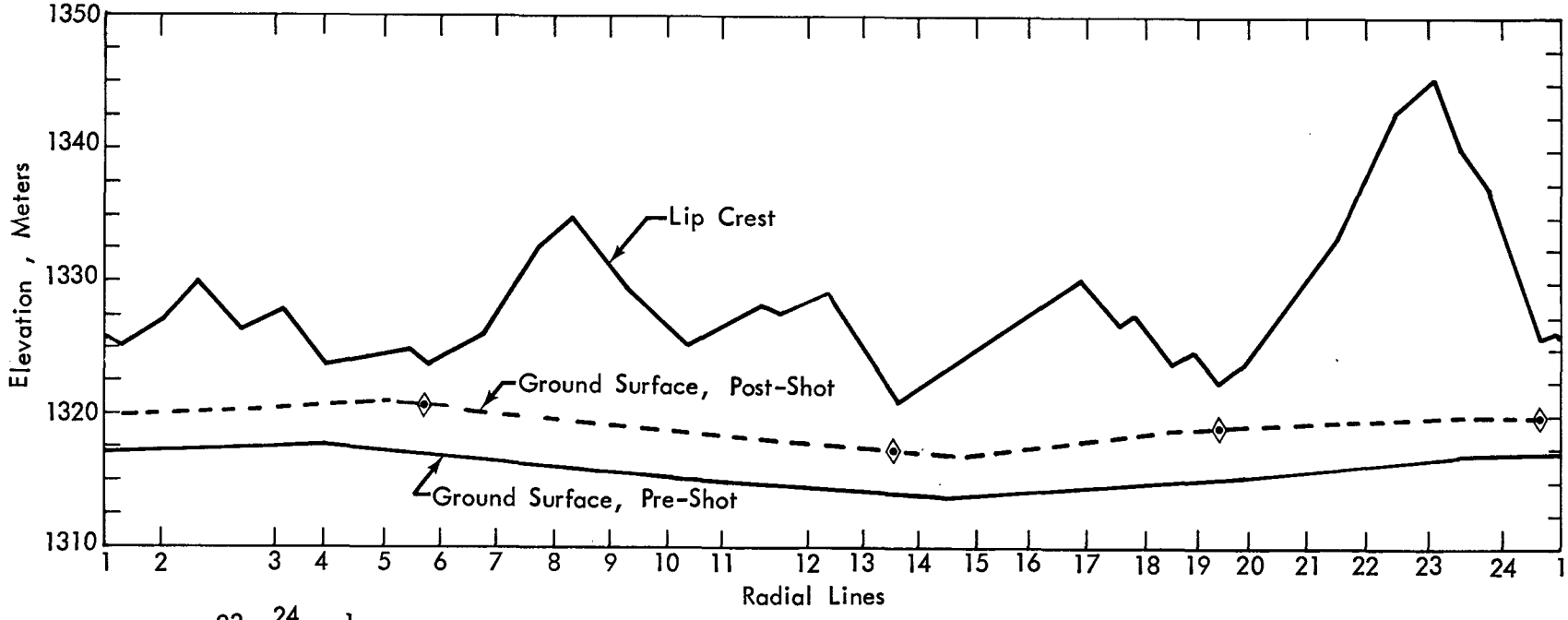

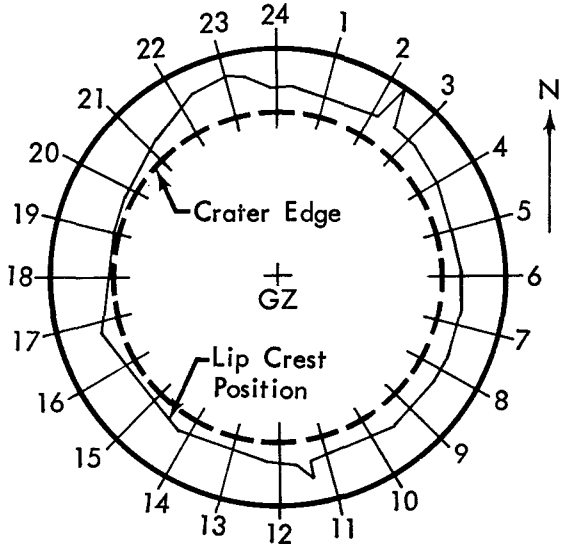

◈ Actual measurements to uplifted ground surface.

Figure 3.13 Sedan lip crest.

The average apparent lip crest height is 12.5 meters (41 feet) obtained by dividing the area under the lip crest graph shown in Figure 3.13 by the length of the circumference at the lip crest position. The average ejecta thickness at the lip crest was 10.2 meters (33.5 feet) determined in the same way.

3.4 MISCELLANEOUS OBSERVATIONS

3.4.1 Deposit of Fused Material. Fused alluvial material is evident in the ejecta beyond the crater. Large fragments of such material are discernible in the ejecta in varying quantities radially outward from the crater. The visible limits are sketched in Figure 3.5, and the abundance is indicated by a subjective scale, where sparse indicates one fragment 1 cm or larger in about 10 square meters, moderate indicates one fragment per square meter, and abundant indicates many fragments per square meter.

The fused material is generally light colored, light grey, green, pink, or brown, and is vesicular similar to pumice. The luster is generally dull, also similar to pumice. Very little vitreous, or glassy, material was observed.

3.4.2 Missile Structural Damage. A significant case of missile damage to a structure was documented. A missile struck the Jangle 3.7 idealized structure causing severe damage to its roof. This structure was located approximately 900 meters (3,000 feet) from ground zero. Photographs of the resulting damage are shown in Figure 3.14.

A small impact crater was located adjacent to the structure oriented

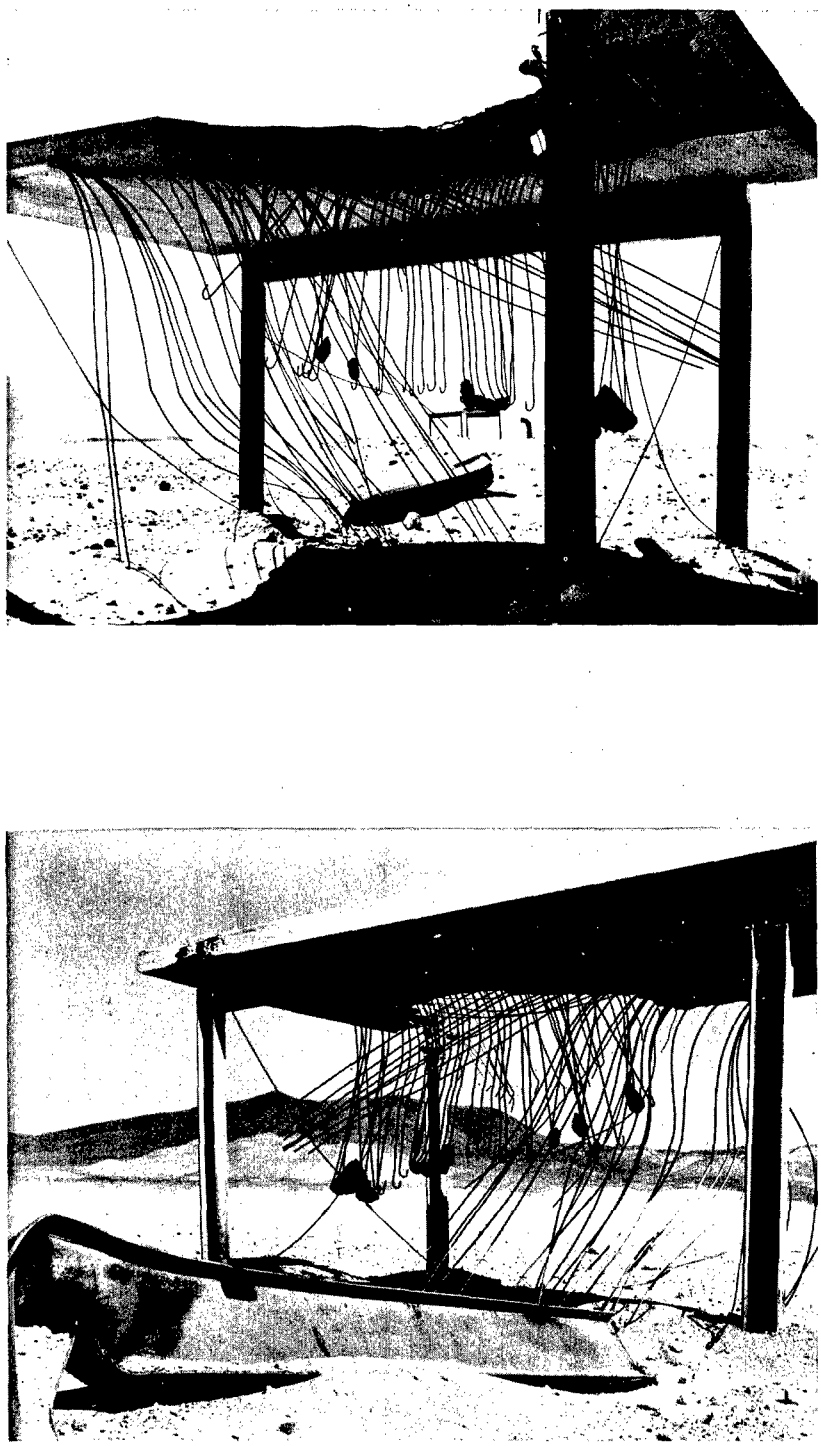

Figure 3.14 Missile damage to Jangle 3.7 structure.

toward ground zero. It probably was caused by part of the same missile which damaged the structure. No rock-like missile was located in the splash crater, but boulders, as well as poorly sorted alluvial material, were scattered on the ground beneath the structure. It is concluded that the structural damage was caused by a discrete mass of desert alluvium which remained intact throughout its flight, but disintegrated upon impact with the structure.

The Jangle 3,7 idealized structure had a roof slab thickness of 18 inches. The roof was designed as a two-way slab with tensile and compression reinforcement consisting of 7/8-inch round steel bars in one direction and 3/4-inch round steel bars in the other direction. All bars were spaced on 12-inch centers. The longitudinal beams supporting the roof slab were wide flange, 33 inches deep and 130 pounds per foot. (One of these beams was damaged and is shown in the lower photograph of Figure 3.14.) The four columns supporting the roof slab were wide flange, 18 inches deep and 114 pounds per foot.

3.4.3 Slumping of Crater Wall. Slumping has occurred around the edge of the crater and is particularly evident in the north quadrant of the crater. Many small slide blocks are evident below the high part of the crater. Slumping is evident just east of the high part of the lip and is visible in Figure 3.15. Some of the small slide blocks are also noted in Figure 3.15.

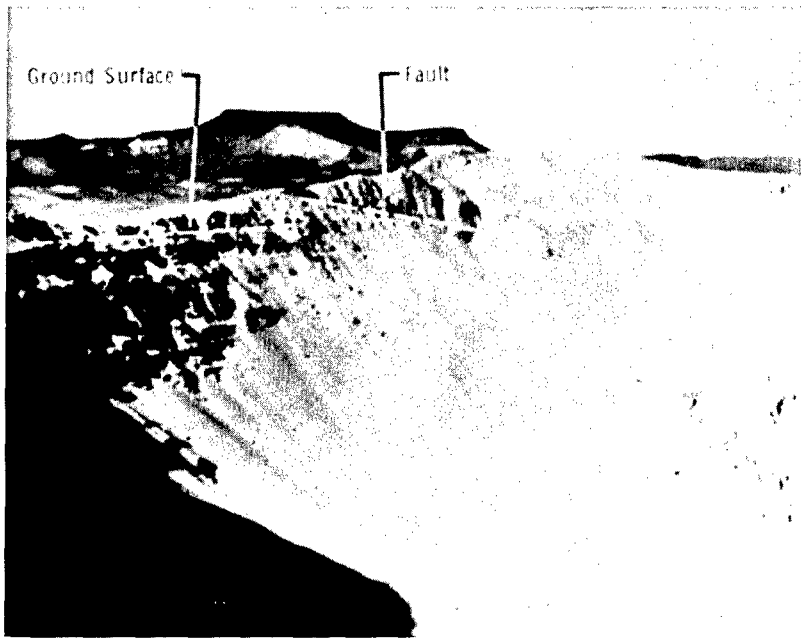

View of highest section of crater lip. (Note fault in debris and slide blocks below.)

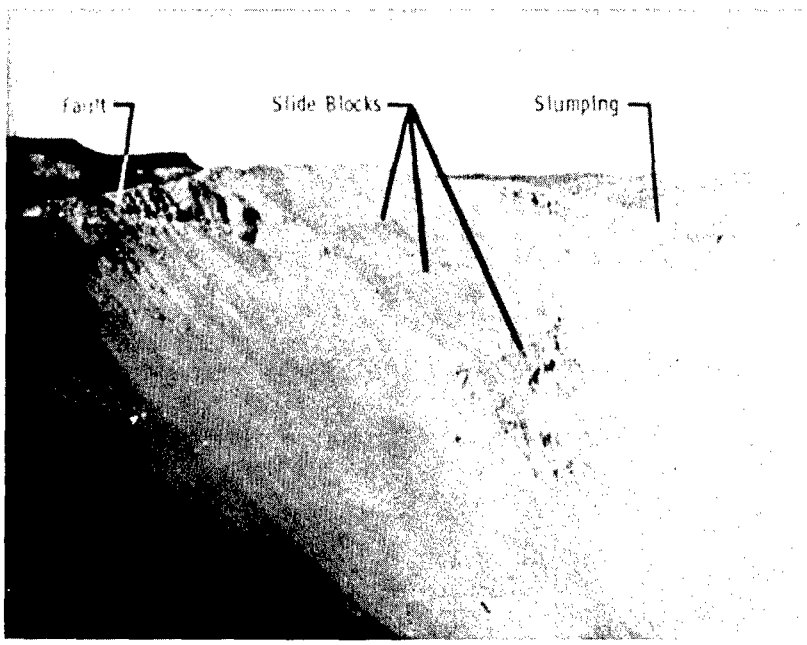

View of highest section of crater lip. (Note slumping in debris and slide blocks.)

Figure 3.15 North edge of Sedan crater.

CHAPTER 4

ANALYSIS AND INTERPRETATION

4.1 EJECTA MASS AND CRATER VOLUME

Sufficient data are available for the Sedan event to compute total ejecta mass by evaluating integrals of the form

$$M_p = 2\pi \int_{D_1}^{D_2} \delta(D)\, D\, dD$$

Where: M_p = that portion of the total ejecta mass falling within the radial distance D_1 to D_2

$\delta(D)$ = the experimentally derived areal density distance function

The experimental ejecta areal density data could not be mathematically fitted with a single function (of the type selected) with sufficient accuracy to be useable for summation of ejecta mass. It was necessary, therefore, to fit several functions to the data, each being applicable only to a specific radial range. The resulting areal density versus distance relationships are shown in Figure 4.1. The estimated thickness of ejecta at the lip crest, 10.2 meters, is included with the experimentally observed data shown in Figure 4.1. This data point was obtained from field observations made along the inner edge of the Sedan crater (see Section 3.3). Areal density relationships shown have been mathematically fitted by the method of least squares to the average of all observations made at a fixed radial distance. The actual relationships and

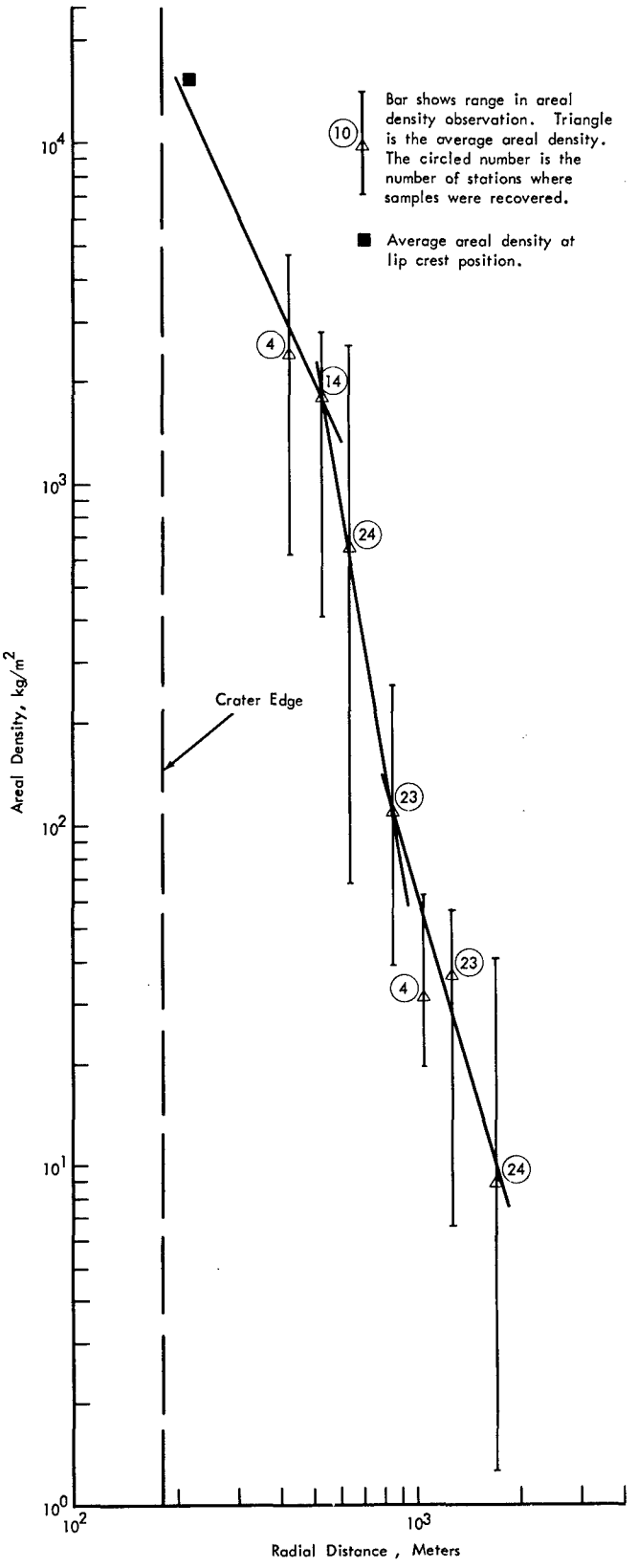

Figure 4.1 Areal density versus distance relationships used for computation of ejecta mass.

their applicable limits are shown in Table 4.1. Thus the total ejecta mass, M_e, is the sum of the incremental ejecta masses, M_p, or:

$$M_e = \sum_{p=1}^{n} M_p$$

The portion of ejecta mass calculated using the relationship fitted to the outermost experimental observations (840 meters to 1,710 meters) is actually computed to an outer limit of infinity. The total ejecta mass calculated between 220 meters (the lip crest position) and infinity is 4.22×10^9 kg.

Radiation fallout samples were collected by Lawrence Radiation Laboratory on D + 1, D + 3 and D + 11 (Reference 9). These data are sufficient to define areal density as a function of distance between 1.7 and 4 km. The mass calculated for fallout within this region is 6×10^7 kg.

The mass of material removed from the area by the wind-blown dust cloud can be calculated using cloud dimensions and an estimated value for its density. Visibility can be related to dust concentration within the cloud (Reference 10). Assuming that the visibility in the dust cloud was not less than 5 meters and not greater than 750 meters, and that the probable visibility was about 50 meters, the mass of material removed can be calculated. If the cloud contains only spherical dust particles approximately 2 microns in diameter and with a specific gravity of 2, the mass per particle is 6.4×10^{-11} grams. A cloud with a visibility of 5 meters contains about 10^5 particles per cm^3, with 750 meters visibility it contains about 500 particles per cm^3, and with 50 meters visibility

TABLE 4.1 AREAL DENSITY RELATIONSHIPS AND LIMITS

Areal Density	Limits	Sum of Residuals Squared*
kg/m^2	m	
$\delta = \frac{2.26 \times 10^9}{D^{2.24}}$	$220 \leq D \leq 550$	6.2×10^6
$\delta = \frac{3.38 \times 10^{19}}{D^{5.98}}$	$550 \leq D \leq 840$	4.4×10^3
$\delta = \frac{2.60 \times 10^{12}}{D^{3.53}}$	$840 \leq D \leq 1710$	5.6×10^2

* Sum of Residuals Squared $= \sum_{i=1}^{n} (K D_i^{-b} - \delta_i)^2$

where δ_i is the field areal density measurement at the D_i^{th} distance and K and b are the least squares coefficients.

it contains about 10^4 particles per cm^3. Using these values and assuming the cloud is hemispherical with a radius of 3.8 km (12,500 feet), the mass of material is less than 6×10^8 kg and more than 3×10^6 kg. If the visibility within the cloud is 50 meters, the fallout mass is about 6×10^7 kg.

There is some fallback material between the lip crest and the edge of the apparent crater. This quantity has been estimated using an 11 foot permanent displacement at the crater's edge and an outward dip of 4.5 degrees (see Figure 4.2). The mass of ejecta in this region, 183 to 210 meters, is calculated to be 1.9×10^8 kg.

The mass inferred from the apparent crater volume may be attributed to various components. Part of the crater void is caused by displacing the original ground surface upward and outward to form the true crater lip. The remaining portion of the crater void may be caused by compaction of the medium surrounding it and the ejection of vaporized material and ballistic debris. For mass computations, it has been assumed that the vaporized material for the Sedan event is included in the ejecta and long-range fallout quantities. The portion of the apparent crater volume caused by the permanent upward distortion of the original ground surface surrounding the crater is equal to the volume of the true lip. The portion of the crater volume resulting from the compression of the surrounding medium is the remainder after the ejecta and true lip mass quantities have been subtracted from the mass inferred from the apparent crater volume.

The apparent crater volume was calculated assuming a frustum of a

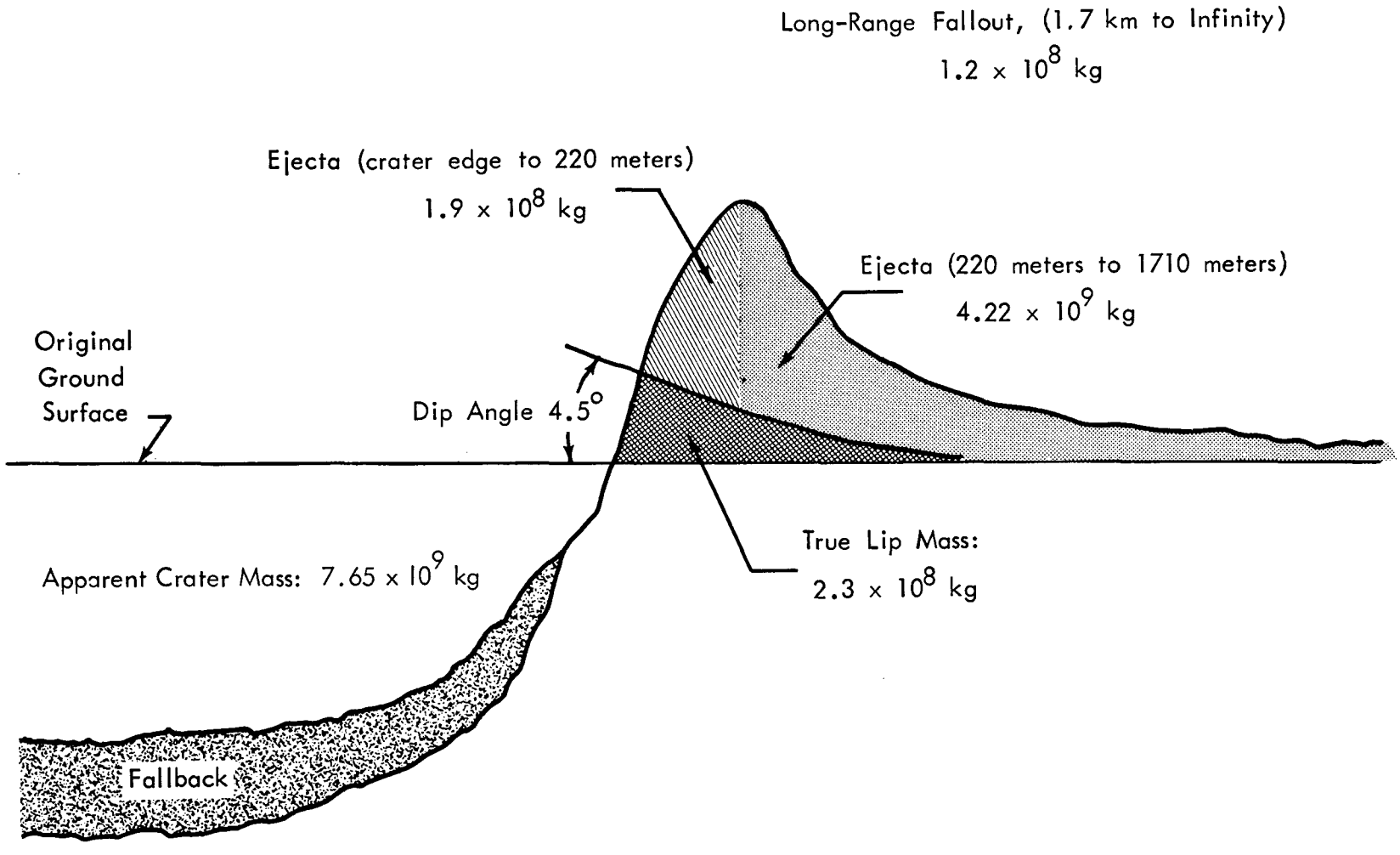

Figure 4.2 Sketch of Sedan crater lip showing mass quantities.

general cone for segments between each 25-foot contour line on the topographic map of the Sedan crater prepared from aerial photographs. The apparent volume calculated in this way is 5.1×10^6 m^3 (1.79×10^8 ft^3). Thus, the total displaced mass of the crater is calculated to be 7.65×10^9 kg.

The permanent uplift at the crater's edge was observed to be about 3.4 meters at two points along the west edge of the crater. Using 3.4 meters, a density of 1.5 gm/cm^3 and assuming that the uplift decreases uniformly outward to two crater radii, a maximum of 9.13×10^8 kg (2.15×10^7 ft^3) is calculated for the true lip. If the dip is assumed to be 6 degrees radially outward, a minimum mass of 9.36×10^7 kg (2.2×10^6 ft^3) is calculated for the true lip. The volume of the true crater lip was calculated by assuming a uniform uplift at the edge of the crater of 3.35 meters (11 feet), the maximum uplift observed, and a uniform average radial dip outward of 4.5 degrees. (That is, a constant circumferential true lip area as shown in Figure 4.2.) Thus, the true lip mass was calculated to be 2.3×10^8 kg.

Thus, the total ejecta, excluding the remote fallout, is 4.47×10^9 kg, the fallout is estimated to be between 3×10^6 kg and 6.8×10^8 kg and is probably about 6×10^7 kg. The total ejecta, then, is estimated to be about 4.53×10^9 kg (between 5.15 and 4.48×10^9 kg).

The total mass displaced as ejecta and true lip is estimated to be between 4.57 and 6.06×10^9 kg and is probably about 4.81×10^9 kg. Thus, the compression fraction of the apparent crater volume, assuming the areal density samples as

representative of the true averages at their respective distances, is between 21 percent and 40 percent with a more probable estimate of about 37 percent. It should be remembered in making mass computations such as those outlined above, that the ejecta data are least accurate within the region near the lip crest, the region wherein the largest quantity of ejecta is deposited. The mass computations do indicate, however, that a significant portion of the apparent crater volume results from compression of the surrounding medium. Mass quantities are summarized in Table 4.2.

4.2 RELATIVE EJECTA MASS DISTRIBUTION

The distribution of ejecta mass relative to the crater is shown in Figure 4.3. In this figure, the ratio M_i/M_e is plotted as the ordinate versus the ratio D/R as the abscissa, where M_i is the cumulative ejecta mass between the crater edge and any distance of interest, M_e is total ejecta mass, D is distance, and R is the radius of the apparent Sedan crater. This mass distribution curve was derived by integrating successive increments of the areal density versus distance curve shown in Figure 4.1. Figure 4.3 indicates that 50, 79, and 92 percent of the total Sedan ejecta mass was deposited between the crater edge and 2, 3, and 5 crater radii, respectively.

4.3 OTHER APPLICABLE CRATER EJECTA DATA

Although a planned ejecta experiment was not part of the Teapot ESS shot, there are certain data available that permit ejecta quantity versus distance

TABLE 4.2 COMPONENT MASSES OF CRATER AND LIP (SEDAN)

Component	Calculated Mass			Percentage of Apparent Crater Mass
	Maximum	Minimum	Estimated	
	kg	kg	kg	
Apparent Crater			7.65×10^9	--
True Lip	9.13×10^8	9.36×10^7	2.3×10^8	3
Ejecta (crater edge to 220 m)			1.9×10^8	3
Ejecta (220 m to 1710 m)			4.22×10^9	55
Fallout (1.7 to 4 km)			6.0×10^7	1
Fallout (beyond 4 km)	6.8×10^8	3×10^6	6.0×10^7	1
Compression	3.08×10^9	1.59×10^9	2.89×10^9	37

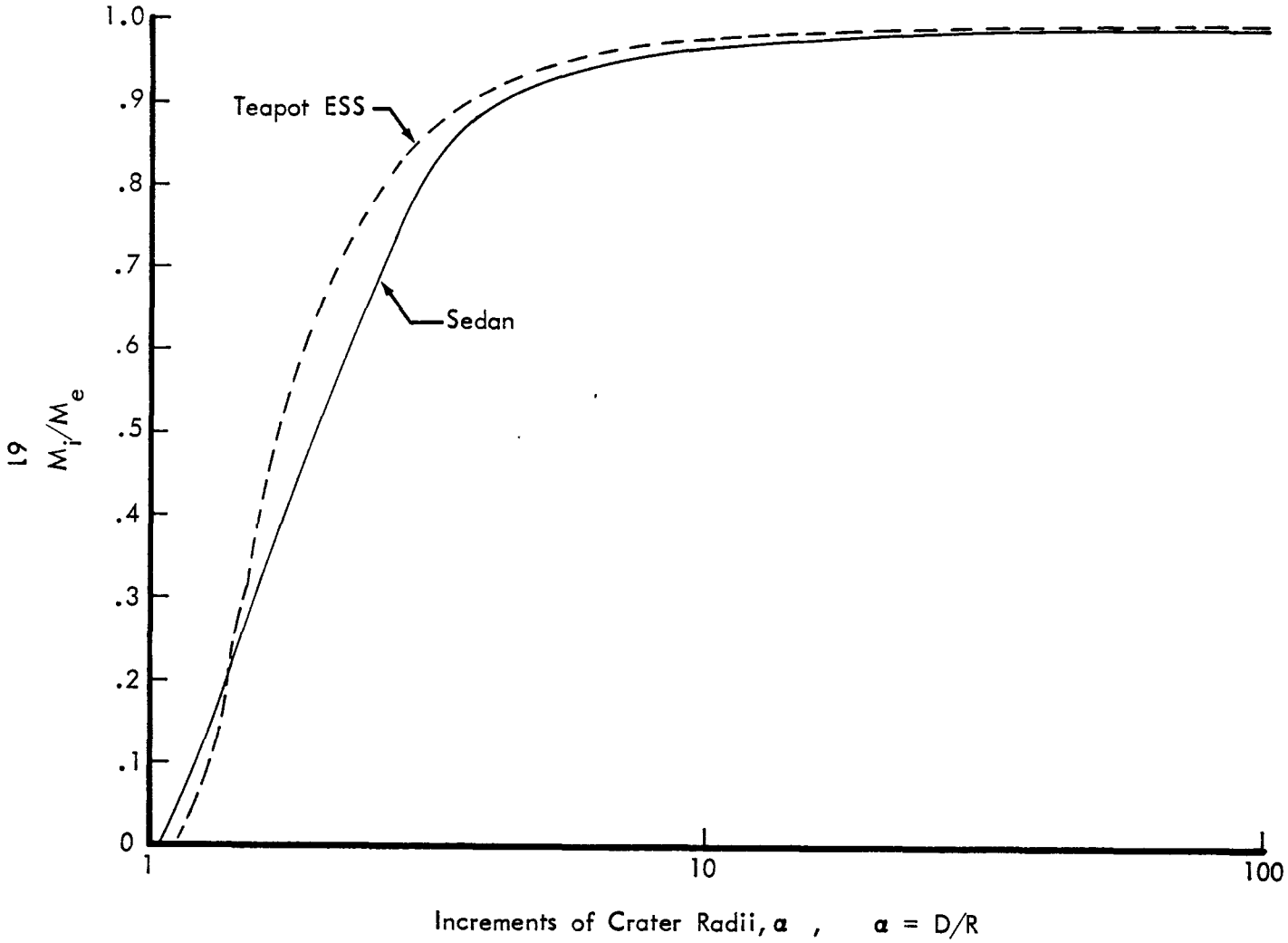

CALCULATED DATA POINTS

α	Sedan $\frac{M_i}{M_e}$	Teapot $\frac{M_i}{M_e}$
1.14	.0424	—
1.2	.0869	.0492
1.4	.2150	.2294
1.6	.3231	.4208
1.8	.4152	.5542
2.0	.4957	.6463
2.3	.6001	.7366
2.7	.7143	.8135
3.0	.7872	.8495
3.3	.8309	.8755
3.7	.8722	.8999
4.0	.8913	.9131
5.0	.9210	.9402
6.0	.9379	.9541
7.0	.9489	.9628
8.0	.9566	.9688
10.0	.9660	.9764
30.0	.9859	.9913
70.0	.9891	.9937
100.0	.9896	.9944

Figure 4.3 Ejecta mass distribution relative to the crater.

relationships to be developed. Teapot ESS was a 1.2-kt (1.1×10^6 kg) nuclear shot detonated 20.3 meters beneath the surface of desert alluvium on the Nevada Test Site. An extensive radioactive fallout experiment included circumferential stations commencing at a radial distance of about 270 meters from ground zero and extending to about 15,000 meters (Reference 11). Fallback quantities at close-in distances were obtained from topographical profiles of the crater lip and the permanent ground surface uplift data given in References 12 and 13, respectively. The resulting areal density versus distance relationships used for ejecta mass computations are shown in Figure 4.4. Also shown in this figure are the apparent and true lip profiles from which the close-in ejecta areal density determinations were made.

Component masses of the crater and lip computed for Teapot ESS using techniques such as those described for the Sedan crater are listed in Table 4.3. No attempt was made to compute the mass of the long-range fallout because it appeared to be a relatively small quantity for the Sedan crater. These mass quantities indicate that 32 percent or less of the apparent crater volume can be attributed to compression of the surrounding medium. Inasmuch as the Teapot ESS scaled burst depth was significantly less than for Sedan, the lesser relative portion of the crater volume attributed to compression seems reasonable (about 41 percent compression for Sedan); the Teapot ESS true lip represents a much greater portion of the apparent crater mass (18 percent for Teapot compared to 3 percent for Sedan). This is also consistent with observation: that is, greater

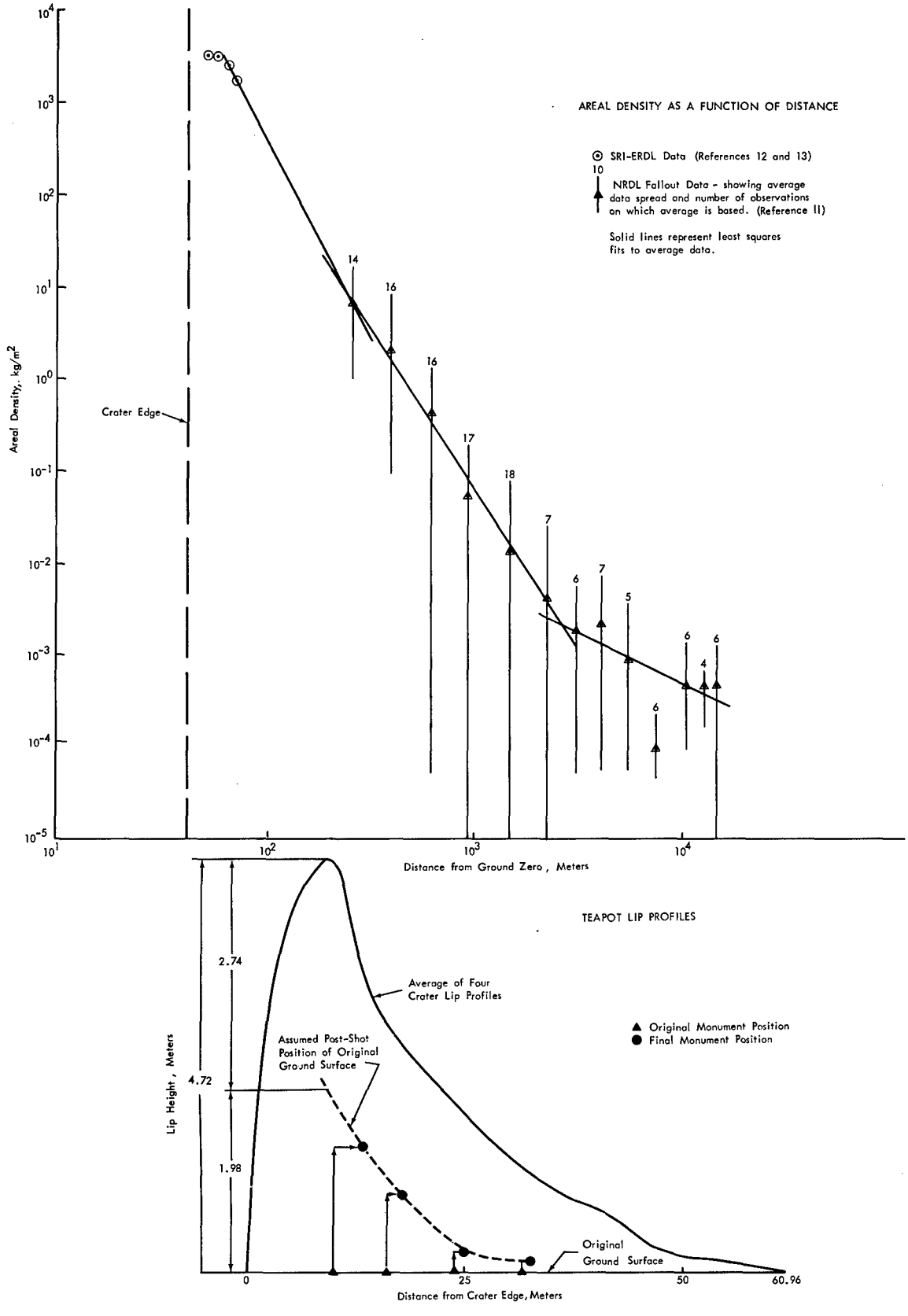

Figure 4.4 Ejecta areal density as a function of distance and lip profiles for the Teapot ESS crater.

Table 4.3 COMPONENT MASSES OF CRATER AND LIP (TEAPOT ESS)

Component	Calculated Mass	Percentage of Apparent Crater Mass
	kg	
Apparent Crater	1.18×10^8	--
True Lip	2.1×10^7	18
Ejecta (crater edge to 53 m)	8.1×10^6	7
Ejecta (53 m to infinity)	5.12×10^7	43
Compression (also includes long range fallout mass)	3.8×10^7	32

ground distortion occurs for craters resulting from shallow underground or surface detonations.

An ejecta mass distribution curve relative to the Teapot crater is shown in Figure 4.3. The ejecta mass lies relatively closer to the crater for Teapot than for Sedan. If both the Sedan and Teapot charges had been of equivalent energy release one would expect the ejecta mass from the more shallow burst (teapot) to lie relatively farther from the crater than that from the deeper burst (Sedan).

High explosive cratering events for which ejecta mass calculations can be made are the HE-2 shot, the 100-ton Suffield shot, and two of the Stagecoach shots. A summary of these cratering events is given in Table 4.4. Mass quantities for these high explosive craters and for the Sedan and Teapot ESS nuclear craters are given in Table 4.5.

Total ejecta mass versus apparent crater volume is plotted in Figure 4.5. The expression relating ejecta mass to apparent crater volume is:

$$M_e = 1.1 \times 10^3 V_c^{0.98}$$

Where: M_e = total ejecta mass in kg

V_c = the volume of the apparent crater in m^3

This relationship is only good for a desert alluvium medium.

4.4 PREDICTED EJECTA DISTRIBUTION

The Sedan crater was predicted to have a radius of about 213 meters (700 feet) (Reference 7). The predicted ejecta thickness as a function of radial distance was based on data correlations using this predicted radius. It was necessary

TABLE 4.4 SUMMARY OF HIGH EXPLOSIVE CRATERING EVENTS APPLICABLE TO THE STUDY OF EJECTA DISTRIBUTION

Shot	Energy Release		Burst Depth	Apparent Crater		Medium	Reference
				Radius	Depth		
	kg	tons	m	m	m		
Stagecoach 2	1.8×10^4	20	5.2	15.4	7.2	Desert alluvium	14
Stagecoach 3	1.8×10^4	20	10.4	17.8	8.6	Desert alluvium	14
Suffield	9.1×10^4	100	0	23.5	6.2	Silt and clay	4
HE-2	1.8×10^4	20	1.4	12.1	4.5	Desert alluvium	15

TABLE 4.5 MASS QUANTITIES FOR EJECTA AND CRATERS

Shot	Apparent Crater Volume, V_c	Apparent Crater Mass, M_c	Ejecta Mass, M_e	Ratio M_e/M_c
	m^3	kg	kg	
Sedan	5.07×10^6	7.65×10^9	4.41×10^9	0.58
Teapot ESS	7.36×10^4	1.18×10^8	5.12×10^7	0.43
HE-2	9.91×10^2	1.59×10^6	9.70×10^5	0.62
Suffield	3.55×10^3	5.85×10^6	3.98×10^6	0.68
Stagecoach 2*	2.37×10^3	3.79×10^6	3.30×10^6	0.87
Stagecoach 3*	4.11×10^3	6.57×10^6	4.80×10^6	0.73

* Ejecta mass quantities were obtained from Reference 14.

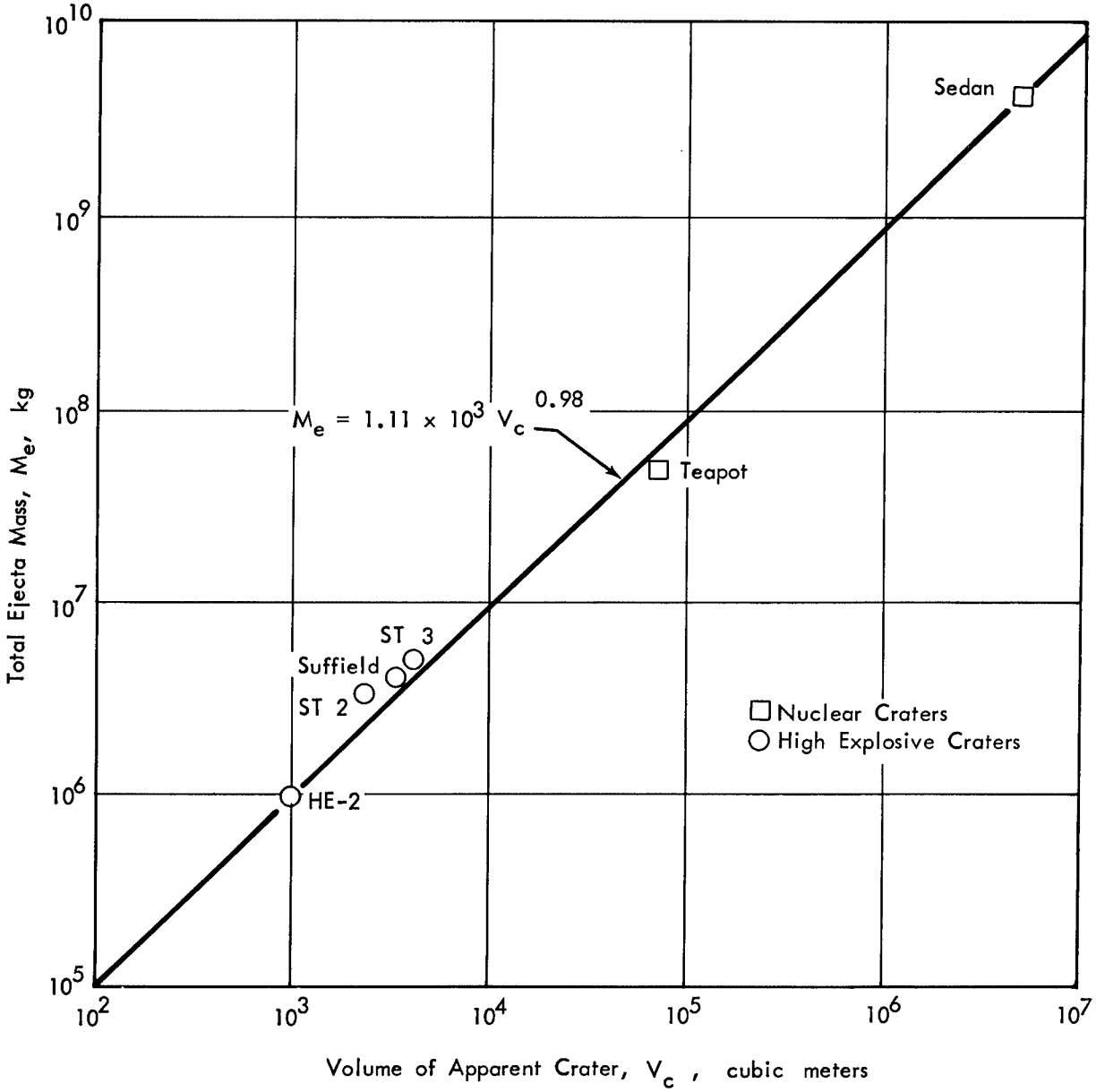

Figure 4.5 Ejecta mass versus apparent crater volume.

to make the following assumptions:

1. Ejecta thickness for a given crater can be approximated using a relationship of the form:

$$t = K\alpha^{-b}$$

where α is distance in increments of crater radii and K and b are constants determined by experimental data. A functional relationship of the above form was observed to fit ejecta data for several high explosive cratering experiments prior to Sedan (References 1, 2, 3 and 4).

2. The shape of the apparent lip profile is independent of explosive energy release within the region of interest.

3. The permanent deformation of the original ground surface is a constant portion of the lip crest height regardless of explosive energy release.

4. The thickness of fallback at the lip crest is equal to one half of the apparent lip crest height.

When apparent lip crest heights are correlated with apparent crater dimensions for high explosive craters, the variance of data was smallest for the relationship between lip crest height and apparent crater radius. This correlation is shown in Figure 4.6. These data are for dry sand, dry clay, desert alluvium, silt, and caliche at scaled depths between -0.02 and 0.4, less than optimum for crater volume. (The scaled depth is the actual depth in meters divided by the cube root of the charge weight in kilograms.) The charges were both spheres and hemispheres.

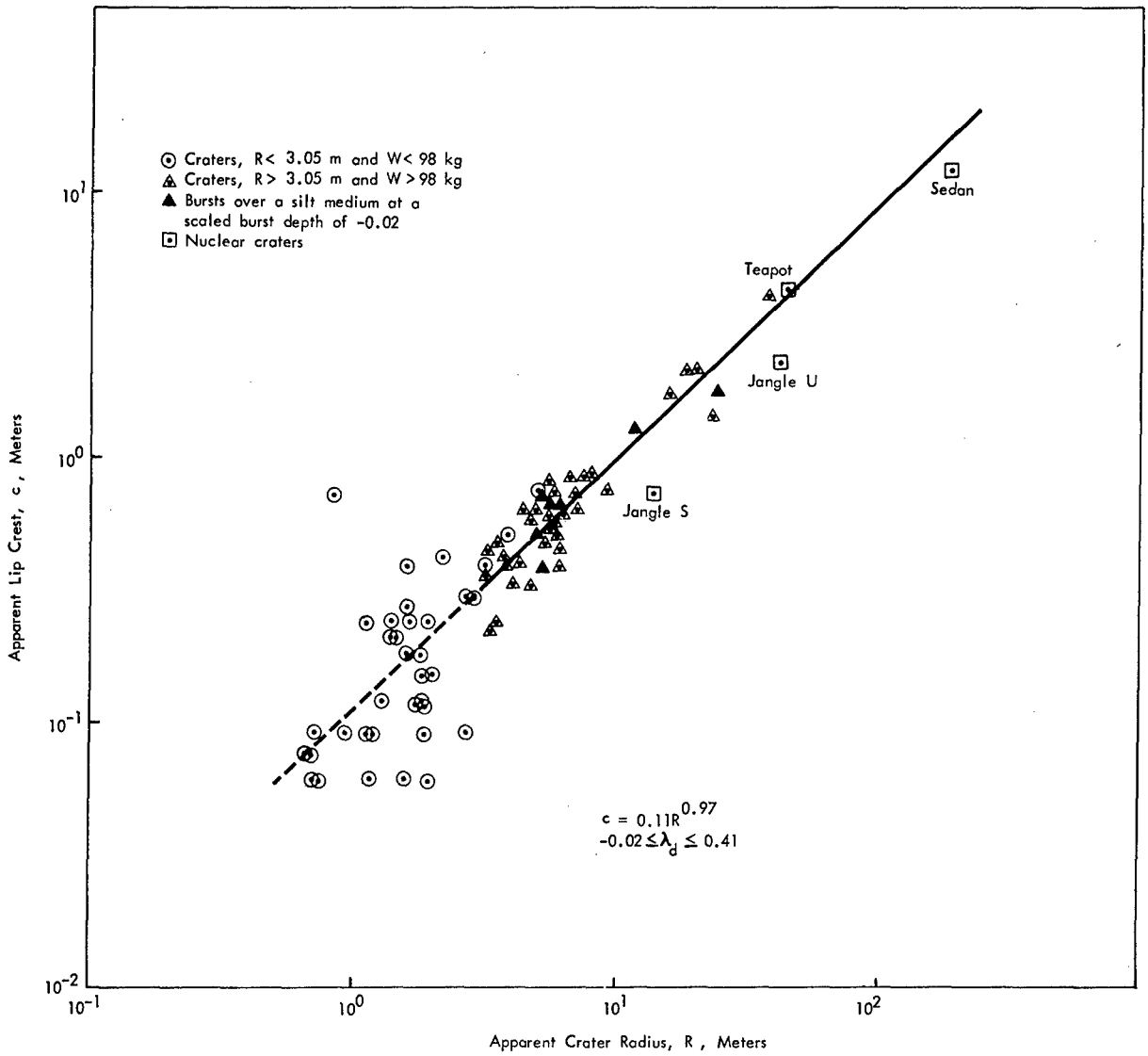

Figure 4.6 Lip crest height as a function of apparent crater radius.

Restricting the data to a single medium, charge type, or shape, at a single scaled burial depth provides only limited data for correlation and does not appear to reduce the variance greatly. This is illustrated in Figure 4.6 by the solid triangles for lip crest height and crater radius data for hemispherical charges fired at a scaled burst depth of -0.02 in silt at the Suffield Experimental Station, Ralston, Alberta, Canada. In short, the lip crest height appears to be a function of the crater size for craters formed at burst depths less than optimum regardless of the explosive energy release or medium.

The lip crest height versus radius relationship shown in Figure 4.6, determined mathematically, is

$$c = 0.11\ R^{0.97} \cong 0.1\ R$$

Where: c = the lip crest height

R = apparent crater radius

Observations of many craters indicate that the lip crest position occurs at about 1.2 apparent crater radii.

Before the above relationship can be used, the portion of the lip crest which is actually ejecta must be estimated. Ejecta made up about one-half the total lip crest height for the Teapot ESS crater (see Figure 4.4). Assuming that the fallback at the lip crest would be one-half the total (apparent) lip crest height for the Sedan crater, or 0.05 times its apparent crater radius, the constant in the selected thickness equation can be determined as follows:

$$t = K\alpha^{-b},$$

but $t = 0.05\ R$ at $\alpha = 1.2$, therefore:

$$K = 0.05\ R\ (1.2)^b$$

The exponent, b, in the region of interest was about 3.6 for the Suffield crater (Reference 4) and about 3.7 for the Teapot ESS crater. Inasmuch as the burst depth for Sedan was to be about optimum, it was felt that the decay exponent would be greater than for either the Teapot or the Suffield crater. (That is, a greater fraction of the total ejecta mass would be deposited closer to the crater.) Thus, b was chosen to be 4.0 and the following expression was used in making the pre-shot estimate of ejecta distribution for the Sedan crater:

$$t = 22\alpha^{-4}\ \text{(meters)}$$

Figure 4.7 shows the spread of actual ejecta observations made at each sampling range and a plot of the above expression. Also shown, for comparative purposes, are the mathematical fit to mean data and the multiple fits made to the mean data for the purpose of total ejecta mass determinations.

4.5 MISSILE TRAJECTORIES

Natural missiles originating in the Sedan crater region were located within predetermined sectors along each of the primary radial sampling lines. A map of the distribution of recovered missiles is shown in Figure A.1. Missile weights and approximate size of the associated impact craters are listed in Table A.8.

The original position of these missiles within the crater region is not known. The Sedan crater geometry indicates that throwout exit angles must have

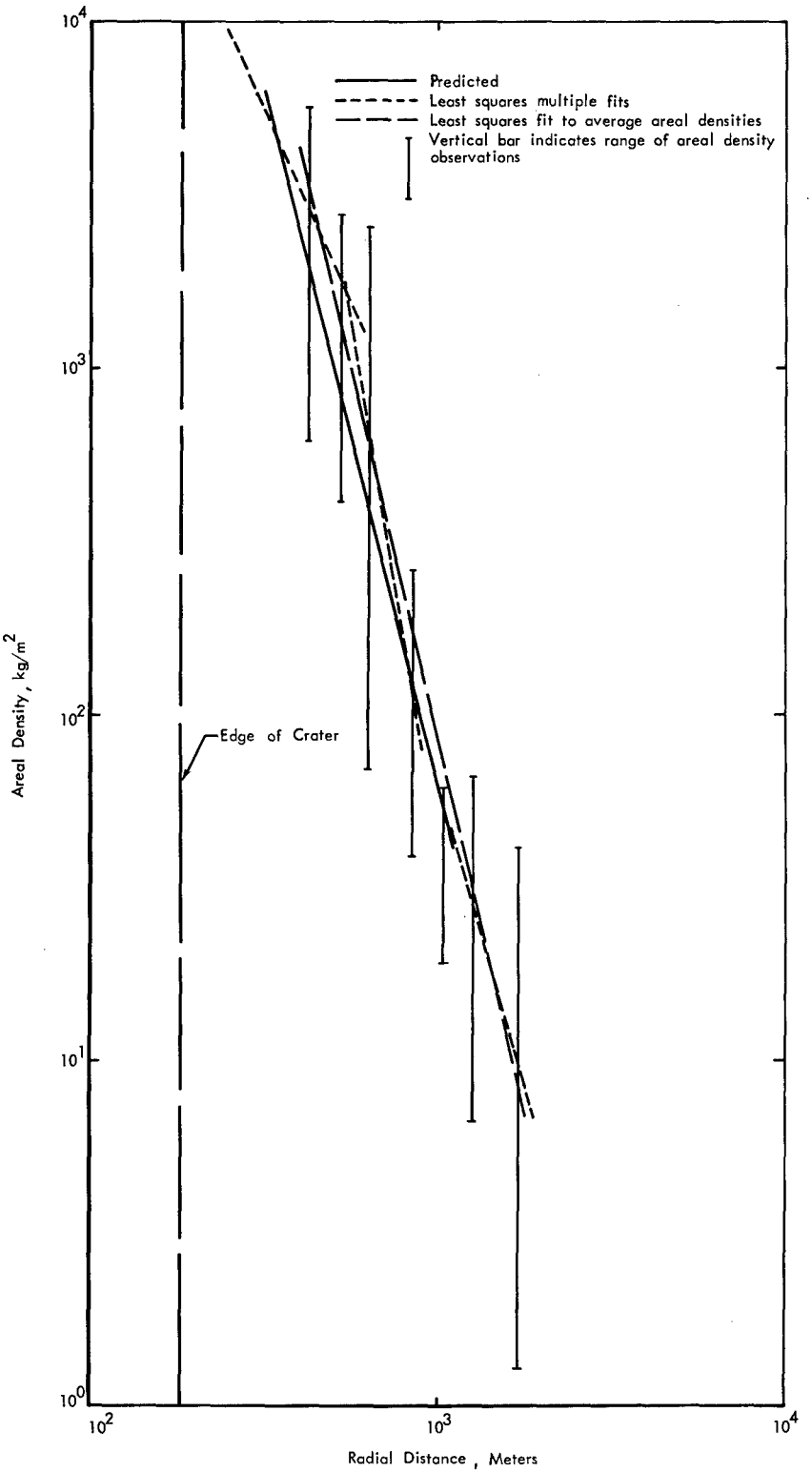

Figure 4.7 Predicted and measured ejecta areal density.

been between 85 degrees and 50 degrees. The results of prior missile experiments indicate that the exit angle is probably the angle of the slant radius (between the missile and the charge) to the horizontal. Employing the classical ballistic formula:

$$R = \frac{v^2 \sin 2\theta}{g}$$

Where: R = missile range

v = missile exit velocity

θ = exit angle

g = gravitational acceleration

and neglecting atmospheric drag, a minimum velocity range can be computed for the missiles listed in Table A.8. The results of this computation are given in Table 4.6.

Shoemaker (Reference 16) in making throwout computations for an impacting bolide, derived the following relationship for particle velocity:

$$\mu = \left[\frac{3E}{4\pi\rho r^3}\right]^{1/2}$$

Where: μ = particle velocity

E = total shock energy

ρ = medium density

r = slant radius from shock origin to the surface

If it is assumed that missiles will leave the surface at velocities close to the particle velocity then for the above expression surface missile exit velocities would be about 94 and 65 meters per second for exit angles of 85 and 50 degrees, respectively.

TABLE 4.6 RANGE OF MINIMUM MISSILE VELOCITIES

Missile	Weight	Range	Range of Velocities for Exit Angles from 50 degrees to 85 degrees		
	kg	m	m/sec		m/sec
1*	17.7	2,060	143	to	341
	1.87				
2	1.53	2,060	143	to	341
	10.7				
	7.03				
	8.16				
	1.31				
3	13.4	2,030	142	to	339
	21.4				
4	15.1	2,030	142	to	339
5	0.14	1,950	139	to	332
	5.05				
	12.4				
	7.80				
6	136 est.	1,800	134	to	319
7	6.49	1,780	133	to	317
8	18.1	1,770	132	to	316
9	10.3	1,770	132	to	316
10	11.3	1,770	132	to	316
11	13.7	1,770	132	to	316
12	136 est.	1,640	128	to	304
13	(3 small splash craters. No missiles. Pile of poorly sorted rubble in one splash crater.)	1,540	124	to	294
14	91 est.	1,560	125	to	297
15	4.82	1,510	122	to	292
16	19.3	1,520	123	to	293
17	4.45	1,660	128	to	306
18	10.6	1,770	132	to	316
19	10.5	1,780	133	to	317
20	7.03	1,520	123	to	293
21	7.20	1,580	126	to	299
22	7.34	1,610	127	to	302
23	21.7	1,420	119	to	283
	41.7				
	9.10				
	12.4				
	9 est.				

TABLE 4.6 RANGE OF MINIMUM MISSILE VELOCITIES (CONTINUED)

Missile	Weight	Range	Range of Velocities for Exit Angles from 50 degrees to 85 degrees		
	kg	m	m/sec		m/sec
24	3.03	1,510	122	to	292
25	8.87	1,510	122	to	292
26	4.56	1,510	122	to	292
27		1,540	124	to	295
28	19.5	1,540	124	to	295
29	7.77	1,720	131	to	312
30	27.1	1,720	131	to	312
31	7.97	1,860	136	to	324
	10.9				
	4.42				
32	11.9	1,840	135	to	322
	9.79				
	4.25				
33	9.07	1,710	130	to	310
34	No missiles.	1,300	114	to	270
	2 splash craters.				
35	10.7	2,130	146	to	347
	Most remote missile.				

* Number refers to missile number on Figure A.1.

(The assumption that missiles are ejected at the exit angle, θ, and at an exit velocity equal to the particle velocity simply means that the kinetic energy imparted by the rarefaction wave reflected from the ground surface is minor.) These velocities are comparable to velocities calculated using the classical ballistic formula for close-in ranges (200 to 400 meters). It is within ranges of this order of magnitude that the major portion of crater ejecta is deposited.

4.6 EJECTA MASS AS A FUNCTION OF EXPLOSIVE YIELD

Observations on the scaling of crater dimensions and on the experimentally developed relationship between ejecta areal density and distance can be used to determine a scaling law for ejecta mass.

The apparent crater volume, V_c, can be correlated with explosive energy release by the general expression:

$$V_c = K_1 \ W^m \tag{1}$$

Where: W = yield

m = 1.0 if cube root scaling is assumed

Total ejecta mass, M_e, can be related to apparent crater volume by a similar general expression

$$M_e = K_2 \ V_c^n \tag{2}$$

where n would be close to 1.0. Combining Equations 1 and 2

$$M_e = K_2 K_1^n \ W^{mn} \tag{3}$$

Total ejecta mass, M_e, can also be calculated by evaluating the following integral:

$$M_e = 2\pi \int_{D_o}^{\infty} \delta(D)\, D\, dD \tag{4}$$

Where: D_o = approximately 1.2 crater radii

$\delta(D)$ = the experimentally determined relationship between ejecta areal density and distance, D

Existing crater ejecta experimental data can usually be described with an areal density relationship of the following form

$$\overline{\delta}(\alpha) = K_3 \alpha^{-b} \qquad 1.2 \leq \alpha < \infty, \; b > 2 \tag{5}$$

where α is actual distance D, divided by the apparent crater radius R, or $\alpha = D/R$. It seems reasonable to assume that K_3 is some function of explosive energy release. Therefore:

$$\delta(D) = \frac{R^b f(W)}{D^b} \qquad 1.2R \leq D < \infty \tag{6}$$

Substituting Equation 6 into Equation 4 and evaluating between the limits of 1.2R to ∞, the following expression results:

$$M_e = \frac{2\pi R^2 f(W)}{(b-2)(1.2)^{b-2}} \tag{7}$$

Substituting Equation 3 and rearranging terms:

$$\frac{R^2 f(W)}{W^{mn}} = \frac{K_2 K_1^n (b-2)(1.2)^{b-2}}{2\pi} \tag{8}$$

but $R = K_4 W^a$.

Therefore Equation 8 becomes:

$$\frac{W^{2a} f(W)}{W^{mn}} = \frac{K_2 K_1^n (b-2)(1.2)^{b-2}}{2\pi K_4^2} \tag{9}$$

The right hand term of Equation 9 is a constant if b is a constant. Assuming that b is a constant is probably valid for bursts at the same scaled depth in the same kind of geologic medium over a limited radial region, say between 1.2 and 5 crater radii. Making this assumption:

$$\frac{W^{2a} f(W)}{W^{nm}} = K_5 \tag{10}$$

and

$$f(W) = K_5 W^{nm-2a} \tag{11}$$

Substituting in Equation 5

$$\bar{\delta}(\alpha) = \frac{K_4 W^{nm-2a}}{\alpha^b} \tag{12}$$

This means that if cube root scaling is valid for crater radius and crater depth, the quantity mn is about 1.0 and a is 0.33. Thus,

$$\bar{\delta}(\alpha) \propto W^{0.33}.$$

If cube root scaling holds for crater radius and quarter root for crater depth, the quantity mn is about 0.92 and:

$$\delta(\alpha) \propto W^{0.25}$$

Unfortunately, applicable ejecta data are not available whereby the above dependence on explosive energy can be verified.

CHAPTER 5

DISCUSSION

5.1 RECOVERY

Sample recovery was delayed until D + 23 because of the high radiation levels at the ejecta stations. During the delay and during the recovery, sporadic winds, common to the desert, generally blowing from a southerly direction, continually eroded the upper layer of ejecta, removing much of the fines from the region sampled. A light rain on D + 21 temporarily halted the aeolian transport of the finely divided material.

Recovery commenced on D + 23 at the G ring and continued inward until all of the D samples and the four primary C samples had been collected. At this time the quarterly allowable radiation dose had been reached for recovery personnel. Further recovery began again on D day plus 6 months (15 January, 1963) and continued inward, until all C stations, 14 B stations and four A stations had been visited and either excavated by hand or bulldozer. At each station actual ejecta thickness measurements were made or areal densities were determined using the thin wall samples.

The tray at F8 could not be found. This station was located in a region of heavy ejecta concentration; that is, under a ray extending about S 60° E from the crater. Investigation of the F8 area indicated that the ejected material was entirely eroded from ridges on the pre-shot ground surface. Drifted dust concentrations were as much as 15 cm deep in depressions in the pre-shot ground

surface; however, the average ejecta depth for this area was about 5 cm.

The tarp at Station D20 could not be located. Re-survey of this station established its location under the lip crest of a large splash crater. Probing in this region indicated that ejecta at this station was 100 to 150 cm in depth. The tarp at D7 also was not located; however, several samples were obtained using the thin-wall sampler.

Many of the tarps were not located on the inner stations (C, B, and A). Those tarps found are noted in Table A.4.

5.2 AEOLIAN EROSION

The amount of material removed by the wind is thought to be relatively unimportant for the inner region of the sampled area; however, at the distant stations, much of the total deposit was finely divided material deposited by the base surge.

There was considerable difference in the outer samples between the areal densities collected in the recessed trays and those collected along the primary radial arrays where tarps were mounted flush with the surface of the ground. Examination of Figure 3.8 indicates that the paucity of ejecta deposited along the four primary radials is a depositional deficiency rather than differences in erosional degradation. All stations inside the F ring were tarps.

Data on fallout collected on D + 1 were obtained from Lawrence Radiation Laboratory (Reference 9). Most of the fallout samples were collected beyond

the outermost ejecta sampling stations. At the G ring, the value of areal density calculated from the mass throwout study was approximately 1 1/2 times larger than the value calculated using the least squares fit to the fallout data. This would seem to indicate accretion by the trays rather than depletion; however, the slope of the exponential decay curve, areal density to radial distance, changes with radial distance and these values are influenced by the data both inside and outside the G ring. The net effect of the predominantly southerly winds should be one of depletion of the fine near-surface material in the layer of ejecta.

There is no consistent difference in the grain size distribution between samples collected on the tarps and samples collected on the trays. Differences between individual samples appear to be related to the pattern of missile type ejecta rather than to wind action. No correction factor for aeolian erosion can be computed on the basis of the sorting of samples collected by the flat tarps and recessed trays.

Aeolian transport is evident in and beyond the region sampled. Windblown material, predominantly sand, silt, and fine-grained detrital pumice-like fused material is concentrated north of small hummocks and bushes and in the bottoms of the impact craters. (Prevailing winds are from the south.)

5.3 CIRCUMFERENTIAL VARIATION

The circumferential variation observed for the B, C, D, F, and G sampling rings is shown in Figure 3.8. At these radial distances, (2.9, 3.5, 4.7, 7.0, and 9.3 crater radii) the ratios of the highest to the lowest observed areal density were

6.7, 37, 7, 10, and 32, respectively. This ratio was approximately 9.4 at the lip crest position. The ratio of 6.7 for the B ring represents circumferential sampling only within the northeast and southwest quadrants. The frequency distribution of areal density observations for the C, D, F, and G rings is shown in Figure 5.1.

The increase in variability at the 3.5 crater radii distance appears to be anomalous; however, in the northwest quadrant, radially outward from the high part of the crater lip, the lower characteristic ejecta layer (bulk ejecta) was missing and this circumference actually intersects the outer edge of the missile-like ejecta deposit.

There is a change in the character of the ballistic deposits radially outward. Poorly sorted material, relatively unaffected by atmospheric winnowing, is deposited to some distance beyond the crater. The ejected material (bulk ejecta) is apparently transported in mass. Beyond the edge of this blanket, the throwout material occurs principally as missiles sorted by the atmosphere. The fine material is semi-suspended and is sorted by the viscosity of the atmosphere, to be deposited later from the base surge cloud as long-range fallout.

Rays are represented by both bulk ejecta debris and the missile-type debris. The large ray occuring at the D, F, and G rings S 60° E from Sedan is marked by a relatively shallow debris depth at the C ring. The B stations were not sampled in this quadrant; however, the debris appears to be relatively shallow here also. The light deposit at the C ring in the northwest quadrant occurs inside two small rays along radii extending N 75° W and N 30° W from Sedan. In this quadrant,

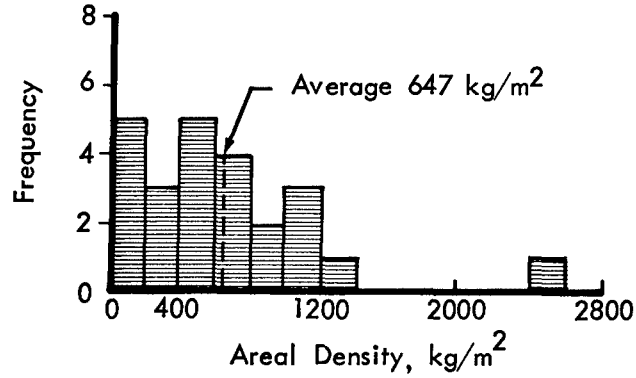

C Ring (640 meters)

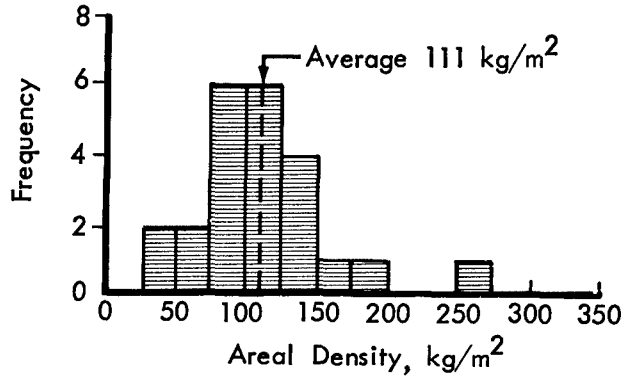

D Ring (850 meters)

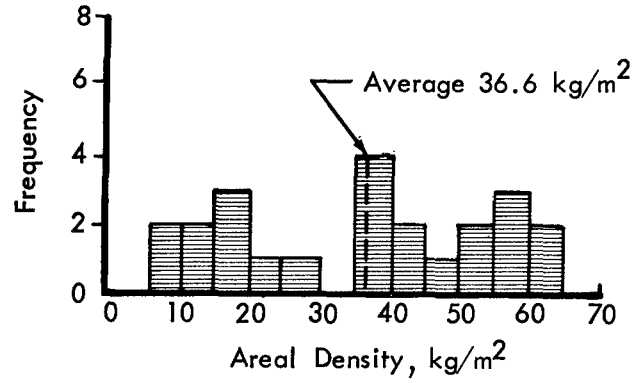

F Ring (1270 meters)

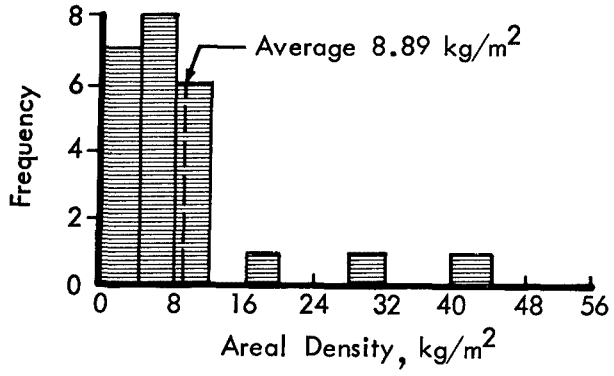

G Ring (1700 meters)

Figure 5.1 Frequency distribution of areal density observations.

the bulk ejected debris was not ejected over as large an area as in the other quadrants. This resulted in the high part of the lip occurring along the northwest edge of the crater.

The light deposits along the outer north, south, and west radii occur beyond high portions in the Sedan crater lip. The lowest portion of the lip occurs approximately east of Sedan ground zero, and ejecta deposits are consistently light along the east radius. This could possibly be related to the venting pattern of the gases from the cavity formed by the Sedan detonation which would impart tangential velocity components to the alluvium being ejected eastward. The tangential character of certain rays may be related to this tangential velocity component caused by high pressure gases injected into fissures forming in the alluvium as the earth mass swells and cracks from tension along inherently weak zones in the ejected mass.

Rays formed of bulk ejecta appear to be more or less continuous with rays formed of missile-type ejecta and may, therefore, represent regions between venting fissures as the crater formed.

The circumferential variation in the ejecta areal density is the measured expression of the ray systems visible in aerial photographs of explosion-formed craters. These rays, characterized by relatively large amounts of ejecta visibly concentrated in longitudinal mounds, are generally oriented radially. The ray system for Sedan is not clearly defined in the aerial photographs since aeolian dust deposited from the base surge extends to approximately twice the radial extent

of the ballistic debris. This base surge deposit was generally thick enough to color the region and obscure the rays which are generally marked by the lighter colored fragmented ejecta. Isolated mounds of ejecta a meter or more in thickness are common inside the D ring, particularly south of the crater.

5.4 VERTICAL LAYERING

Correlation of the vertical layering in the ejecta and the original layering in the alluvium was attempted at the ejecta sampling stations; however, stratification was not maintained in sufficient detail at these distances and this correlation was not possible.

A distinct depositional layering is evident at most of the C stations and at all of the A and B stations which were sampled. This vertical stratigraphy is predominantly a two-layer system, although two C stations showed evidence of stratification (a third layer, that of the deposit by the base surge cloud, originally present, had been partially eroded and was not recognizable as a distinct layer in the field). Within the two-layer framework, the relative positions and magnitudes of these ejecta strata are shown in Figure 5.2.

The upper layer, present at all C, B, and A stations, is a light grey, poorly sorted material containing moderate to abundant grains of fused alluvial material. Unfused material ranges from silt size to pebble size with local cobbles and boulders. The lower layer is a light yellowish-brown, poorly sorted material with scattered pebbles, cobbles, and boulders in a matrix of finer material. The thickness of these

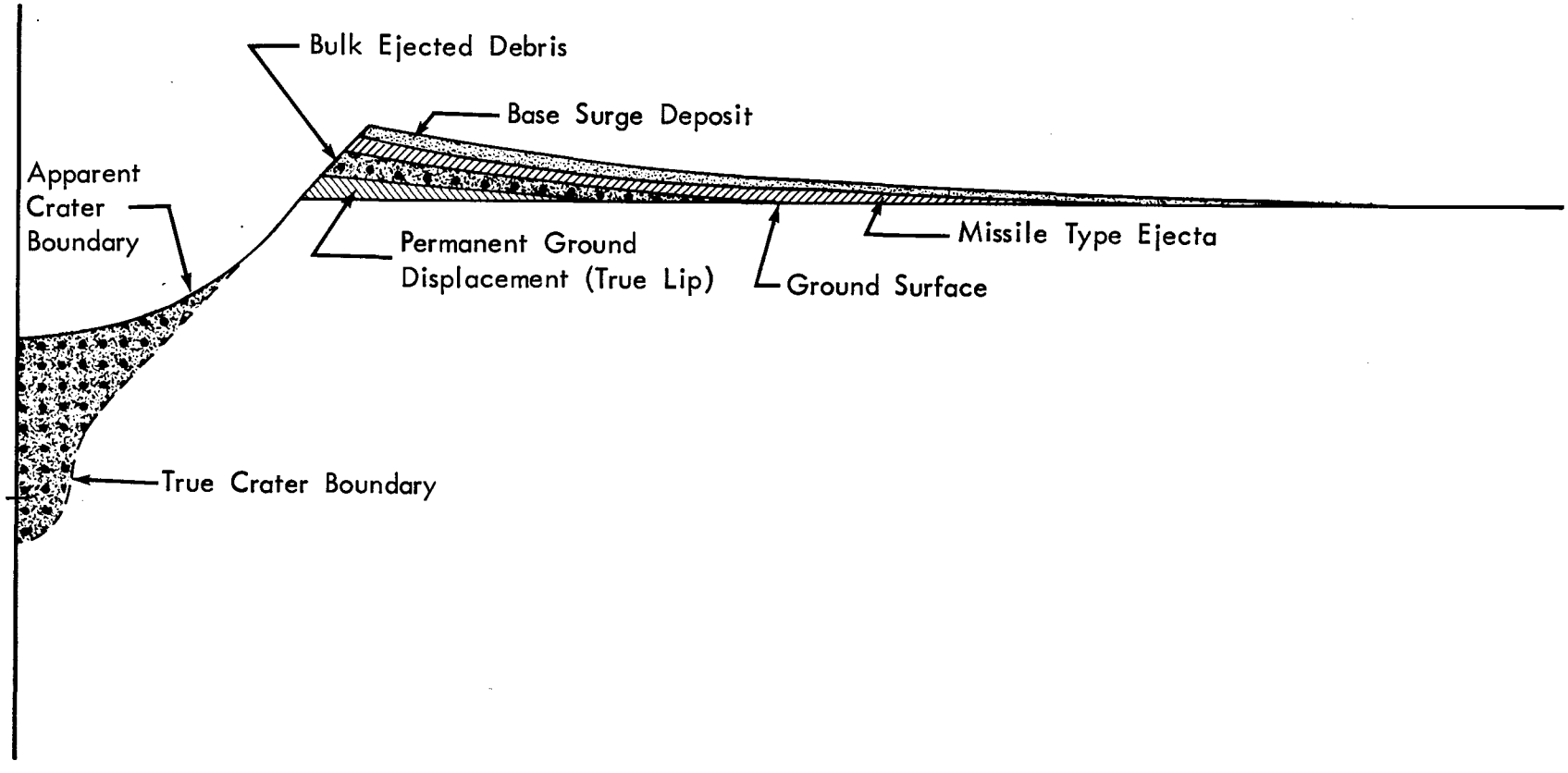

Figure 5.2 Diagrammatic section of Sedan crater lip.

two layers is summarized in Table 3.3. Evidence of sorting by the atmosphere was observed in the upper layer with aeolian material deposited mostly after D-day occurring at the top. The contact between these two debris types is obviously gradational, but the color change noted in the field and probably caused by the admixture of abundant fused material takes place generally in less than a centimeter.

Material in the lower layer is believed to be ejected in mass and relatively unaffected by the atmosphere. Fused material was not observed when this lower layer was sampled; however, occasional fragments were found when samples were sorted into grain-size groupings. The lower layer is believed to be composed of material ejected in bulk at relatively low velocities. This material was unaffected by atmospheric action and was probably deposited by fluid flow mechanism superimposed on initial ballistic trajectories.

The upper layer is composed of material from the base surge deposit; debris from high-angle, high-exit velocity trajectories; and fused material similar to primary fallout.

The limits of the bulk ejected and missile-type debris deposits are shown in Figure 3.5. These limits are not precisely known because of limited control. The bulk ejecta is not present at any of the D stations examined and is missing at Station C23, so that the limit is known to lie inside C23 and between the C and D rings at all other sampled radii. The outer limit of the missile-type debris is very difficult to locate since the missile frequency appears to decrease gradually rather than abruptly. This limit is based on the missile survey along the four principal radii and on the

relative abundance and size of pebbles present in the trays at the F and G rings. The average size of the missiles near the outer limit of missile-type debris appears to increase outward.

The missile-type and bulk ejected debris were sampled separately where recognized; namely, at the A, B, and C rings. The cumulative percent curves for the samples taken from the two layers at each ring are shown in Figure 5.3. Note that median grain size is uniformly larger in the upper layer or missile-type debris. Fine-grained material, mostly silt sized and light pumice-like fused material has locally been redeposited, and accretion of this material did occur at several of the inner samples. Some depletion of the fines must also have occurred. This post-ejecta aeolian material has been included in the samples of the top layer and tends to reduce the median grain size of the missile-type ejecta samples which depletion of the fines would tend to increase the median grain size. Because of the random nature of the positions of the different size grains within the layer, it is believed that the net effect on median grain size by aeolian action would be that of reduction and that this would be a minor effect.

The median grain size of the upper debris layer missile-type ejecta is 0.089, 0.094, and 0.076 cm at the A, B, and C rings and 0.064, 0.064, and 0.061 cm in the lower debris, or bulk ejecta layer. At ring C, the cumulative percent curves of the two samples cross twice at about the 17 and 74 percentiles, but the greater portion of the bulk ejected sample is smaller than the missile-type sample.

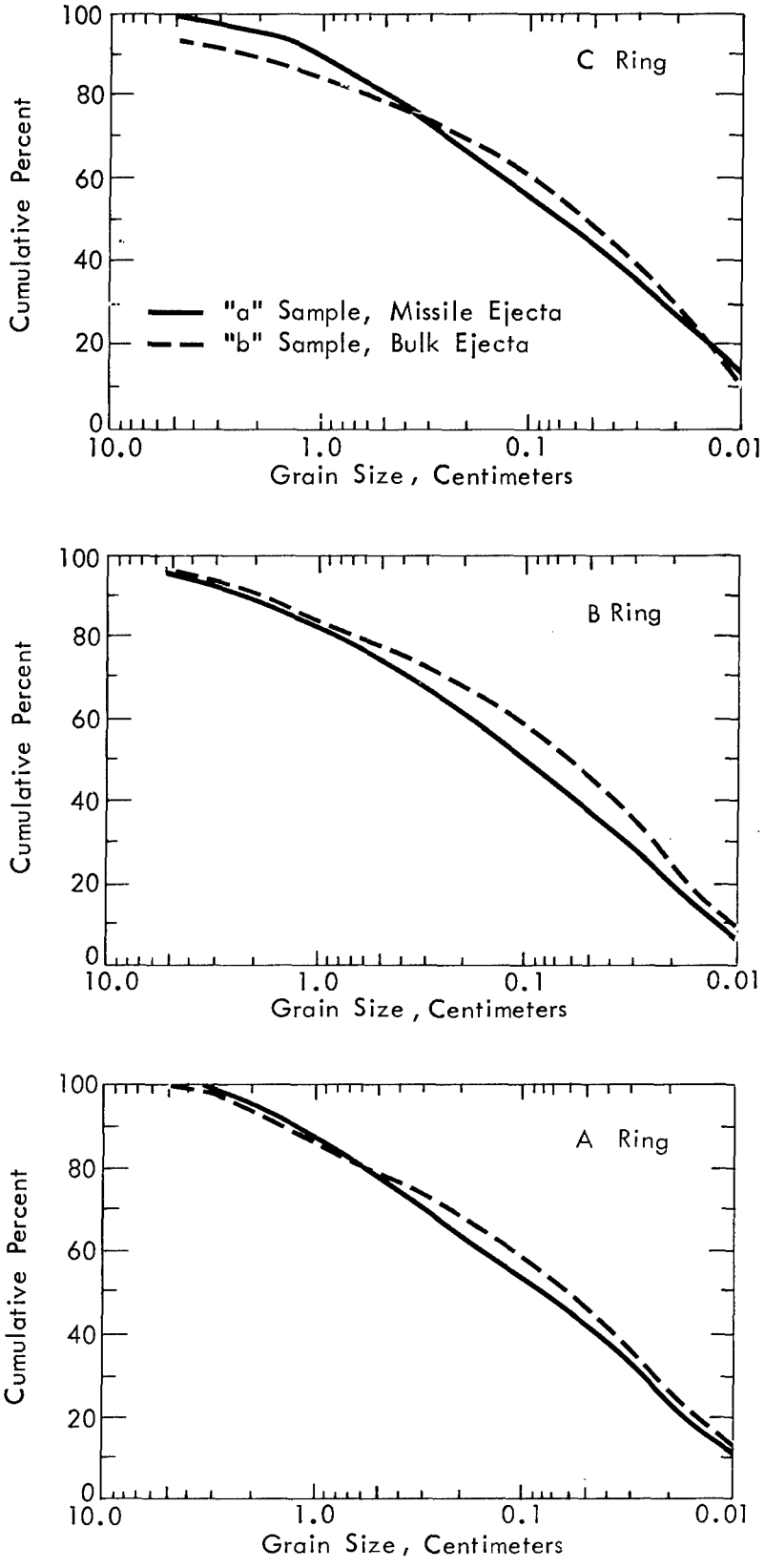

Figure 5.3 Grain size distribution of the two distinct debris layers.

5.5 INVERSE LIP STRATIGRAPHY

There is distinct stratification in the ballistic debris exposed inside the Sedan crater. This layering is shown in Figure 3.4. The layers are variable in thickness, decreasing and increasing along the crater periphery.

Detailed stratigraphic mapping of these layers above the original ground surface, in addition to detailed mapping below the original ground surface in the sediments exposed along the crater wall, may yield enough information to correlate the debris with the original alluvium at the lip crest. It is believed that the stratigraphy in the debris will be the inverse of the stratigraphy in the alluvium, similar to the conditions determined by Shoemaker (Reference 17) at Meteor Crater, Arizona. An equivalent layer in the debris above the original ground surface is much thinner than the original bed it represents and may even be missing at certain locations. At the crater's edge, roots in soil above the original ground surface were broken and the material appeared to be sheared with the upper portion moving radially outward. Many of the cobbles in the debris just beyond the lip crest were shattered. This outward shearing of the ejected beds is responsible for thinning in the layers and locally may completely shear out a bed or a contiguous series of beds, resulting in missing portions of the stratigraphic section where exposed. The sheared beds in the debris are sub-lenticular and beds vary in thickness along the strike giving an appearance of braided structure.

There is some evidence of the inverse character of the ejecta exposed along the Sedan crater wall. A photograph and interpretive sketch of the crater wall are

shown in Figure 5.4.

The medium-brown colored bed just below the original ground surface is massive, where seen, and the small details of bedding cannot be traced around the "hinge-line." The lighter colored bed just below is cemented slightly and some details of bedding are visible. This bed appears to be wrapped around the folded original ground surface and the massive brown unconsolidated bed. Fragments of the massive brown bed are evident just above the original ground surface.

5.6 GRAIN SIZE DISTRIBUTION AND COMMINUTION

Pre-shot samples of the alluvium in the region cratered by the Sedan device are inadequate for determination of a bulk average sorting. Sampling in the alluvium in Area 10 has been done by split spoon sampling apparatus at regular intervals. In general, the sampling technique used tends to select the finer-grained material and to exclude the coarser lenses of gravel due to the size of the tube (about 3 inches in diameter) driven into the alluvium and the difficulty encountered in forcing the tube into the alluvium when the alluvium being sampled contains numerous pebbles or cobbles. Thus, the average sorting of the samples of pre-shot alluvium tends to be smaller than was actually the case.

The grain size distribution for samples taken from the G, F, D, C, B, and A rings is shown in Figure 3.7. Also shown are the two extreme grain size distribution curves for a 56-meter hole from which pre-shot alluvium samples were taken prior to the Jangle cratering events. (Reference 8). It must be remembered when comparing these pre-shot distribution curves to the grain size distribution for

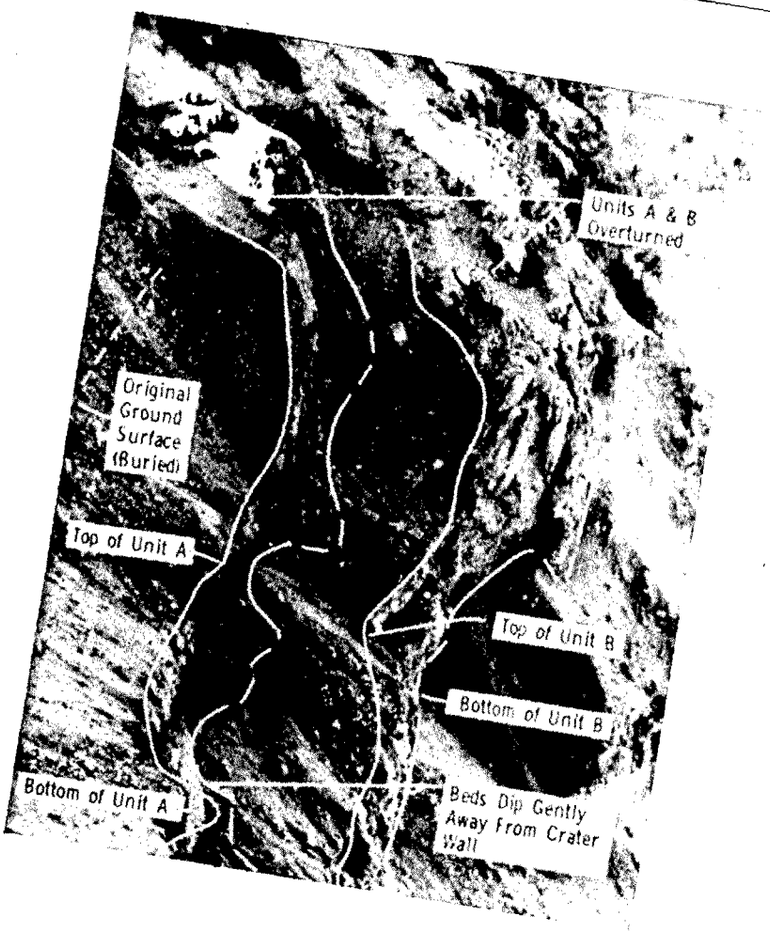

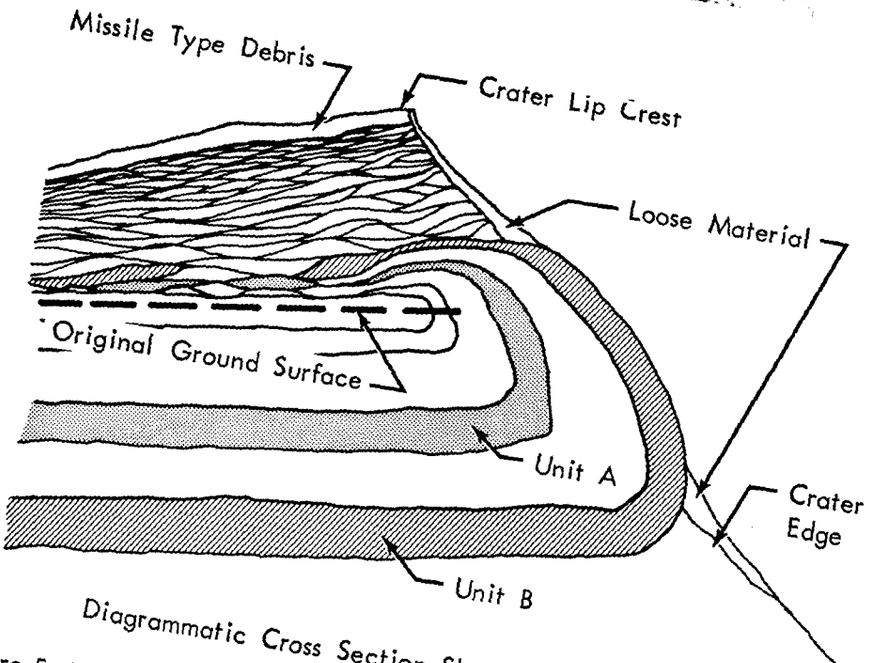

Diagrammatic Cross Section Showing Bed Overturn

Figure 5.4 Photograph and interpretation of ejecta along original ground surface near crater edge.

specific post-shot ejecta samples that the sampling hole was less than one-third the Sedan device placement depth and that the pre-shot holes represent extremes.

The change in grain size distribution from coarser to finer particles is apparent from Figure 3.7. It should be noted that some of the fine-grained material was removed by the wind and by the base surge. This means, in effect, that the distribution curves shown for each sampling ring would actually have indicated a somewhat finer grain size distribution if unaltered samples had been obtained.

There is insufficient data available from which to determine the extent of comminution which resulted from the explosive shock.

5.7 ORIGINAL GROUND SURFACE

The original ground surface was located at several points around the edge of the crater. The soil horizon is evident at other locations. The original ground surface is marked by soil, vegetation, artifacts such as rags, and (near the north-east portion) a hardened layer probably representing the much-watered surface of a graded road.

The original ground surface is shown in Figure 5.5. Vegetation with roots extending upward into the soil for a short distance, with the top pointing inward, were located, tending to indicate that the soil was folded over and inverted above the original ground surface. Roots extending upward and outward in the inverted soil zone were short, indicating that the inverted soil layer was sheared. The soil layer above the original ground surface is thinner than the soil layer beneath the original ground surface and was probably thinned and sheared by the radially outward

Northeast crater edge showing original ground surface.

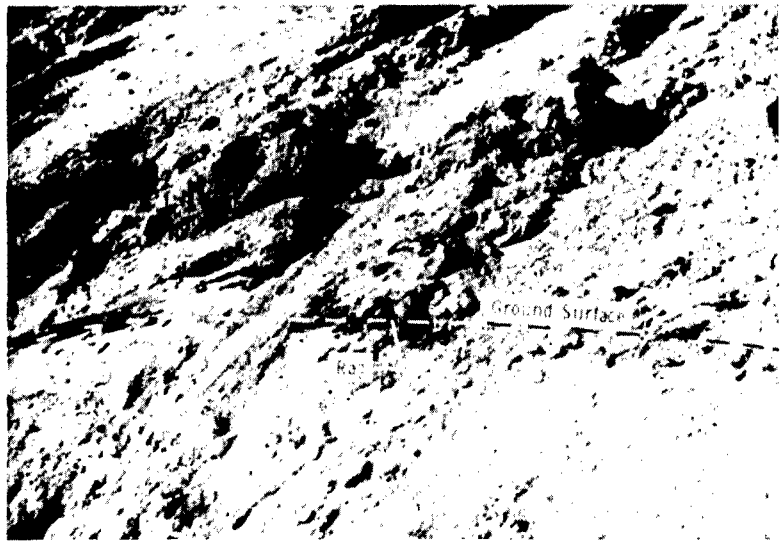

Original ground surface outcropping at northwest edge of crater.

Soil zone at original ground ground surface exposed at south edge of crater.

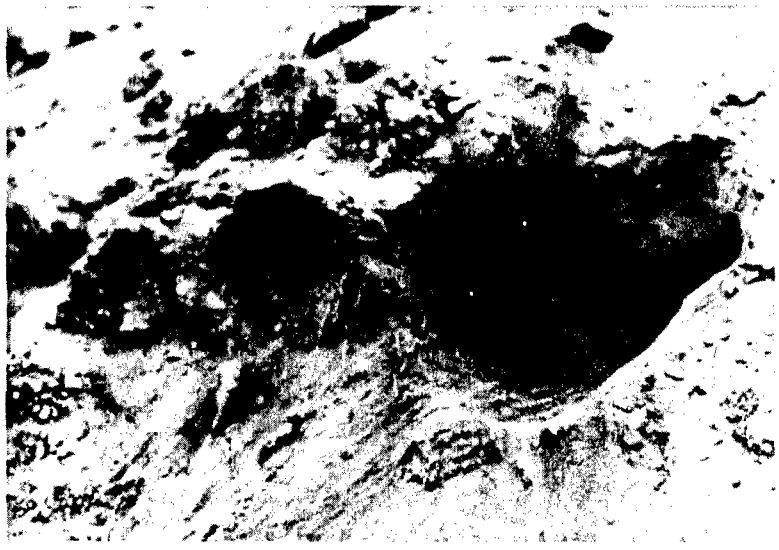

Figure 5.5 Exposures of original ground surface.

motion of the ejecta caused by the radial inertia of the debris after impact with the original ground surface.

5.8 IMPACT CRATERS

Boulder-like missiles were not recovered when impact craters were excavated. The high impact velocities and the tendency of the missile to ricochet would make it difficult to find definite evidence of impact craters that were formed by boulder-like missiles; however, the lack of this evidence does not eliminate the possibility that some of these craters were so formed.

Impact crater ejecta was deposited asymmetrically around the edge of the impact crater. Apparently the missile was a large discrete mass of alluvium ejected intact from the Sedan crater. The impacting mass depressed the original ground surface marked by vegetation and organic debris, deformed the ground surface to form a raised lip outward, and ricocheted outward shearing off part of the deformed lip. A diagrammatic section of a typical impact crater is shown in Figure 3.11.

Large impact craters, those over 3 meters in diameter, were counted using aerial photographs of the Sedan crater and the surrounding area. The radial distribution of these craters is shown in Table 5.1. (An impact crater location map is shown in Figure 3.10). Over fifty percent of the total number of large impact craters are located between 550 and 730 meters from the Sedan ground zero.

Table 5.2 indicates the frequency of impact craters occurring at fixed radial distances from ground zero. Shown in this table is the percentage of each circumference covered by impact craters. This percentage is actually calculated

TABLE 5.1 RADIAL DISTRIBUTION OF LARGE IMPACT CRATERS*

Distance Range from Sedan Epicenter		Number of Impact Craters within Area Defined by Distance Range	Percent of Total
meters	crater radii		
180 to 370	1 to 2	7	2
370 to 550	2 to 3	84	19
550 to 730	3 to 4	244	52
730 to 920	4 to 5	109	23
920 to 1100	5 to 6	20	4
1100 to 1280	6 to 7	1	< 1

* A large impact crater is over 3 meters in diameter.

TABLE 5.2 IMPACT CRATER PROBABILITIES

Distance		Probability
meters	crater radii	percent
370	2	3.3
410	2 1/4	3.3
460	2 1/2	6.0
500	2 3/4	4.8
550	3	5.0
590	3 1/4	4.8
640	3 1/2	4.6
690	3 3/4	3.4
730	4	4.4
780	4 1/4	1.5
820	4 1/2	1.6

using the following expression:

$$p = \frac{\sum l_D}{C}$$

where $\sum l_D$ is the sum of the lip-to-lip diameters of all impact craters which are tanget to, or lie on, any sampling ring of circumference, C. A maximum probability of being struck by an impacting missile (if the percentage p is defined as a probability) occurs at about 460 meters (2 1/2 crater radii) and is approximately 6 percent. All probabilities are over 4 percent within the region between 460 meters and 640 meters (2 1/2 and 3 1/2 crater radii).

It is also of interest to note the percentage of impact craters occurring circumferentially. These percentages, for the region between 550 and 750 meters from ground zero, are shown in Figure 3.10. The percentages shown are based on area; that is, the ratio of impact crater lip-to-lip area to the area of the 10-degree sector within the region specified above. There does not appear to be an obvious correlation between the circumferential distribution of impact craters shown in Figure 3.10 and the circumferential variation of ejecta areal density for the C sampling ring shown in Figure 3.8. (The C ring is located at approximately 3 1/2 crater radii.). Careful study of aerial photographs also indicates no correlation for circumferential variability between impact craters and ejecta areal densities for the more distant sampling rings.

5.9 TOPOGRAPHIC CHARACTER OF THE EJECTA SURFACE

Between the lip crest and two to three apparent crater radii, the ejecta surface topography is quite hummocky and irregular. The hummocks decrease in

size and frequency per unit area radially outward and are sparse beyond three crater radii. The surface in this region is infrequently spotted with boulders and impact craters; however, from two or three crater radii outward to about five crater radii the surface is littered with boulders and cobbles and marked with clusters of impact craters. The large impact craters all occur within 7 crater radii. Small impact craters occur beyond this out to the limit of ballistic ejecta decreasing in frequency radially outward.

Surface rubble is locally abundant and locally absent. Figure 5.6 shows the rubbly nature east of the crater in the region about four to six crater radii from ground zero. The irregular topography in the lip is also evident. The hummocky nature of the topography near station A24 is also shown in Figure 5.6. The horizon in the center of this picture is the southern lip of the Sedan crater. The two peaks to the east are mountains. The hummocky topography on the west horizon is the eastern part of the highest section of the Sedan lip.

5.10 APPLICATION TO NUCLEAR DITCHING

Ejecta distribution and its prediction is of interest because it represents one of the hazards associated with potential Plowshare projects falling within the earth-moving category. First, there is the potential danger associated with the ballistic character of the throwout itself; in fact, missiles ejected from the ditch or crater may in certain cases represent a greater lethal radius than the blast wave. Secondly, if there is radioactivity associated with the nuclear explosive, the contamination that

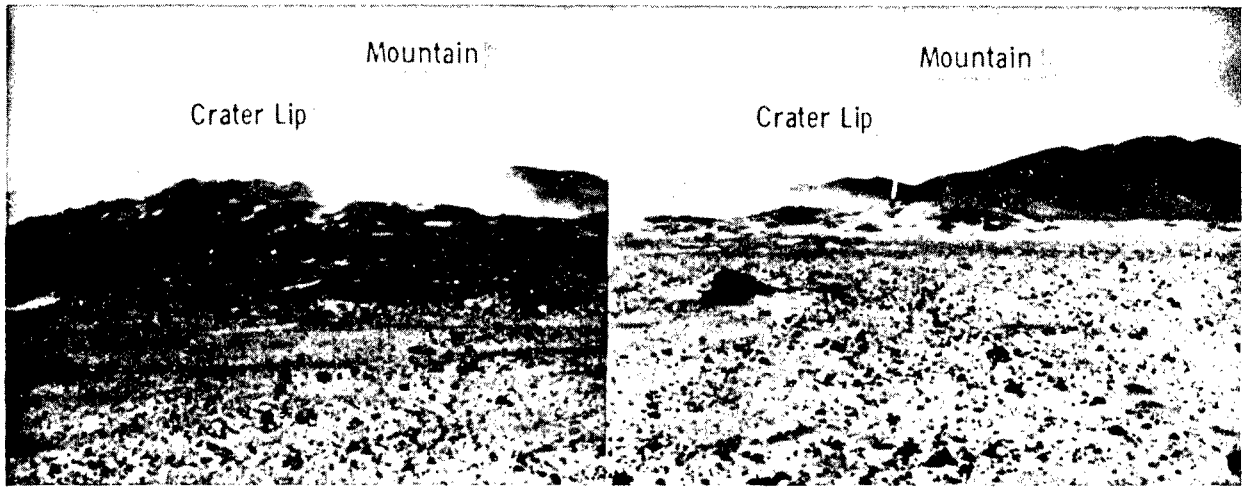

Composite view from Station D2 looking Southeast

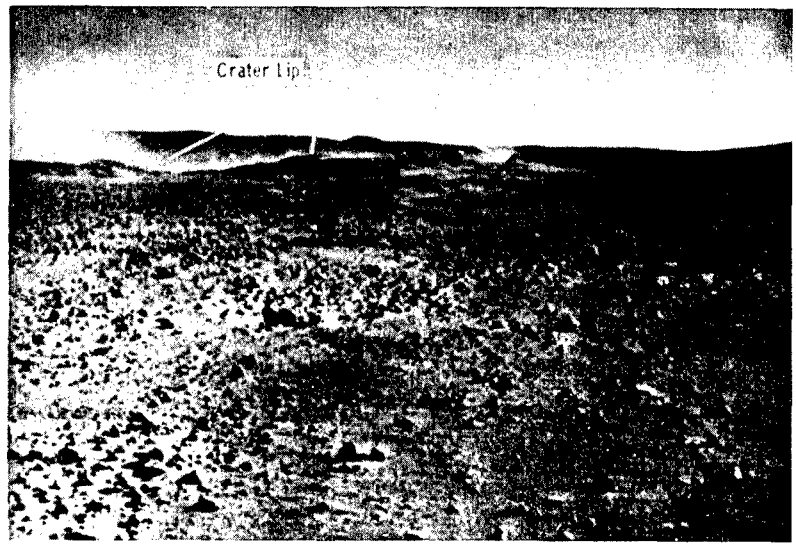

View from Station E14 looking Northeast

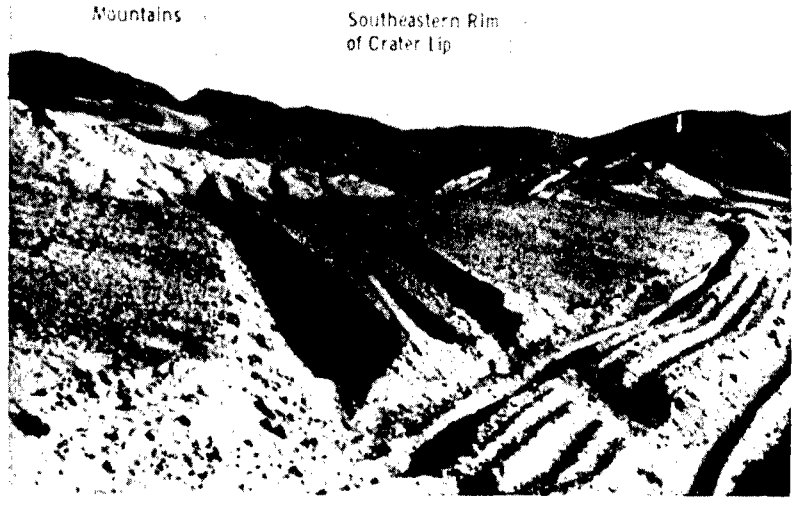

View near Station A24 looking South

Figure 5.6 Topographic character of ejecta surface.

results will be almost wholly trapped in the ejected debris. It may therefore be of some interest to be able to predict ejecta distribution empirically until applicable theory has been developed and verified.

The analytical work done on Sedan ejecta data suggests a procedure whereby ejecta distribution could be determined for explosive ditches. The required relationships sketched in Figure 5.7 must be derived from experimental data.

The first relationship (Figure 5.7a) is essentially the scaling law for linear spaced-point ditching charges. Experimental work has already been done by Sandia Corporation and Lawrence Radiation Laboratory to determine this relationship for high-explosive charges (see, for example, Reference 18).

The second relationship (Figure 5.7b) is that between the mass of the material ejected from the ditch and the mass inferred from the ditch volume. Total ejecta mass can only be determined for a given ditch (or crater) if sufficient observations are made within the region in which the largest quantity of ejecta is deposited. This region is about 10 radii for craters and is probably 5 widths for ditches.

The third required relationship (Figure 5.7c) describes the location of ejecta relative to the ditch. In the sketch, M_i is the ejecta mass between the ditch edge and any distance of interest, M_{de} is total mass ejected from the ditch, D is distance, and R_d is one-half of the apparent ditch width.

The three relationships described above must be described for optimum charge burial depth, that is, the charge depth at which the maximum apparent crater volume is created. These relationships also must be determined for the same geologic medium

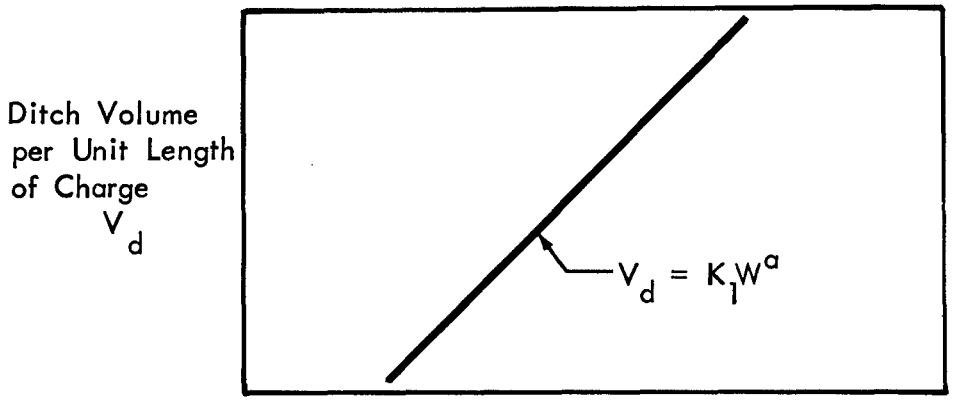

(a)

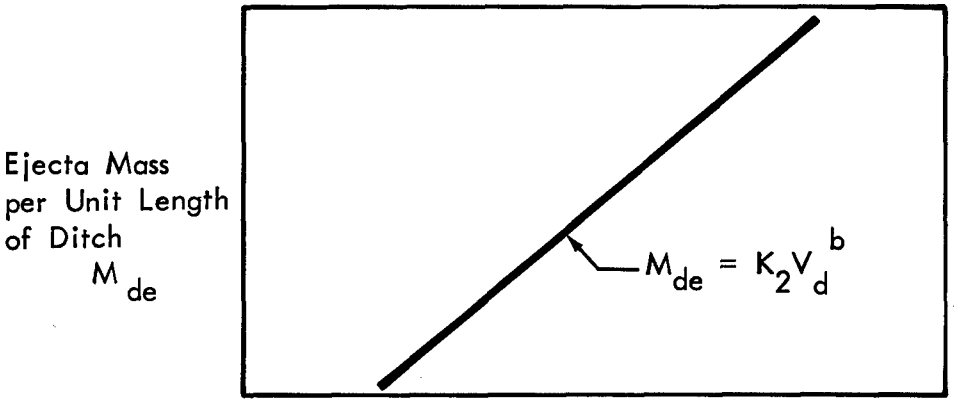

(b)

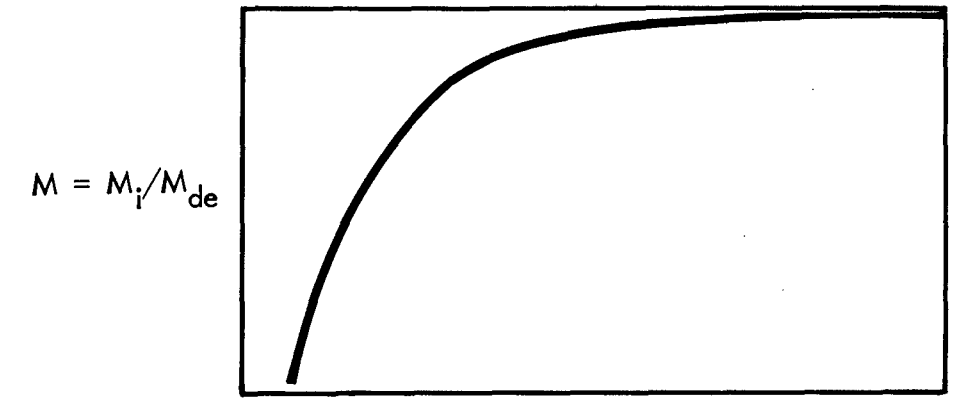

(c)

Figure 5.7 Relationships required for estimation of ejecta distribution along explosive ditches.

and in all cases are defined for a unit length of the explosive charge. The ejecta mass distribution shown in Figure 5.7c is a typical curve based on many other specific distribution curves which, for prediction purposes, is considered the most representative.

Once the relationships shown in Figure 5.7 are determined, ejecta distribution can be determined for a full-scale Plowshare ditching event by the following steps:

1. Estimate apparent volume per unit charge length of the ditch to be constructed (refer to Figure 5.7a).

2. Determine total ejecta mass per unit charge length (refer to Figure 5.7b).

3. Calculate ejecta distribution normal to the ditch longitudinal axis (refer to Figure 5.7c). The areal density, δ, relationship is:

$$\delta(\alpha) = \frac{M_{de}}{2\pi R_d^2 d} \frac{dM}{d\alpha}$$

4. Evaluate longitudinal ejecta variation.

Linear ditching experiments using nuclear row charges are currently being planned for the near future. Chemical explosive ditching experiments are in progress at the present time. It is recommended that ejecta experiments designed to provide data applicable to deriving the above relationships be included in both nuclear and chemical explosive ditching programs.

It may also be possible to use ejecta data obtained on cratering experiments to predict throwout distribution on ditching events. A method of equating crater and ditch volumes is given in Reference 18. If ditch volume can be established from crater data, then steps in estimating ejecta distribution are as outlined briefly above.

CHAPTER 6

CONCLUSIONS AND RECOMMENDATIONS

6.1 CONCLUSIONS

The following specific conclusions are drawn:

1. Several expressions can be developed relating ejecta areal density to distance. If a single mathematical fit is made to all observations, this relationship is:

$$\delta = \frac{6.98 \times 10^{14}}{D^{4.3}}$$

When only the observations considered are those along the four primary sampling lines the relationships derived are:

$$\delta = \frac{6.32 \times 10^{16}}{D^{5.1}}$$

If several fits are made using all data, but arbitrarily restricting each fit to a specific region, the following relationships are derived:

$$\delta = \frac{2.26 \times 10^{9}}{D^{2.2}} \qquad 220 \leq D \leq 550$$

$$\delta = \frac{3.88 \times 10}{D^{6.0}} \qquad 550 \leq D \leq 840$$

$$\delta = \frac{2.60 \times 10}{D^{3.5}} \qquad 840 \leq D \leq 1710$$

In the above relationships, δ is areal density in kg/m^2, and D is distance in

meters. In all cases, the mathematical fits have been made to the arithmetic mean of the data.

2. The areal density varies significantly at constant radial distances. The ratios of the highest to the lowest observations of areal density were 32, 10, 7, and 37 at the G, F, D, and C sampling rings, respectively.

3. The total mass of material ejected from the Sedan crater represents about 58 percent of the mass inferred from the apparent crater volume. After appropriate corrections are made, it is concluded that about 37 percent of the apparent crater volume results from compression of the surrounding desert alluvium.

4. Fifty percent of the material ejected from the crater is deposited on the ground surface between the crater edge and two crater radii, eighty percent is within three crater radii, and ninety-seven percent is within ten crater radii.

5. A distinct layering is observable in the ejecta profile. The upper layer is made up of the larger particulate material whereas the lower layer consists of fine, silt-like material. It is suggested that the material in the lower layer is ejected from the crater in mass, is relatively unaffected by the atmosphere, and is deposited early in the time history of ejecta deposition. The material in the upper layer exhibits ballistic characteristics; that is, the individual particles were probably ejected along ballistic trajectories, being influenced by the atmosphere, and came down late in the time history of ejecta deposition.

6. Numerous impact craters mark the debris layer surrounding the crater, with their greatest frequency occurring between 550 and 730 meters from ground zero. The outermost impact crater was observed at 2,140 meters from ground zero.

These impact craters were generally caused by individual boulders and large discrete masses of alluvium falling back to the ground very late in the time history of ejecta deposition.

7. The pre-shot stratification existing in the upper region of the desert alluvium medium can be observed in inverse order in the ejecta immediately surrounding the crater.

6.2 RECOMMENDATIONS

It is recommended that similar experimentation be included in future cratering shots, both chemical and nuclear. It is necessary for the success of any such planned experiment that the ejecta sampling program include sufficient stations to measure adequately the throwout close to the crater (within 5 crater radii), the region in which more than ninety percent of the ejecta was deposited for Sedan. Following are specific types of cratering events which would yield useful ejecta data:

1. Several cratering events at the surface (or some scaled burst depth) of the same geologic medium but each differing in energy release from the other by about two orders of magnitude. This would provide data on the relationship between ejecta quantity and explosive energy release for the same actual and scaled distance from the charge epicenter.

2. A cratering event similar to Sedan in hard rock. This would provide data on the ejecta-mass-to-crater-mass ratio for a nearly noncompressible medium.

3. Cratering and ditching events designed to determine their relative equivalence. Thus, information would be available from cratering events which would permit the determination of ejecta distribution for large yield ditching charges.

APPENDIX A

SUMMARY OF RAW DATA

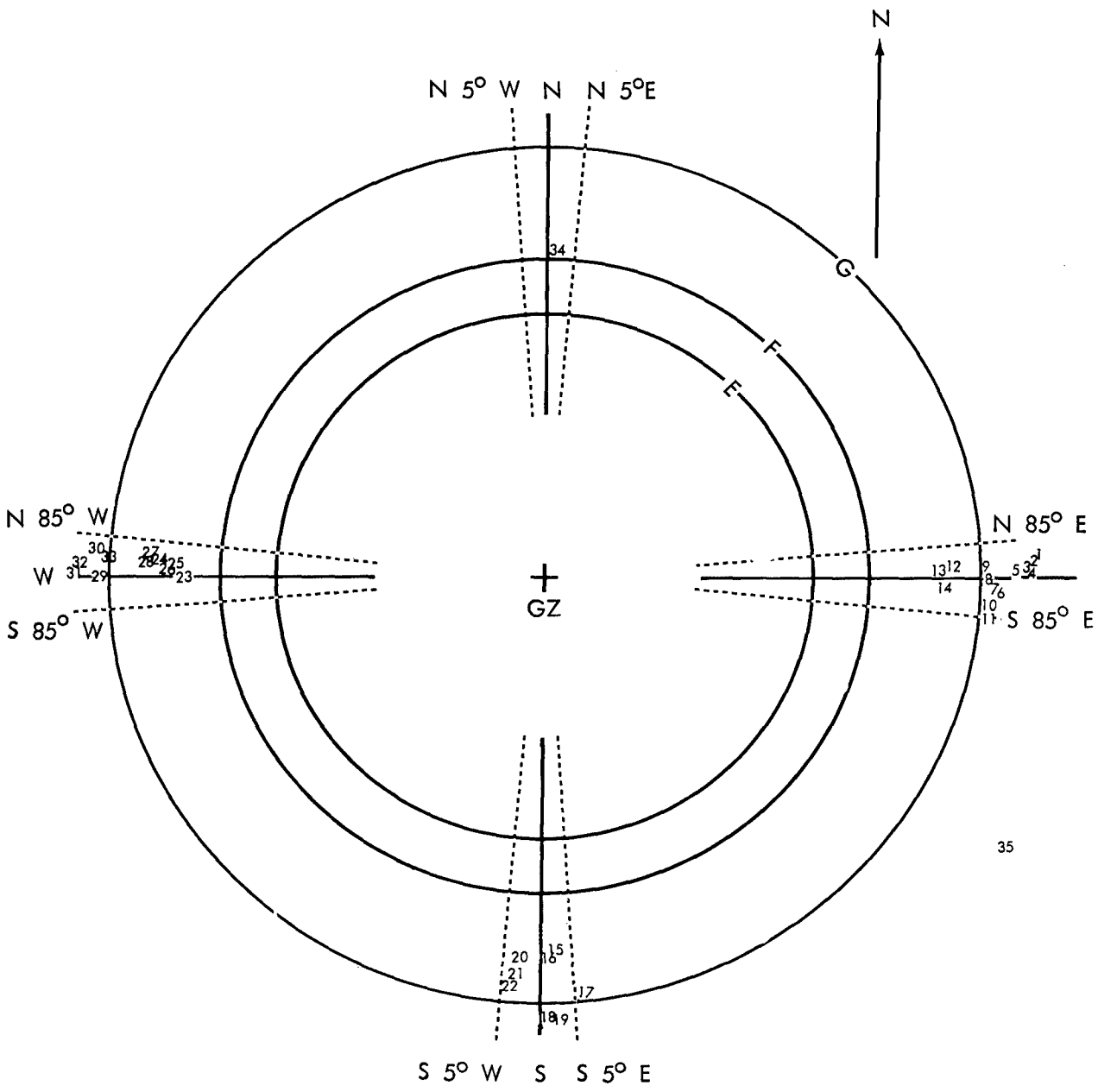

Figure A.1 Missile survey.

TABLE A.1 EJECTA AREAL DENSITY SAMPLES--PRIMARY ARRAY

Station	Tarp Number	Weight of Sample Plus Tarp*	Weight of Sample	Areal Density
		pounds	pounds	lb/ft^2
G6	G6a	6.94	5.50	0.68
	G6b	4.63	3.19	0.395
	G6c	5.88	4.44	0.55
	G6d	9.19	7.75	0.96
	G6e	5.69	4.25	0.525
G12	G12a	7.00	5.56	0.69
	G12b	7.25	5.81	0.72
	G12c	5.19	3.75	0.465
	G12d	6.19	4.75	0.59
	G12e	7.13	5.69	0.705
G18	G18a	4.56	3.12	0.386
	G18b	3.38	1.94	0.24
	G18c	3.25	1.81	0.224
	G18d	3.25	1.81	0.224
	G18e	3.44	2.00	0.248
G24	G24a	5.19	3.75	0.465
	G24b	3.81	2.37	0.294
	G24c	4.00	2.56	0.317
	G24d	3.75	2.31	0.386
	G24e	4.94	3.50	0.434
F6	F6a	16.25	14.81	1.84
	F6b	16.25	14.81	1.94
	F6c	22.25	20.81	2.58
F12	F12a	12.94	11.50	1.42
	F12b	57.38	55.94	6.92
	F12c	58.31	56.87	7.04
F18	F18a	6.25	4.81	0.595
	F18b	22.81	21.37	2.64
	F18c	13.2	11.76	1.46

TABLE A.1 EJECTA AREAL DENSITY SAMPLES--PRIMARY ARRAY (CONTINUED)

Station	Tarp Number	Weight of Sample Plus Tarp*	Weight of Sample	Areal Density
		pounds	pounds	lb/ft^2
F24	F24a	12.38	10.94	1.35
	F24b	5.56	4.12	0.51
	F24c	19.75	18.31	2.26
E6	E6a	---	84.44	10.4
	E6b	---	130.16	16.1
	E6c	---	93.87	11.6
E12	E12a	34.06	32.62	4.05
	E12b	55.25	53.81	6.66
	E12c	23.38	21.94	2.72
E18	E18a	19.88	18.44	2.28
	E18b	30.75	29.31	3.63
	E18c	68.25	66.81	8.27
E24	E24a	38.25	36.81	4.56
	E24b	26.50	25.06	3.1
	E24c	36.25	34.81	4.31
D6	D6a	---	133.66	16.6
	D6b	---	161.88	20.0
D12	D12a	158.81	157.37	19.5
	D12b	158.88	157.44	19.5
D18	D18a	---	76.94	9.52
	D18b	---	62.26	7.7
D24	D24a	72.50	71.06	8.8
	D24b	56.75	55.31	6.85
C1			11.38**	113.8
			10.88**	108.8
			11.56**	115.6
C2				215***

TABLE A.1 EJECTA AREAL DENSITY SAMPLES--PRIMARY ARRAY (CONTINUED)

Station	Tarp Number	Weight of Sample Plus Tarp*	Weight of Sample	Areal Density
		pounds	pounds	lb/ft^2
C3			12.75**	128
			14.44**	144
C4			12.50**	125
			13.13**	131
C5			11.06**	111
			12.00**	120
C6			6.62**	66.2
C7				164***
C8			10.88**	109
			10.00**	100
			9.81**	98.1
C9				206***
C10			10.38**	104
			11.56**	116
			10.56**	106
C11				524***
C12			12.94**	129
C13				243***
C14			5.75**	57.5
			6.38**	63.8
			5.88**	58.8
C15				286***
C16				178***

TABLE A.1 EJECTA AREAL DENSITY SAMPLES--PRIMARY ARRAY (CONTINUED)

Station	Tarp Number	Weight of Sample Plus Tarp*	Weight of Sample	Areal Density
		pounds	pounds	lb/ft^2
C17			13.00**	130
			14.19**	142
C18			3.75**	37.5
			5.63**	56.3
C19			1.688**	16.9
			1.75**	17.5
			1.688**	16.9
C20			1.625**	16.3
			1.75**	17.5
			2.188**	21.9
C21			1.50**	15.0
			1.813**	18.1
			1.813**	18.1
C22	C22a	86.25	84.81	10.5
	C22b	146.50	145.10	18.0
C23	C23a	304.75	303.31	39.5 (7.67 ft^2 sample area)
C24			11.50**	115
B6			8.75**	87.5
			8.38**	83.8
			8.50**	85.0
B12				262***
B18			12.94**	129
			12.88**	129
B24				478***

TABLE A.1 EJECTA AREAL DENSITY SAMPLES--PRIMARY ARRAY (CONTINUED)

Station	Tarp Number	Weight of Sample Plus Tarp*	Weight of Sample	Areal Density
		pounds	pounds	lb/ft^2
A6			12.50**	125
A12				449***
A18				225***
A24				1170***

* Average tarp weight 1.44 pounds
Average tarp area 8.08 ft^2 (see Table A.6)

** Estimated, using thin-walled sampling tube and steel plate base at visually identified debris-pre-shot interface (see Table A.6)

*** Estimated, using measured depths to debris-pre-shot interface and density of 1.5 gm/cm^3.

TABLE A.2 EJECTA AREAL DENSITY SAMPLES--TRAYS

Station	Weight of Tray* Plus Sample	Weight of Sample	Areal Density
	pounds	pounds	lb/ft^2
G1	1.75	1.28	1.66
G2	1.44	0.97	1.26
G3	1.88	1.41	1.83
G4	1.69	1.22	1.58
G5	3.13	2.66	3.46
G7	1.50	1.03	1.34
G8	6.94	6.47	8.4
G9	5.25	4.78	6.2
G10	1.19	0.72	0.935
G11	1.06	0.59	0.765
G13	1.19	0.72	0.935
G14	2.19	1.72	2.24
G15	2.25	1.78	2.31
G16	1.63	1.16	1.51
G17	1.44	0.97	1.26
G19	1.56	1.09	1.42
G20	0.69	0.22	0.286
G21	1.00	0.53	0.69
G22	1.94	1.47	1.91
G23	1.81	1.37	1.78
F1	3.56	3.09	4.01
F2	6.31	5.84	7.58
F3	4.25	3.78	4.91
F4	8.75	8.28	10.8
F5	7.19	6.72	8.74
F7	9.44	8.97	11.7
F8	lost	---	---
F9	9.25	8.78	11.4
F10	3.25	2.78	3.61
F11	6.38	5.91	7.7

TABLE A.2 EJECTA AREAL DENSITY SAMPLES--TRAYS (CONTINUED)

Station	Weight of Tray* Plus Sample	Weight of Sample	Areal Density
	pounds	pounds	lb/ft^2
F13	11.25	10.78	14.0
F14	9.69	9.22	12.0
F15	6.06	5.59	7.25
F16	6.69	6.22	8.09
F17	3.31	2.84	3.69
F19	11.00	10.53	13.7
F20	3.19	2.72	3.53
F21	7.44	6.97	9.05
F22	8.81	8.34	10.8
F23	8.13	7.66	9.96

* Average tray weight 0.47 pounds and average tray area 0.77 ft^2 (see Table A.6)

TABLE A.3 EJECTA AREAL DENSITY SAMPLES--SECONDARY TARPS

Station	Weight of Sample	Collector Area	Areal Density	Sampling Techniques*	Remarks
	pounds	ft^2	lb/ft^2		
D1	2.19	0.1	21.9	B	Tarp destroyed.
	2.94	0.1	29.4		
	2.81	0.1	28.1		
D2	41.75	2.0	20.9	A	Tarp intact.
	36.75	2.0	18.4		
	33.56	2.0	16.8		
D3	20.13	1.0	20.1	A	Tarp intact.
	24.13	1.0	24.1		
	22.56	1.0	22.6		
	18.00	1.0	18.0		
D4	26.63	1.0	26.7	A	Tarp partially destroyed.
	24.75	1.0	24.7		
D5	30.06	1.0	30.1	A	Tarp partially destroyed.
D7	11.75	0.3	39.2	B	Tarp not found.
D8	50.81	1.0	50.8	A	Tarp intact.
	51.00	1.0	51.0		
	58.94	1.0	58.9		
D9	28.31	1.0	28.3	A	Tarp partially destroyed.
	25.31	1.0	25.3		
	22.94	1.0	23.0		
	19.94	1.0	20.0		
D10	2.06	0.1	20.7	C	Tarp badly damaged Thickness estimates: 3.0 inches, 2.75 inches, 3.75 inches.

TABLE A.3 EJECTA AREAL DENSITY SAMPLES--SECONDARY TARPS (CONTINUED)

Station	Weight of Sample	Collector Area	Areal Density	Sampling Techniques*	Remarks
	pounds	ft^2	lb/ft^2		
D11	22.69	2.0	11.3	A	Tarp intact.
	21.19	2.0	10.6		
D13	15.06	1.0	15.1	A	Tarp intact.
	14.44	1.0	14.4		
	18.56	1.0	18.5		
	23.75	1.0	23.7		
D14	19.81	1.0	19.8	A	Tarp intact.
	14.94	1.0	15.0		
	13.81	1.0	13.8		
	15.81	1.0	15.8		
D15	36.88	1.0	36.9	A	Tarp intact.
	36.69	1.0	36.7		
	34.88	1.0	34.9		
	36.94	1.0	36.9		
D16	35.50	1.0	35.5	A	Tarp intact.
	30.75	1.0	30.7		
	16.00	1.0	16.0		
	19.06	1.0	19.1		
D17	34.56	1.0	34.5	A	Tarp intact.
	23.31	1.0	23.3		
	21.94	1.0	22.0		
	30.00	1.0	30.0		
D19	22.38	1.0	22.3	A	Tarp was folded where lightest sample taken.
	25.81	1.0	25.8		
	24.06	1.0	24.1		
	15.88	1.0	15.9		

TABLE A.3 EJECTA AREAL DENSITY SAMPLES--SECONDARY TARPS (CONTINUED)

Station	Weight of Sample	Collector Area	Areal Density	Sampling Techniques*	Remarks
	pounds	ft^2	lb/ft^2		
D20					Tarp location under splash crater and lip. Probe thickness: 32, 44, 54 inches. Average 43 inches.
D21	20.44	1.0	20.4	A	Tarp intact.
	23.56	1.0	23.5		
	22.19	1.0	22.2		
	26.94	1.0	26.9		
D22	258.19	16.20	16.0		Entire tarp picked up. Weight of tarp plus sample, 260.94 lb. Weight of tarp, 2.58 lb.
D23	11.50	1.0	11.5	A	Tarp intact.
	9.19	1.0	9.16		
	16.75	1.0	16.7		
	9.56	1.0	9.59		
B1	-	-	421	D	
B2	-	-	487	D	
B3	-	-	290	D	
B4	-	-	262	D	
B5	-	-	543	D	
B13	-	-	571	D	
B14	-	-	356	D	
B15	-	-	506	D	

TABLE A.3 EJECTA AREAL DENSITY SAMPLES--SECONDARY TARPS (CONTINUED)

Station	Weight of Sample	Collector Area	Areal Density	Sampling Techniques*	Remarks
	pounds	ft^2	lb/ft^2		
B16	-	-	328	D	
B17	-	-	496	D	

* Sampling Techniques:

A. Sample box inserted in debris until base rested on tarp. Sample removed and weighed.

B. Debris excavated and original ground surface identified. Steel plate inserted along the original ground surface and thin-walled sampling tube inserted until base rested on steel plate. Tube and plate removed and sample inside tube weighed.

C. Thin-walled sampling tube inserted until base rested on tarp. Sample recovered and weighed.

D. Debris excavated to original ground surface; thickness of debris measured. Areal density estimated using specific gravity equal to 1.5 gm/cm^3.

TABLE A.4 EJECTA THICKNESS OBSERVATIONS

Station	Ejecta Thickness	Station	Ejecta Thickness
	feet		feet
C1**	1.3	B1	4.5*
C2	2.3	B2	5.2*
C3**	1.9	B3	3.1*
C4	1.4	B4**	2.8*
C5	1.2	B5	5.8*
C6**		B6**	0.9
C7	1.8	B12**	2.8*
C8**	1.0	B13	6.1*
C9	2.2	B14	3.8*
C10**	1.3	B15	5.4*
C11**	5.6*	B16	3.5*
C12**	1.8	B17	5.3*
C13	2.6	B18	1.5*
C14**	0.7	B24	5.1*
C15	3.1		
C16	1.9	A6**	1.4
		A12**	4.8*
C17	1.5	A18**	2.4*
C18**		A24	12.5*
C19	0.2		
C20	0.2		
C21	0.2		
C22**			
C23**			
C24			

* Excavation by bulldozer. All other stations hand excavated.

** Tarp found.

TABLE A.5 EJECTA THICKNESS--PIPE GAGES

Station	Ejecta Thickness
	feet
D2	0.27
	0.26
	0.27
	0.27
D11	0.14
	0.15
	0.10
	0.09
D22	0.10
	0.10
	0.08
	0.09

TABLE A.6 SAMPLE COLLECTOR DATA

Sampler Collector	Number of Collectors	Average Dimensions	Average Area	Average Weight
		feet	ft^2	pounds
Primary Tarps	18	2.05 by 3.94	8.08	1.44
Secondary Tarps	10	4.02 by 4.03	16.20	2.58
Trays	10	0.71 by 1.08	0.77	0.48
Thin-walled Sampling Tube	1		0.1	

TABLE A.7 VOLUMETRIC DENSITY OF DEBRIS

Sample	Station	Moist Density	Remarks
		lb/ft^3	
1	E6	98	Sample taken at surface
2	D6	100	Sample taken at surface
3	C6	85	Sample taken at surface
4	A6	95	Sample taken at surface
5	X6	111	Sample taken at surface
6	C12	87	Sample taken about 3 inches below surface
7	A12	95	Sample taken about 4 to 5 inches below surface
8	C24	90	Sample taken about 2 inches below surface
9	B24	95	Ejecta very loose. Sample taken one inch below surface
10	F8	87	Drifted dust
11	C18	101	
12	B18	89	Sample taken 2 inches below surface

TABLE A.8 MISSILE SURVEY DATA

Radius	Note Number on Figure A.1	Lip-to-Lip Splash Crater Dimensions	Splash Crater Depth from Lip Crest	Weight of Missiles	Distance and Direction from Splash Crater	Remarks
		inches	inches	pounds	feet	
6	1	22 by 24		39.0	34 ft E	
				4.13	Adjacent	
6	2	30 by 30		3.38	1 ft S	Circular crater
				23.63	10 ft S	
				15.50	11 ft S	
				18.00	15 ft NW	
				2.88	Scattered	10 small fragments
6	3	54 by 54		29.50	60 to 70 ft E	Circular crater
				47.25	50 ft SE	
6	4	24 by 24		33.38	6 ft N	Circular crater in bush
6	5	24 by 30	6	0.31	6 ft N	
				11.31	10 ft E	
				27.25	12 ft NE	
				17.19	15 ft N	
6	6	30 by 40	6	300 est.		Missile ≈15 by 15 by 17 inches

TABLE A.8 MISSILE SURVEY DATA (CONTINUED)

Radius	Note Number on Figure A.1	Lip-to-Lip Splash Crater Dimensions	Splash Crater Depth from Lip Crest	Weight of Missiles	Distance and Direction from Splash Crater	Remarks
		inches	inches	pounds	feet	
6	7			14.31		No splash crater found
6	8	18 by 30		39.94	8 ft E	
6	9	24 by 24		22.69	6 ft E	Circular crater
6	10	30 by 48		24.88	up to 50 ft E	6 fragments
6	11	20 by 22	2	30.13	8 ft SE	
6	12			300 est.		3 fragments
6	13	Small				3 small splash craters. No missiles. Pile of poorly sorted rubble in one splash crater.
6	14	30 by 42	6 to 7	200 est.		4 fragments. Two about 10 pounds each and two totalling about 1.5 ft^3.
12	15	36 by 36	3	10.63	50 ft S	Circular crater

TABLE A.8 MISSILE SURVEY DATA (CONTINUED)

Radius	Note Number on Figure A.1	Lip-to-Lip Splash Crater Dimensions	Splash Crater Depth from Lip Crest	Weight of Missiles	Distance and Direction from Splash Crater	Remarks
		inches	inches	pounds	feet	
12	16	24 by 32		42.63	Adjacent	
12	17	24 by 36	3	9.81	Adjacent	
12	18	28 by 28	6	23.44	3 ft SW	Circular crater
12	19	24 by 24	5	23.19	Adjacent	Circular crater
12	20	26 by 26		15.50	In crater	Circular crater almost drifted full
12	21	24 by 28	3	15.88	18 ft S	
12	22	20 by 20		16.19	In crater	Circular crater almost drifted full
18	23	55 by 55	8 to 9	47.75 92.00 20.06 27.25 20.00 est.		Circular crater Numerous small fragments

TABLE A.8 MISSILE SURVEY DATA (CONTINUED)

Radius	Note Number on Figure A.1	Lip-to-Lip Splash Crater Dimensions	Splash Crater Depth from Lip Crest	Weight of Missiles	Distance and Direction from Splash Crater	Remarks
		inches	inches	pounds	feet	
18	24	15 by 15	1	6.69		Almost drifted full
18	25	20 by 20	1	19.56		Almost drifted full
18	26	18 by 18	1	10.06		Almost drifted full
18	27					11 missiles 15 to 40 pounds within an area about 150 ft. in diameter
18	28	35 by 43	3	43.00	Adjacent	
18	29	25 by 27	3	17.13		
18	30	26 by 47	3	59.75	75 ft W	Long crater dimensions oriented N of Sedan crater
18	31	30 by 40	4	17.56 24.00 9.75		 4 fragments 3 fragments

TABLE A.8 MISSILE SURVEY DATA (CONTINUED)

Radius	Note Number on Figure A.1	Lip-to-Lip Splash Crater Dimensions	Splash Crater Depth from Lip Crest	Weight of Missiles	Distance and Direction from Splash Crater	Remarks
		inches	inches	pounds	feet	
18	32	27 by 35	4 to 5	26.19 21.56 9.38	90 ft E	Long crater dimensions oriented toward Station D-24
18	33	20 by 20 20 by 20		20.00	Adjacent	Two splash craters and one missile
24	34	12 by 12 8 by 8				No missiles two small possible splash craters
8	35			23.5	4 ft SE	Most remote missile

TABLE A.9 GRAIN SIZE DISTRIBUTION LARGER THAN 0.185 INCH

Sample Number	Weights of Sample Size Groups*							Remarks**
	A	B	C	D	E	F	G	
				grams				
G1			2.2			1.0	582	
G6					67.6	53.7	3212	
G8			22.0	16.0	122.5	300.9	2524	
G12						2.8	4117	
G13						0.1	258	
G18			15.1		33.0	25.5	1581	
G19					30.4	6.8	473	
G24					14.8	21.4	2101	
F1						5.3	1338	
F6				61.4	167.6	63.2	4723	
F7				29.2	134.7	166.7	3764	
F12		53.9	97.8	74.0	91.3	93.8	3286	
F13		96.6	26.7		49.9	47.9	2263	
F18			71.9	217.6	575.8	159.3	3071	
F19				52.5	363.2	443.5	3441	
F24				10.5	16.1	14.4	3694	
E12	331.9	126.2	82.4	89.3	185.7	243.2	4182	
E18		147.9	169.1	7.9	91.2	190.9	4172	
E24				37.7	86.6	57.8	4881	
D6		27.8	13.0	28.9	140.7	158.3	1496	
D12		98.6	70.5	66.1	380.6	788.9	3917	
D18			49.9	21.3	200.3	246.4	4115	
D24				24.9	113.9	143.8	5312	
C6a				18.3	201.1	141.5	613	Upper
C6b		105.2	19.7	124.8	194.5	276.1	2657	Lower
C11a		157.0	216.5	232.7	511.2	463.5	1740	Upper
C11b				48.2	225.1	265.5	3173	
C12a			20.5		32.7	37.1	554	Upper
C12b	1721.0		48.1	154.8	308.1	390.8	3989	Lower
C18a			24.6		29.4	48.2	690	Upper
C18b				29.1	87.7	79.9	1717	
C24a		60.9			53.4	40.2	588	Upper
C24b	234.3	151.5	120.8	49.3	245.5	244.8	4164	Lower

TABLE A.9 GRAIN SIZE DISTRIBUTION LARGER THAN 0.185 INCH (CONTINUED)

Sample Number	Weights of Sample Size Groups*							Remarks**
	A	B	C	D	E	F	G	
	grams							
B6a	176.3		45.9	50.2	62.4	39.2	525	Upper
B6b	566.0			58.7	87.8	141.5	1940	Lower
B12a			23.3	92.9	407.3	706.1	2142	Upper
B12b			68.4	44.0	294.1	344.9	3740	Lower
B18a					5.6	35.2	526	Upper
B18b			169.0	84.8	314.9	289.4	4337	Lower
B24a		103.6	135.1	32.3	149.1	141.6	2170	Upper
B24b		172.5	301.5	185.7	533.8	435.2	4640	Lower
A6		236.3	105.3	71.6	324.0	447.2	4319	13 lb 4 oz
A6a				21.2	69.1	94.7	645.5	Upper
A6b			23.2	65.4	208.0	435.6	3542	Lower
A12		98.6	118.1	73.8	445.1	536.7	3868	All
A12a			15.3	119.8	499.8	691.2	2843	Upper
A12b			127.0	136.5	491.2	469.9	3881	Lower
A18a			374.0	53.2	235.1	213.7	2669	Upper
A18b		131.7	40.8	51.7	223.4	226.2	3106	Lower
A24a				16.5	80.9	72.3	664	Upper
A24b		116.5	365.3	255.7	536.7	414.2	3791	Lower

* Sample size groups are:
- A S > 2 in.
- B 1.5 in. < S < 2 in.
- C 1.0 in. < S < 1.5 in.
- D 0.75 in. < S < 1.0 in.
- E 0.375 in. < S < 0.75 in.
- F 0.185 in. < S < 0.375 in.
- G S < 0.185 in.

** Samples designated upper were generally within 0.2 ft of the ejecta surface. Samples designated lower were taken near the tarp.

TABLE A.10 GRAIN SIZE DISTRIBUTION SMALLER THAN 0.185 INCH

Sample Number	Weights of Sample Size Groups*							Remarks**
	H	I	J	K	L	M	N	
	grams							
G1		0.3	2.4	8.8	47.1	22.8	126.2	
G6	5.4	14.8	34.4	38.4	68.5	17.6	32.3	
G8	14.5	17.9	26.2	33.4	67.4	17.2	31.5	
G12	1.3	5.3	14.8	23.7	69.9	24.1	57.8	
G13	0.4	1.4	8.4	21.5	57.5	23.3	79.6	
G18	3.5	3.4	13.0	22.6	69.6	26.7	71.7	
G19	2.4	8.4	18.5	27.0	71.4	21.1	85.1	
G24	3.3	3.2	5.4	14.6	69.7	29.3	79.7	
F1	1.2	5.0	13.2	20.5	50.8	23.0	84.1	
F6	8.5	16.8	27.5	36.5	70.2	17.8	22.4	
F7	12.7	27.7	38.1	41.1	60.8	12.7	18.3	
F12	13.0	20.9	24.5	25.4	56.4	18.3	25.3	
F13	7.9	24.0	34.0	37.1	60.1	14.0	31.2	
F18	5.7	13.2	23.6	29.4	73.7	21.3	38.1	
F19	23.6	32.4	30.2	27.2	45.0	11.9	24.1	
F24	1.4	3.4	10.8	21.6	75.3	29.5	78.8	
E12	18.4	30.0	29.2	27.5	49.5	13.2	17.5	
E18	13.8	18.5	22.5	23.5	48.5	14.9	35.6	
E24	3.5	9.4	19.5	26.4	69.4	23.1	57.7	
D6	26.1	36.7	38.0	40.4	68.4	16.4	27.1	
D12	40.7	38.5	35.6	30.0	49.8	12.9	21.2	
D18	27.7	36.0	34.0	29.8	52.5	16.5	35.6	
D24	10.8	20.0	26.6	29.3	62.1	17.6	40.0	
C6a	62.3	43.9	37.2	32.0	46.3	10.1	12.9	Upper
C6b	30.8	35.3	34.7	30.7	47.7	10.3	12.6	Lower
C11a	39.9	41.4	32.9	26.1	37.9	8.9	11.1	
C11b	20.5	25.9	26.9	25.8	47.5	12.6	20.3	
C12a	30.7	39.9	32.9	27.6	41.1	9.8	17.6	Upper
C12b	29.0	35.9	36.6	33.8	55.7	11.2	19.6	Lower
C18a	36.4	43.6	34.8	27.4	40.9	11.2	25.4	Upper
C18b	24.0	38.9	34.5	28.4	48.7	12.1	19.3	
C24a	32.4	32.5	32.4	31.4	57.0	15.8	35.2	Upper
C24b	20.9	24.8	26.6	30.8	77.8	17.9	26.8	Lower

TABLE A.10 GRAIN SIZE DISTRIBUTION SMALLER THAN 0.185 INCH (CONTINUED)

Sample Number	Weights of Sample Size Groups*							Remarks**
	H	I	J	K	L	M	N	
	grams							
B6a	35.7	43.4	42.8	37.5	60.9	14.7	18.8	Upper
B6b	26.4	36.6	36.5	33.3	56.3	13.1	17.4	Lower
B12a	56.0	47.6	36.9	29.9	48.6	11.4	13.0	Upper
B12b	26.5	32.8	34.5	33.6	52.5	11.4	17.8	Lower
B18a	45.4	50.9	40.3	31.9	47.2	11.5	21.3	Upper
B18b	27.6	35.9	35.3	34.3	63.3	13.5	19.5	Lower
B24a	30.3	38.2	40.2	38.3	61.7	12.0	19.9	Upper
B24b	37.7	40.0	37.4	35.9	57.7	11.7	21.1	Lower
A6	26.4	32.6	33.0	29.0	46.5	12.6	17.9	
A6a	36.5	40.2	35.8	30.7	49.0	13.0	16.2	Upper
A6b	42.9	47.7	45.0	49.7	66.0	16.0	24.3	Lower
A12	26.6	34.6	33.3	30.3	49.9	12.1	22.3	All
A12a	40.3	38.5	33.8	27.3	43.8	10.4	12.7	Upper
A12b	33.9	50.1	48.6	42.7	60.5	13.7	28.2	Lower
A18a	55.2	58.0	51.1	42.5	65.6	15.0	25.8	Upper
A18b	25.9	35.1	34.4	31.3	57.0	14.2	17.3	Lower
A24a	30.9	32.0	32.5	28.5	51.3	14.8	23.1	Upper
A24b	29.3	34.6	33.4	30.7	48.0	11.8	23.1	Lower

* Sample size groups are:
H 0.078 in. < S < 0.185 in.
I 0.0328 in. < S < 0.078 in.
J 0.0164 in. < S < 0.0328 in.
K 0.0097 in. < S < 0.0164 in.
L 0.0041 in. < S < 0.0097 in.
M 0.0029 in. < S < 0.0041 in.
N S < 0.0029 in.

** Samples designated upper were generally within 0.2 ft of the ejecta surface. Samples designated lower were taken near the tarp.

TABLE A.11 PERCENT BY WEIGHT OF GRAIN SIZES

Sample Number	Percent by Weight for Sample Size Groups*												
	A	B	C	D	E	F	H	I	J	K	L	M	N
G6					2.03	1.61	2.46	6.75	15.68	17.50	31.23	8.02	14.72
G12						0.07	0.66	2.69	7.51	12.03	35.47	12.23	29.34
G18			0.91		1.99	1.54	1.59	1.54	5.90	10.26	31.59	12.12	32.56
G24					0.69	1.00	1.58	1.53	2.59	6.99	33.39	14.04	38.19
F6				1.22	3.34	1.26	4.01	7.92	12.97	17.21	33.12	8.39	10.56
F12		1.46	2.64	2.00	2.47	2.54	6.29	10.11	11.85	12.28	27.27	8.85	12.24
F18			1.76	5.31	14.06	3.89	2.08	4.83	8.63	10.75	26.96	7.79	13.94
F24				0.28	0.43	0.39	0.63	1.52	4.84	9.68	33.73	13.21	35.29
E12	6.33	2.41	1.57	1.70	3.54	4.64	7.92	12.92	12.57	11.84	21.34	5.68	7.54
E18		3.09	3.54	0.16	1.91	3.99	6.79	9.11	11.08	11.57	23.89	7.34	17.53
E24				0.74	1.71	1.14	1.61	4.34	8.99	12.18	32.02	10.66	26.61
D6		1.49	0.69	1.55	7.54	8.49	8.27	11.63	12.05	12.81	21.69	5.20	8.59
D12		1.85	1.32	1.24	7.15	14.82	13.10	12.39	11.46	9.66	16.04	4.15	6.82
D18			1.08	0.46	4.32	5.32	10.60	13.78	13.01	11.40	20.10	6.31	13.62
D24				0.44	2.04	2.57	4.97	9.20	12.24	13.48	28.57	8.09	18.40
C6		2.26	0.42	3.20	9.82	9.90	13.09	13.07	12.44	10.93	16.77	3.63	4.47
C6a				1.88	20.65	14.53	16.02	11.29	9.57	8.23	11.91	2.60	3.32
C6b		3.11	0.58	3.69	5.76	8.17	11.99	13.74	13.51	11.95	18.59	4.01	4.90
C12**	22.51		1.06	2.02	4.72	5.89	8.61	10.77	10.53	9.56	15.49	3.21	5.63
C12a			3.18		5.07	5.76	13.23	17.19	14.17	11.89	17.71	4.22	7.58
C12b	26.03		0.73	2.34	4.66	5.91	7.89	9.77	9.96	9.19	15.14	3.05	5.33
C18**			1.03	1.01	4.29	4.81	11.78	17.06	14.62	11.87	19.58	4.99	8.96

TABLE A.11 PERCENT BY WEIGHT OF GRAIN SIZES (CONTINUED)

Sample Number	Percent by Weight for Sample Size Groups*												
	A	B	C	D	E	F	H	I	J	K	L	M	N
C18a			3.10		3.72	6.08	14.43	17.29	13.80	10.86	16.21	4.44	10.07
C18b				1.52	4.58	4.18	10.46	16.95	15.03	12.38	21.22	5.27	8.41
C24**	4.14	3.33	2.13	0.87	4.91	4.76	7.68	8.96	9.53	10.88	26.88	6.26	9.67
C24a		8.20			7.19	5.41	10.84	10.87	10.84	10.51	19.07	5.29	11.78
C24b	4.50	2.91	2.32	0.95	4.71	4.70	7.40	8.79	9.42	10.91	27.56	6.34	9.49
B6**	20.10		1.47	3.10	4.23	4.86	8.31	11.11	11.05	9.98	16.71	3.92	5.16
B6a	19.63		5.10	5.58	6.94	4.36	8.21	9.98	9.85	8.63	14.01	3.38	4.33
B6b	20.27			2.10	3.14	5.06	8.35	11.57	11.54	10.53	17.80	4.14	5.50
B12**			1.46	1.11	6.96	8.67	10.90	13.01	13.43	12.96	20.27	4.42	6.81
B12a			0.69	2.75	12.08	20.95	14.62	12.42	9.63	7.80	12.69	2.98	3.39
B12b			1.52	0.98	6.54	7.68	10.55	13.06	13.74	13.38	20.92	4.54	7.09
B18**			2.61	1.31	5.06	5.70	11.40	14.23	13.28	12.37	21.99	4.79	7.26
B18a					0.99	6.21	16.95	19.02	15.05	11.91	17.63	4.29	7.95
B18b			3.25	1.63	6.06	5.57	10.04	13.06	12.85	12.48	23.06	4.91	7.09
B24**		2.78	4.81	2.91	8.43	6.89	11.51	12.27	11.51	11.05	17.77	3.60	6.47
B24a		3.79	4.94	1.18	5.46	5.18	10.00	12.61	13.27	12.65	20.39	3.96	6.57
B24b		2.75	4.81	2.96	8.52	6.94	11.55	12.26	11.46	11.00	17.69	3.59	6.47
A6		4.29	1.91	1.30	5.88	8.13	10.43	12.92	13.08	11.55	18.43	4.99	7.09
A6a				2.55	8.32	11.40	12.81	14.11	12.57	10.77	17.22	4.56	5.69
A6b			0.54	1.53	4.86	10.19	12.19	13.55	12.79	14.12	18.77	4.55	6.91
A12		1.92	2.30	1.44	8.65	10.44	9.57	12.45	11.98	10.90	17.97	4.35	8.03
A12a			0.37	2.91	10.92	16.78	13.45	12.85	11.28	9.11	14.62	3.47	4.24
A12b			2.48	2.67	9.62	9.20	9.28	13.71	13.30	11.69	16.58	3.75	7.72
A18**		3.15	1.97	1.38	5.98	5.99	10.21	13.45	13.04	11.79	21.22	5.25	6.57

TABLE A.11 PERCENT BY WEIGHT OF GRAIN SIZES (CONTINUED)

Sample Number	Percent by Weight for Sample Size Groups*												
	A	B	C	D	E	F	H	I	J	K	L	M	N
A18a			10.55	1.50	6.63	6.03	13.26	13.94	12.28	10.22	15.73	3.66	6.20
A18b		3.48	1.08	1.37	5.91	5.99	9.89	13.40	13.13	11.95	21.77	5.42	6.61
A24**		2.11	6.61	4.64	9.79	7.57	9.63	11.35	10.97	10.07	15.79	3.88	7.59
A24a				1.98	9.70	8.67	11.55	11.96	12.15	10.65	19.18	5.53	8.63
A24b		2.13	6.66	4.66	9.79	7.56	9.61	11.35	10.96	10.07	15.76	3.87	7.58

* Size groups are in inches. (See Tables A.9 and A.10 for sample size groups.)

** Adjusted percent based on the a and b layer percentages.

REFERENCES

1. W. A. Roberts and J. A. Blaylock; "Distribution of Debris Ejected by the Stagecoach Series of High Explosive Cratering Bursts"; D2-6955-1, October 1961; The Boeing Company, Seattle, Washington; Unclassified.

2. W. A. Roberts; "Outer Crater Lip Debris Ejected by Scooter--A Buried High Explosive Cratering Shot"; D2-90086, April 1962; The Boeing Company, Seattle, Washington; Unclassified.

3. R. H. Carlson and W. A. Roberts; "Local Distribution of Material Ejected by Surface Explosions: White Tribe Interim Report"; D2-6955-2, August 1961; The Boeing Company, Seattle, Washington; Unclassified.

4. R. H. Carlson and W. A. Roberts; "Ejecta Study of 100-Ton Suffield Explosive Cratering Shot"; D2-90203, August 1962; The Boeing Company, Seattle, Washington; Unclassified.

5. Engineering Research Associates, Inc.; "Underground Explosion Test Program"; Final Report, Volume 1--Soil, August 1952, Volume 2--Rock, April 1953; Engineering Research Associates, Inc., St. Paul, Minnesota; Unclassified.

6. W. N. Hess and M. D. Nordyke; "Throwout Calculations for Explosion Craters"; Journal of Geophysical Research, October 1961, Vol. 66, No. 10; The American Geophysical Union, Washington, D. C.; Unclassified.

7. Private communication with M. D. Nordyke; University of California, Lawrence Radiation Laboratory, Livermore, California; Unclassified.

8. J. A. Bishop and F. E. Lowance; "Physical Characteristics of Crater and Lip"; Project 4.2, Operation Jangle, WT-399, May 1952; U. S. Naval Civil Engineering Research and Evaluation Laboratory, Port Hueneme, California; Unclassified.

9. W. R. Wray, U. S. Army Engineer Nuclear Cratering Group, Corps of Engineers, Lawrence Radiation Laboratory, Livermore, California; Letter to: W. A. Roberts, The Boeing Company, Seattle, Washington; Subject: "Sedan Fallout Data," 8 January 1963; Unclassified.

10. M. G. El-Fandy, "On the Physics of Dusty Atmospheres"; Quarterly Journal of the Royal Meteorological Society, April 1953, Vol. 79, No. 340, Pages 284-287; Unclassified.

11. R. L. Stetson and others; "Distribution and Intensity of Fallout from the Underground Shot"; Project 2.5.2, Operation Teapot, WT-1154, March 1958; U. S. Naval Radiological Defense Laboratory, San Francisco, California; Unclassified.

12. J. G. Lewis; "Crater Measurements"; Project 1.6, Operation Teapot, WT-1105, August 1958; Engineer Research and Development Laboratories, Fort Belvoir, Virginia; Unclassified.

13. D. C. Sachs and L. M. Swift; "Underground Explosion Effects"; Project 1.7, Operation Teapot, WT-1106 (Del.), July 1959; Stanford Research Institute, Menlo Park, California; Unclassified.

14. R. H. Bishop and others; "20-Ton HE Cratering Experiments in Desert Alluvium, Final Report, May 1962"; Project Stagecoach, SC-4596(RR); Sandia Corporation, Albuquerque, New Mexico; Unclassified.

15. D. C. Campbell; "Some HE Tests and Observations on Craters and Base Surges"; Project 1(9)-3, Operation Jangle, WT-410, November 1951; Armed Forces Special Weapons Project, Kirtland Air Force Base, Albuquerque, New Mexico; Unclassified.

16. E. M. Shoemaker; "Ballistics and Throwout Calculations for the Lunar Crater Copernicus"; UCRL-6438; Proceedings of the Geophysical Laboratory-Lawrence Radiation Laboratory Cratering Symposium held in Washington, D.C., March 28-29, 1961; U. S. Geological Survey, Menlo Park, California; Unclassified.

17. E. M. Shoemaker; "Impact Mechanics at Meteor Crater, Arizona"; Open File Report, July 1959; U. S. Geological Survey, Menlo Park, California; Unclassified.

18. R. H. Carlson; "High Explosive Ditching from Linear Charges"; Journal of Geophysical Research, June 1963, Vol. 68, No. 12; The American Geophysical Union, Washington, D.C.; Unclassified.

TECHNICAL REPORTS SCHEDULED FOR ISSUANCE
BY AGENCIES PARTICIPATING IN PROJECT SEDAN

AEC REPORTS

AGENCY	PNE NO.	SUBJECT OR TITLE
USPHS	200F	Off-Site Radiation Safety
USWB	201F	Analysis of Weather and Surface Radiation Data
SC	202F	Long Range Blast Propagation
REECO	203F	On-Site Rad-Safe
AEC/USBM	204F	Structural Survey of Private Mining Operations
FAA	205F	Airspace Closure
SC	211F	Close-In Air Blast From a Nuclear Event in NTS Desert Alluvium
LRL-N	212P	Scientific Photo
LRL	214P	Fallout Studies
LRL	215F	Structure Response
LRL	216P	Crater Measurements
Boeing	217P	Ejecta Studies
LRL	218P	Radioactive Pellets
USGS	219F	Hydrologic Effects, Distance Coefficients
USGS	221P	Infiltration Rates Pre and Post Shot
UCLA	224P	Influences of a Cratering Device on Close-In Populations of Lizards
UCLA	225P Pt. I and II	Fallout Characteristics

TECHNICAL REPORTS SCHEDULED FOR ISSUANCE BY AGENCIES PARTICIPATING IN PROJECT SEDAN

AGENCY	PNE NO.	SUBJECT OR TITLE
BYU	226P	Close-In Effects of a Subsurface Nuclear Detonation on Small Mammals and Selected Invertabrates
UCLA	228P	Ecological Effects
LRL	231F	Rad-Chem Analysis
LRL	232P	Yield Measurements
EGG	233P	Timing and Firing
WES	234P	Stability of Cratered Slopes
LRL	235F	Seismic Velocity Studies

DOD REPORTS

AGENCY	PNE NO.	SUBJECT OR TITLE
USC-GS	213P	"Seismic Effects From a High Yield Nuclear Cratering Experiment in Desert Alluvium"
NRDL	229P	"Some Radiochemical and Physical Measurements of Debris from an Underground Nuclear Explosion"
NRDL	230P	Naval Aerial Photographic Analysis

ABBREVIATIONS FOR TECHNICAL AGENCIES

STL	Space Technology Laboratories, Inc., Redondo Beach, Calif.
SC	Sandia Corporation, Sandia Base, Albuquerque, New Mexico
USC&GS	U. S. Coast and Geodetic Survey, San Francisco, California
LRL	Lawrence Radiation Laboratory, Livermore, California
LRL-N	Lawrence Radiation Laboratory, Mercury, Nevada
Boeing	The Boeing Company, Aero-Space Division, Seattle 24, Washington
USGS	Geological Survey, Denver, Colorado, Menlo Park, Calif., and Vicksburg, Mississippi
WES	USA Corps of Engineers, Waterways Experiment Station, Jackson, Mississippi
EGG	Edgerton, Germeshausen, and Grier, Inc., Las Vegas, Nevada, Santa Barbara, Calif., and Boston, Massachusetts
BYU	Brigham Young University, Provo, Utah
UCLA	UCLA School of Medicine, Dept. of Biophysics and Nuclear Medicine, Los Angeles, Calif.
NRDL	Naval Radiological Defense Laboratory, Hunters Point, Calif.
USPHS	U. S. Public Health Service, Las Vegas, Nevada
USWB	U. S. Weather Bureau, Las Vegas, Nevada
USBM	U. S. Bureau of Mines, Washington, D. C.
FAA	Federal Aviation Agency, Salt Lake City, Utah
REECO	Reynolds Electrical and Engineering Co., Las Vegas, Nevada

SUPPLEMENTARY DOD DISTRIBUTION FOR PROJECT SEDAN

PNE NO.	DIST. CAT.	PNE NO.	DIST. CAT.	PNE NO.	DIST. CAT.
200	26, 28	214	26	226	42
201	2, 26	215	32	228	42
202	12	216	14	229	26, 22
203	28	217	14	230	100
204	32	218	12, 14	231	22
205	2	219	14	232	4
211	12	221	14	233	2
212	92, 100	224	42	234	14
213	12, 14	225	26	235	14

In addition, one copy of reports 201, 202, 203, 211, 214, 215, 216, 217, 218, 221, 225, 229, 230, 232, 234, and 235 to each of the following:

The Rand Corp.
1700 Main St.,
Santa Monica, California

Attn: Mr. H. Brode

U. of Illinois,
Civil Engineering Hall
Urbana, Illinois

Attn: Dr. N. Newmark

Stanford Research Institute
Menlo Park, California

Attn: Dr. Vaile

E. H. Plesset Associates
1281 Westwood Blvd.,
Los Angeles 24, California

Attn: Mr. M. Peter

Mitre Corp.
Bedford, Massachusetts

General American Transportation Corp.
Mechanics Research Div.
7501 N. Natchez Ave.,
Niles 48, Illinois

Attn: Mr. T. Morrison; Dr. Schiffman

Dr. Whitman
Massachusetts Institute of Technology
Cambridge, Massachusetts